INFORMATION TO USERS

This manuscript has been reproduced from the microfilm master. UMI films the text directly from the original or copy submitted. Thus, some thesis and dissertation copies are in typewriter face, while others may be from any type of computer printer.

The quality of this reproduction is dependent upon the quality of the copy submitted. Broken or indistinct print, colored or poor quality illustrations and photographs, print bleedthrough, substandard margins, and improper alignment can adversely affect reproduction.

In the unlikely event that the author did not send UMI a complete manuscript and there are missing pages, these will be noted. Also, if unauthorized copyright material had to be removed, a note will indicate the deletion.

Oversize materials (e.g., maps, drawings, charts) are reproduced by sectioning the original, beginning at the upper left-hand corner and continuing from left to right in equal sections with small overlaps. Each original is also photographed in one exposure and is included in reduced form at the back of the book.

Photographs included in the original manuscript have been reproduced xerographically in this copy. Higher quality 6" x 9" black and white photographic prints are available for any photographs or illustrations appearing in this copy for an additional charge. Contact UMI directly to order.

UMI

A Bell & Howell Information Company
300 North Zeeb Road, Ann Arbor MI 48106-1346 USA
313/761-4700 800/521-0600

Université d'Ottawa · University of Ottawa

CALCIUM, ACTIN AND THE SPECTRIN SKELETON: RESPONSES TO SWELLING AND SHRINKING PERTURBATIONS

Thesis submitted to the
School of Graduate Studies and Research
University of Ottawa
in partial fulfillment of the requirements for the
M.Sc. degree in the

Ottawa-Carleton Institute of Biology

PREFACE

Chapters two and three of this thesis were initially written as manuscripts for publication. I had the job of writing the first manuscript, which was then modified by Cathy and myself in collaboration. Chapter 2 was published in January 1998 by the American Journal of Physiology. Chapters 3 and 4 are in preparation.

Ian Slotin, a summer student in Cathy's lab during the summer of 1995, perfected the FURA-2-AM loading protocol which I later used for my calcium experiments, presented in chapter 2. Along with this he acquired data for the calcium calibration curve, which is presented with my calibration curve in chapter 2.

Dr. Jay Baltz, a principal investigator at the Loeb Institute, taught and allowed me to use his ratio imaging microscope and equipment, which was needed to perform the calcium experiments. For the experiments where I accumulated the $[Ca]_{int}$ every 2 seconds, he helped by adjusting the microscope focus and beginning the ratioing software as I did the solution changes.

Jenni McNally, a summer student in Cathy's lab, characterized osmotically induced VLDs in tissue culture rat skeletal myotubes, L6E9 cells, during the summer of 1996. Then during the summer of 1997 she performed Western blots using L6E9 myoblasts and myotubes and the 4I12 antibody specific for β-spectrin and β-fodrin. These results were required before I could begin my spectrin skeleton immunocytochemistry studies. Her data is presented in the appendix.

Drs. Chris Cohan and Elizabeth Welnhofer, from the University of Buffalo, performed the high resolution microscopy and live F-actin *Lymnaea* experiments, presented in chapter 3, in collaboration with Cathy and myself when we visited their lab during the spring of 1997.

TABLE OF CONTENTS

ACKNOWLEDGEMENTS

I would like to thank my mother and father, Linda and James Herring, for their emotional and financial support, especially over the past six years of university. Specifically I would like to thank my dad for instilling the idea that once I begin something I must see it through. This often became my reason to continue my Master's over many frustrating days and nights. I would like to thank my mom for always telling me, during my bouts of frustration, to try it one more time. For some reason she was always right, it was better the next time.

To my husband and best friend, Andrew Nelson, I would like to thank him for his continual emotional support. His pressuring to start and finish writing my thesis was much needed on many occasions. Also thank-you for just listening.

To my supervisor, Dr. Cathy Morris, I would like to thank her for giving me the chance to join her lab, extend my scientific knowledge and for telling me to try it again. But most of all for her continual guidance.

To Dr. Jay Baltz I would like to thank him for devoting a lot of his time to me and for having such patience when the calcium experiments did not initially work. His talks about how the experiments would eventually work and how we could approach the next set of experiments always reassured me. Also for volunteering as an extra pair of hands when I had to go back a year later and do some additional calcium experiments for the paper.

To Drs. Chris Cohan and Elizabeth Welnhofer at the University of Buffalo, I would like to thank them both for allowing me to invade their lab for two weeks. If it hadn't been for their generosity and commitment to helping me, my actin experiments may have went on indefinitely.

To my lab mates, Cicely Gu, Peter Juranka, Xiaodong Wan and Lorin Gaertner, thank-you for the days of commiserating when my experiments were not working and for sharing in those days when they actually did.

ABSTRACT

As cells change their size and shape they must also make coordinated surface area changes. To understand how cells regulate their surface area, responses to exogenously applied osmotic swelling and shrinking perturbations were studied. Previous studies in molluscan neurons revealed that excess surface membrane is retrieved, during large shrinking perturbations, as vacuole-like dilations (VLDs) (Reuzeau *et al.*, 1995). VLDs begin as membrane invaginations of the substrate-adherent surface that can grow up to 10μm in diameter in about 1 minute, reverse upon reswelling and recover by cell-mediated processes, sensitive to actomyosin inhibitors, by pinching off at the substrate (Reuzeau *et al.*, 1995). From these observations it was postulated that cells regulate their surface membrane in response to membrane tension gradients. Increases in membrane tension, brought about by swelling, should therefore elicit addition of membrane to the cell surface, whereas decreases in membrane tension, brought about by shrinking, should cause retrieval of excess surface membrane.

If increased membrane tension increases membrane area via enhanced calcium dependent exocytosis, then $[Ca]_{int}$ rather than membrane tension may be the primary signal used in surface area regulation. $[Ca]_{int}$ in swelling molluscan neurons was measured by FURA-2 ratiometric microscopy using perturbations which induced VLDs. $[Ca]_{int}$ was measured in either normal (3.5mM) or low (0.5μM) extracellular calcium. The small but statistically significant changes observed were well below the levels which would stimulate exocytosis. In BAPTA loaded neurons, resting $[Ca]_{int}$ was about one-half its normal value and did not change with osmotic perturbations. BAPTA was therefore effective at chelating neuronal intracellular calcium. BAPTA loaded neurons, like control neurons yielded VLDs using either normal or low extracellular calcium. These results are consistent with the idea that neurons have an $[Ca]_{int}$ independent means of adjusting their surface area and thus lends weight to the hypothesis that membrane tension may directly mediate surface area regulation.

Previous investigations revealed that neurons incubated in cytochalasin, a drug that promotes actin depolymerization, do not undergo VLD recovery (Reuzeau *et al.*, 1995). Microscopy studies into how neuronal F-actin responded to osmotic perturbations and how the F-actin is related

to VLDs were therefore initiated. In *Lymnaea* neurons that had swelled then reshrunk to form VLDs, F-actin rapidly reorganized around the VLDs. At the substrate, F-actin formed rings of newly constituted leading edge (filopodia and lamellipodia) that we termed actipodia. Microinjection of live molluscan neurons with fluorescent G-actin also indicated that F-actin could reorganize as actipodia around the VLD membrane within 5 minutes. Cytochalasin incubated neurons formed VLDs but no actipodia were observed in association with these VLDs. It was concluded that F-actin rich actipodia may be the structures which help the VLD pinch off from the substrate and therefore begin reinternalization of excess surface membrane, also known as VLD recovery.

Fodrin and spectrin are cytoskeletal proteins thought to provide mechanical support to surface membranes. Fodrin and/or spectrin line a variety of intracellular vacuoles and vesicles, leading us to investigate whether VLD membranes are likewise lined by membrane skeleton. VLDs can be generated in rat skeletal muscle myotubes and since an appropriate antibody specific for spectrin and fodrin was available for this preparation, myotubes were used rather than molluscan neurons. Myotube VLDs were found to be lined by the spectrin skeleton as early as 3 minutes after first being induced to form. It is likely therefore that during surface area regulation newly invaginating membrane is mechanically stabilized by the membrane skeleton.

To explain how surface membrane is reinternalized in the form of VLDs upon shrinking, the membrane invaginations that become VLDs are thought to experience an increase in membrane tension. The results of this thesis show that intracellular calcium signalling is not critical for any of the steps in this process and have implicated the actin and the spectrin skeleton in events occurring as shrinking cells reduce their surface area.

LIST OF FIGURES

ABBREVIATIONS

α-MEM	alpha minimum essential medium
(-AM)	acetoxymethyl ester
4-bromo-A23187	4-benzoxazolecarbcxylic acid, 6-bromo-5-(methylamino)-2-((3,9,11-trimethyl-8-(1-methyl-2-oxo-2-(1H-pyrrol-2-yl)-ethyl-1,7-dioxaspiro(5,5)undec-2-yl)methyl)-,(6S-(6α(2S*,3S*),8β(R*),9β,11α))
BAPTA	1,2-bis(o-aminophenoxy)-ethane-N,N,N',N'-tetraacetic acid
BFA	brefeldin A
BSA	bovine serum albumin
$CaCl_2$	calcium chloride
[Ca]	calcium concentration
$[Ca]_{int}$	intracellular calcium concentration
$[Ca]_{ext}$	extracellular calcium concentration
CB	cytochalasin B
C_m	membrane capacitance
DIC	differential interference contrast
DMSO	dimethyl sulfoxide
EGTA	ethyleneglycol-bis-(β-amino-ethylether)N,N'-tetra-acetic acid
F-actin	filamentous actin
FBS	fetal bovine serum
FURA-2	5-oxazolecarboxylic acid, 2-(6-(bis(2-((acetyloxy)methoxy)-2-oxoethyl)amino)-5-(2-(bis(2-((acetyloxy)methoxy)-2-oxoethyl)amino)-5-methylphenoxy)ethoxy)-2-benzofuranyl)-, (acetyloxy)methyl ester
g	grams
GTP-γ-S	guanosine 5'-O-(3-thiotriophosphate)
h	hours
HEPES	(N-[2-hydroxyethy]piperazine-N'[2-ethanesulfonic acid]
KCl	potassium chloride
L6NS	L6E9 normal saline
min(s)	minute(s)
$MgCl_2$	magnesium chloride
NaCl	sodium chloride
NaOH	sodium hydroxide
nM	nanomolar
NEM	*N*-ethylmaleimide
NS	normal saline
0.5xNS	normal saline diluted with distilled water by 50%
rh-actin	tetramethyl-rhodamine-5-iodoacetamide labelled G-actin
RVD	regulatory volume decrease
S.E.	standard error
PBS	phosphate buffered saline
PMSF	phenylmethylsulfonylfluoride
μM	micromolar
μm	micrometer
μL	microliter
VLDs	vacuole-like dilations

CHAPTER 1: GENERAL INTRODUCTION

INTRODUCTION TO SURFACE AREA REGULATION AND MEMBRANE TENSION

This thesis centers around the general theory that cells must regulate their plasma membrane area to accommodate shape and volume changes. How surface membrane and associated cytoskeletal elements respond to swelling and shrinking osmomechanical perturbations was investigated. Many researchers have examined volume regulation in response to swelling and shrinking. However, it can not be assumed that surface membrane is somehow innately regulated along with cellular volume regulation mechanisms. The surface area and volume of solid objects change at different rates. And since the cell surface membrane is a physically discrete entity it must regulate its area by a mechanism independent of volume regulation mechanisms. How, for instance do cells double their surface area during swelling without bursting? Plasma membrane is very inelastic; it can only stretch by 2-3% (Evans *et al.*, 1976; Nichol and Hutter, 1996a). Stretching beyond this limit results in membrane rupture which is fatal.

Membrane tension, we postulate, maybe a simple signal and effector that could maintain surface area homeostasis in response to normal cellular demands and to emergencies. If surface membrane tension increased, membrane would be added thereby increasing the cell's surface area. By contrast a decrease in membrane tension would initiate retrieval of surface membrane causing a decrease in a cell's surface area. In-plane membrane under low tension will flow to membrane regions under increased tension. Can this fact be used by cells to help avoid cellular rupture? Likewise, can a decrease in surface membrane tension promote reincorporation of excess surface membrane back into the cell? The plasma membrane experiences membrane tension gradients (Dai and Sheetz, 1995a and b; Sheetz and Dai, 1996) but for a tension feedback system to operate, membrane from internal stores must be continually available and somehow be "in communication" with the surface. Because tension in an irregular shaped cell is not isotropic (in the face of an isotropic pressure), membrane tension as described here can work and act locally; then tension differences would provide a source of potential energy.

APPROACHES USED TO STUDY SURFACE AREA REGULATION

Membrane capacitance

The most often used way of measuring a cell's surface area has been to measure its membrane capacitance, since membrane capacitance is directly proportional to membrane area. Therefore if cells regulate their surface area by adding and retrieving membrane during swelling and shrinking perturbations, the membrane capacitance should change. Membrane capacitance (C_m) is defined (Eckert *et al.*, 1988) as the ability of membrane to store or separate charges and results from the fact that the lipid bilayer is a dielectric material that is impermeable to ions. Ion's electrical fields extend over short distances (~50Å) such as the low dielectric constant lipid bilayer and thus interact with ions on the other side of the membrane. When positively charged ions are in excess beneath one side of the membrane, negatively charged ions on the other side of the membrane are attracted and this results in separation of charge by the capacitor. If a cell's surface membrane increases in area, then correspondingly more counter ions can be stored on the opposite sides. The increase in the number of separated ions is measured as increased C_m. Likewise decreases in the number of separated ions is measured as decreased C_m.

Measurements of C_m under voltage clamp include only the membrane at the cell surface. Smoothed out irregular membrane such as surface ruffles would not result in a capacitance increase (Ross *et al.*, 1994). By contrast, any internal membrane stores not at or continuous with the membrane surface, such as cytoplasmic vesicles or occluded membrane invaginations, would not be measured as part of C_m. Therefore when apparent membrane area (from cell diameter measurements and C_m) both increase, internal membranes must be added to the surface membrane (Wan *et al.*, 1995). The C_m value measured for biological membranes is approximately 1μF/cm^2 (Eckert *et al.*, 1988). This is referred to as the membrane's specific capacitance, whereas the general term "membrane capacitance" does not refer to a given area and so does not account for the amount of separated charge per unit membrane area. The units of C_m are farads (F), which is equal to the quantity of charge separated per volt.

Capacitance measurements are usually recorded in order to investigate membrane trafficking during exocytosis and endocytosis. Zorec and Tester (1993) found that intracellular

pressure changes in barley protoplasts could cause cells to undergo either exocytosis or endocytosis. Standard patch-clamp whole-cell recording techniques were used to measure the protoplast's C_m. Exocytosis was initiated, observed when C_m measurements increased, by increasing the cell's intracellular pressure by a patch pipette inserted into the protoplast's interior. Release of this pressure resulted in endocytosis, again observed when C_m decreased.

The fact that C_m can increase upon swelling and decrease upon shrinkage has been documented in various cell types. Okada *et al.* (1992) found that exposure of human small intestinal epithelial cells to a hypotonic bathing solution (an osmolality change of 293 to 161mosM due to a decreased NaCl concentration) caused extensive swelling. This corresponded to an increase in membrane capacitance from 23.2±1.3 to 28.8±1.8pF, which was calculated to correspond to the incorporation of more than 4000 0.2μm diameter vesicles. Upon return to the isotonic media, which caused shrinkage, the membrane capacitance decreased from 28.8±1.8pF to 24.1±1.6pF. Sukhorukov *et al.* (1993) studied how continual dilution of hyposmotic solutions affected C_m measurements and cell morphology. Osmolality reductions below 150mosM, from an isotonic osmolality of 280mosM, resulted in increasing C_m values in murine myeloma, hybridoma and fibroblasts. From 200 to 60mosM, C_m increased about 2 fold in each cell type. It was, therefore, concluded that these hypotonically stressed cells initially used microvilli membrane to overcome these shocks, as evidenced by the cell becoming spherical in shape, but once all this membrane had been exhausted, at approximately 200mosM, incorporation of membrane from internal stores was required. Placing the swollen cells back into their isotonic solution, thereby causing shrinkage, resulted in recovery of the cell's original size and C_m value.

Membrane tension

The hypothesis that membrane addition occurs at the plasma membrane due to increased tension and membrane retrieval occurs due to decreased tension has been hypothesized by a few researchers. Only recently, however, have membrane tension measurements been made (Dai and Sheetz, 1995a; Dai *et al.*, 1998). Bray (1984) first proposed that chicken dorsal root axons increased their surface area due to tension increases. Axonal outgrowth was observed when a

pulling force was applied to axons. Axons pulled at speeds up to 100μm/h increased in length up to 960μm for up to 24 hours. Membrane tensions were not measured in these experiments but along with the above experiments and the observation that neurites undergo an increase in volume during axonal elongation, lead to the conclusion that neurites grow due to applied mechanical tension and the growth occurred by membrane addition at the sites experiencing the tension. Zheng *et al.* (1991) expanded Bray's experiments by measuring the tension and rate of outgrowth in pulled axons. Chick sensory neuronal growth cones were attached to glass needles and pulled for 30-60 minutes at a constant tension followed by numerous pulling steps, which were always of a constant but increased tension for another 30-60 minutes. It was concluded that the relationship between the axonal growth rate and membrane tension is not linear but that an increase in tension is required for axonal growth since a decrease in tension resulted in axonal retraction. Zheng *et al.* (1991) further hypothesized that this form of tension dependent membrane addition could be mediated by axolemmal vesicles fusing with the membrane experiencing the increased tension. Zheng *et al.* (1991) also observed *de novo* neurite extension, as Bray (1984) had likewise observed, by pulling a cell, which had no previous neurite extensions, at its cell body margin. The *de novo* initiation of neurites required application of a tension above a certain threshold. However, these threshold tensions were similar to the tensions required for neurite extension. Observations of *de novo* initiated neurites after the pulling experiments, revealed that these structures developed normal growth cones capable of normal growth cone motility, neurite elongation and elaboration of normal microtubule arrays. This lead to the conclusion that neurite responses to tension differences was part of normal neuronal development.

Dai and Sheetz (1995a) observed membrane tension increases in chick dorsal root ganglia axons and interpreted from this that internally stored membrane was being added at the site of increased membrane tension. Membrane tension values were calculated by using laser optical tweezers to pull on lipid bilayer attached beads at the center of an axon, thus forming a membrane tether. The force required to keep the membrane tether at a constant length was measured and used to estimate the membrane tension, which is expressed in the units of mN/m. These experiments were designed to test if membrane would flow toward the high tension tether site as

indicated by a net movement of other, freely diffusing lipid-attached beads, on the axon towards the tether site. Net bead movements on the cell body side of the tether were almost undetectable, however, beads on the growth cone side of the tether moved towards the tether site. It was therefore concluded that in growing neurons, membrane addition occurs at the growth cone. In later papers, they proposed that membrane tension differences could control surface area regulation (Dai and Sheetz, 1995b), including tension differences brought about by osmotic swelling and shrinking (Sheetz and Dai, 1996).

Lin *et al.* (1995) also studied the relationship between membrane surface area regulation and tension with respect to swelling. Chick dorsal root ganglia neurons in a 50% diluted culture media were pulled at a constant tension. Lin *et al.* (1995) noted that neurons in the osmotically diluted saline grew 50-300% faster than the neurons being pulled in normal isotonic culture media. It was concluded that neurons were more sensitive to tension increases if placed in an osmotically diluted solution due to loosening up of the neuronal cytoskeleton.

Fink and Cooper (1996) observed that *Fundulus heteroclitus* embryos under mechanical deformation had increased rates of apical membrane turnover at sites under increased membrane tension. Mechanical membrane deformations were made by compressing embryos stained with fluorescently labelled lectins and lipids between two coverslips. Measurements of membrane tensions were not made but it was assumed that compression of the embryos resulted in membrane tension increases. Accelerated membrane turnover was observed as loss of fluorescent signal in the areas where the embryos bulged out or was of highest curvature. These experiments also revealed that tension increases at cell-cell contacts corresponded to areas with increased rates of membrane turnover.

A linear relationship between membrane tension and membrane surface area was measured in sarcolemmal vesicles shed from swelling rabbit psoas muscles (Nichol and Hutter 1996a). Membrane tension was recorded by deforming the vesicles by micropipette aspiration. Pipette suction was applied to make the vesicle, outside the pipette, spherical in shape. Subsequent suction or pressure increases caused an increase in the vesicle's membrane tension. Membrane tensions were recorded as the pressure steps were increased until vesicular rupture.

The maximum tension sustained before bursting was 12.4±0.2mN/m. This was calculated to represent a fractional increase in membrane area of 0.0260.005 or approximately 3%. It was concluded that the tension changes brought about membrane addition via vesicle membrane invaginations until vesicular rupture.

Visualizing surface area changes

Understanding how cells regulate their plasma membrane area is most often studied by exocytosis and endocytosis of vesicular membrane. Cytoplasmic vesicles and vacuoles have been observed and a few researchers have hypothesized that theses structures may be involved in surface membrane area regulation. Whether these vesicles and vacuoles are exocytosis and/or endocytosis mediated is not the issue here, only that they have been observed to bring about surface area changes. Lewis and Diamond (1976) observed that stretching of rabbit urinary bladder epithelial cells resulted in macroscopic and microscopic multicellular membrane folds being smoothed out, resulting in flattening of the apical membrane. Further stretching did not result in smoothing out of membrane invaginations, however, the epithelial cells were still able to withstand the stretching stimulus without rupturing. In a later study they hypothesized that it was the fusion of internal cytoplasmic vesicles with the apical membrane of the rabbit urinary bladder epithelial cells that could explain why the cells did not rupture during extensive stretching (Lewis and de Moura, 1982). To study if stretching did bring about fusion of internal vesicles with the surface membrane, the cell's C_m was measured. Stretching did bring about an increase in the cell's C_m, leading to the conclusion that perhaps it was calcium dependent exocytotic vesicles stimulated to fuse with the apical membrane which allowed the cells to undergo the stretching stimuli. However it was not verified if stretching caused intracellular calcium concentrations to increase. Steinhardt *et al.* (1994) hypothesized that calcium mediated membrane addition of cytoplasmic vesicles by exocytosis could be a fundamental cell survival mechanism found in all cells.

A number of other internal membranous structures have been observed, which may be internal membrane stores that could mediate surface area regulation. Cheng and Reese (1987) observed the recycling of lumenless membrane disks, about 1.5µm long, in chick tectal growth

cones under normal conditions (ie. no perturbation). These membranes were found stacked and as single disks interconnected by electron dense crosslinks. The single disks were positioned closer to or connected to the surface membrane in comparison to the stacked internal membrane arrays. They hypothesized that these lumenless membranes represented internal membrane stores which could be added to the neuron's growth cone to facilitate growth. Calculations revealed that these disks, stacked and single, accounted for 80% of the neuron's intracellular membrane. Observations of the recycling process revealed how this membrane was reinternalized. Coated pits were endocytosized from the membrane surface as coated vesicles, which subsequently were uncoated and fused to form vacuoles which eventually collapsed. It was postulated that the collapsed vacuoles would either replenish the stacked disks or be transported directly towards the plasma membrane as single disks, thereby eliminating the step of being incorporated into stacked disks and then only later being transported to the plasma membrane as a single disk.

Dailey and Bridgman (1993) observed vacuole-like organelles in rat superior cervical neurons. These vacuoles were found to be confluent with the surface membrane when cationized ferritin, which labels surface membrane and any membrane that was at the surface during the incubation, was found covering the surface membrane and also the vacuoles in question. These vacuoles were not elicited by a perturbation but spontaneously appeared and disappeared over a number of minutes. Before disappearing, however, all vacuoles were observed moving centripetally back into the growth cone at a rate of 1µm/minute. It was hypothesized that these vacuoles may participate in growth and/or retrieval of membrane at the neuronal growth cone. These vacuoles grew to a diameter of 150nm and greater and formed at the substrate and at the top of neurons (ie. where neuron is not attached to the substrate). The authors suggested that disappearance of the vacuoles represented fusion of vesicular membrane with the growth cone surface but could not rule out that the vacuole disappearance could be due to vesiculation of the vacuoles to smaller, unresolvable organelles, flattening of the vacuole to a lumenless membrane disk, as observed by Cheng and Reese (1987), or fusion of vacuolar membrane with intracellular membrane stores.

Surface area regulation, in a hyposmotic solution, has been observed in rat renal inner medullary collecting duct cells (Czekay *et al.*, 1994). Approximately 100 seconds after swelling,

these cells formed very small vesicles. The vesicles were observed due to the extracellular marker dye, fluorescein isothiocyanite-dextran, had been added to the swelling solution. These cells undergo regulatory volume decrease (RVD), a cellular mechanism that decreases or shrinks a cell's volume back or close to its original volume after initially undergoing swelling. Therefore the observed vesicles actually formed while the cells were shrinking. These researchers hypothesized that the swelling perturbations caused vesicular membrane to fuse with the cell's surface membrane. Then about 100 seconds after swelling, the time when RVD was being initiated, reinternalization of the surface membrane began in the form of vesicles. Surface area regulation appeared to occur very fast in these cells, but may be explained by the fact that inner medullary collecting duct cells contain high concentrations of organic osmolytes and therefore probably swell rapidly upon hyposmotic exposure. Therefore, initiation of RVD within a minute may be critical to the maintenance of proper cellular functioning and survival.

Krolenko *et al.* (1995) observed reversible vacuolation in frog skeletal muscle fibers. Removal of glycerol from the extracellular solution caused cell shrinkage and vacuole formation along the T-tubule system, surface membrane invaginations which penetrate deep into the muscle fiber. Addition of glycerol, which causes cells to swell, caused disappearance of the vacuoles. This phenomena could be repeated within the same muscle fiber a number of times by simply removing and readding glycerol. Larger vacuoles were observed to reform at the same locations within the fiber during cycling of glycerol removal and addition. Addition of RH414, a surface membrane dye, stained the muscle fiber's surface membrane which included the T-tubule system and the vacuoles formed due to glycerol removal. Addition of $DiOC_6$, an intracellular membrane dye, did not however stain the fiber's T-tubules or vacuoles. It was therefore concluded that the vacuolar membrane arose from the fiber's surface membrane. These vacuoles formed over 2-10 minutes, were able to grow in size by fusing with other vacuoles, ranged in size from 0.4-1.5μm in diameter, and failure to disappear was observed in some fibers that had been cycled through a number of vacuolations and devacuolations. Overall, it was speculated by these authors that reversible vacuolation of the T-tubule system may provide additional understanding of skeletal muscle volume regulation, membrane fusion and trafficking.

Aplysia neurons were hypothesized to use membrane invaginations found at, but occluded from, the membrane surface as internal membrane sources during swelling (Fejtl *et al.*, 1995). Upon swelling, the connection occluding the invaginated membrane would be broken, therefore, allowing this membrane to be added and flattened out at the membrane surface. Likewise, during shrinking the excess surface membrane would be pulled back into membranous invaginations. Neuronal membrane invaginations, neuronal surface membrane area increases and decreases, due to swelling and shrinking, were observed, however, quantitative changes of the membrane invaginations due to swelling and shrinking were not measured, so this is purely speculative (Fejtl *et al.*, 1995).

The possible internal membrane stores used during surface area regulation are numerous, as the above literature review testifies. Other structures which may be internal membrane stores include membrane bound organelles. Many of these cellular organelles have been observed to transform into membrane tubules, which extend into the cell periphery, move along microtubules and fuse with other membrane tubules creating polygonal membrane networks. The endoplasmic reticulum (rough and smooth) (Terasaki *et al.*, 1984 and 1986; Dabora and Sheetz, 1988; Lee and Chen, 1988; Allan and Vale, 1994), the Golgi apparatus (Allan and Vale, 1994; Cooper *et al.*, 1990; Lippincott-Schwartz *et al.*, 1990 and 1991; Wood *et al.*, 1991) and endosomes (Swanson *et al.*, 1987; Hopkins *et al.*, 1990) have all been observed to form these tubule projections. These projecting structures have been observed *in vivo* and *in vitro*, but whether any part of the tubular system can communicate with the surface and bring about changes in surface area remains to be determined.

Morphological changes such as changes in cell size and shape may also mediate surface area regulation. Murine myeloma, hybridoma and fibroblast cells pull in their microvilli, extensive membrane structures used in nutrient absorbance, during a moderate hyposmotic perturbation (Sukhorukov *et al.*, 1993). Even when faced with a more severe swelling shock these cells did not rupture. It was postulated, therefore, that one of two processes must have occurred, since the cell's membrane capacitance also increased during swelling. Either there was 1) instantaneous production and transport of "extra" membrane or 2) reutilization and transport of internal membrane

stores to the plasma membrane, both examples of membrane area regulation.

Plant protoplast surface area regulation

Evidence of cells undergoing surface area regulation has been studied more extensively in plant protoplasts (plant cells that have had their cell walls removed, therefore providing direct access to the plasma membrane).

In 1980, Jensen and Palta presented evidence that refuted the long held hypothesis that protoplast surface membrane folded upon shrinkage. Electron micrographs of inner epidermal onion cells magnified up to 150 000 times did not reveal any surface membrane folds. They concluded, therefore, that during osmotic shrinkage, membrane surface area was reduced and did not constitute as part of the surface membrane since it had been internalized into the cell.

As early as 1981 tension experiments with rye leaf protoplasts (*Secale cereale* L. cv. Puma) determined that tensions larger than 4 mN/m resulted in membrane rupture, whereas membrane tensions smaller than this produced increases in the protoplast's surface area (Wolfe and Steponkus, 1981). Similar to animal cells, plant protoplast membrane areas can only, from a resting membrane tension of about 100μN/m, stretch by 2%. Thinning of the lipid bilayer could not account for the 15% increase in protoplast membrane area during increases in tension up to and including 1mN/m. It was therefore proposed that larger changes in membrane area, which appeared to be controlled by membrane tension changes, must have occurred due to exchange of membrane between an intracellular membrane reservoir and the surface membrane. The structure which served this purpose was unknown but it was proposed that it could include internal vesicles or sub-microscopic membrane bucklings or foldings; even though Jensen and Palta (1980) had shown that membrane folds are not observed in onion protoplasts. Gordon-Kamm and Steponkus (1984) confirmed that plant protoplasts do not fold their membrane during shrinking perturbations, lending support to the internal membrane source being cytoplasmic vesicles. It was hypothesized that the chances of stressed protoplasts surviving membrane expansion forces depend on the amount of material available in the reservoir and the rate at which this excess membrane could be incorporated into the plasma membrane.

Subsequently these researchers extended their observations in rye leaf protoplasts (Wolfe *et al.*, 1985). Protoplast membrane area increases were generated by applying pressure. The known pressure step, the radius of the protoplast outside the pipette and inside the pipette allowed for membrane tension calculations. Membrane tension increases ranged from 200μN/m to 5mN/m for 2 minutes. Between 2 and 5mN/m, membrane area dramatically increased as the tension increased. These area increases were interpreted as tension-dependent incorporation of membrane at the membrane surface. This hypothesis was extended to when membrane tensions fell to zero; membrane would become flaccid and, therefore, membrane would be retrieved from the surface and transferred to the membrane reservoir. These experiments further supported the hypothesis that incorporation and retrieval of reservoir membrane at and from the surface membrane was tension-dependent.

Rye leaf protoplast area was further characterized during swelling (Wolfe *et al.*, 1986). The protoplast's membrane surface tension increased rapidly to a maximum and slowly decreased over about a minute of swelling. All protoplasts ruptured when placed in distilled water from an initial isotonic solution of 0.53Osm, whereas 70% of protoplasts survived a dilution of 0.53 to 0.34Osm. Of all the protoplasts analyzed, the larger osmotic dilutions, which resulted in faster membrane expansions, produced the highest membrane tensions; the largest membrane tensions recorded ranged from 3.5-4.8mN/m. It was therefore suggested that the membrane tension during osmotic expansion was determined by the elasticity of the membrane and by the rate at which reserve membrane could be added to the surface in order to overcome the increased tension. It was concluded that the direction of membrane transfer between internal membrane stores and plasma membrane was controlled directly by membrane tension. This was extended to the hypothesis that if the tension dropped below a critical value, surface membrane would become flaccid resulting in vesicle formation. If the critical tension value was exceeded, surface membrane would become stretched resulting in addition of reserve membrane material.

Research on *Chenopodium album* verified that vesicles form when protoplast membrane tension is decreased (Wartenburg *et al.*, 1992). During shrinking, which causes a decrease in membrane tension, vesicles formed within the cytoplasm. Vesicles, ranging in size from 2-3μm,

were observed by addition of a fluorescent extracellular dye in the shrinking solution. Upon swelling of the shrunken protoplasts, the fluorescent vesicles disappeared. Therefore, in plant protoplasts membrane transfer between internal membrane stores and the surface membrane is tension dependent and vesicle formation can be used as an indicator of surface area decrease.

By 1993 it was well accepted that membrane exchange between the protoplast surface membrane and an intracellular membrane reservoir depended upon plasma membrane tension changes mediated by membrane bound vesicles (Kell and Glaser, 1993). This exchange of membrane could occur due to any type of mechanical stress (ie. stretching and releasing of membrane, which includes osmotic swelling and shrinking). This tension-dependent addition and retrieval of membrane is thought to be continuous over the plant cell's life with the rate of membrane incorporation and removal being equal at the membrane's resting tension. But as observed by Wartenburg *et al.* (1992), if the rate of membrane retrieval exceeded the rate of incorporation, vesicle formation occurs. Both processes, membrane incorporation and retrieval in plant protoplasts, appear to be dependent on the intracellular and extracellular calcium concentration. Whether membrane incorporation at the protoplast surface is mediated by calcium dependent exocytosis is still inconclusive, though membrane retrieval occurs by endocytotic-like vesiculations (Kell and Glaser, 1993).

OSMOMECHANICAL APPROACHES USED TO STUDY SURFACE AREA REGULATION

Membrane capacitance

Membrane capacitance studies were performed using *Lymnaea stagnalis* molluscan neurons to study if neuronal C_m varied during osmomechanical perturbations (Wan *et al.*, 1995). Neurons were swollen in hyposmotic NS and returned to NS to bring about shrinkage. Swelling caused an increase in the neuron's size and C_m; neurons left to swell for 1 hour underwent an area increase of about three fold. Similarly, shrinkage brought about a decrease in neuronal size and C_m. These experiments therefore revealed that *Lymnaea* neurons add membrane during swelling and retrieve membrane during shrinking. The relationship between C_m and surface area closely corresponded to 0.7μF/cm^2. The experiments were repeated to determine if C_m depended upon

an influx of extracellular calcium, which would stimulate exocytosis. Omitting calcium, elevating magnesium (from 2 to 5.5mM) and addition of the calcium chelator EGTA (0.1mM) to both the swelling and shrinking solutions revealed that the relationship between C_m and surface area again corresponded to 0.7μF/cm^2, therefore ruling out that the change in C_m was dependent upon the $[Ca]_{ext}$. Also during these experiments, one-third of the rounded, swollen *Lymnaea* neurons exhibited prolonged writhing of their peripheral cell body regions. Writhing was defined as a cycle of bulging and retracting of membrane areas occurring two or more times at the same cellular region (Wan *et al.*, 1995). Single bulge/retraction cycles were not scored as writhing, suggesting that repeated writhing required contractile restorative forces. Incubation of the neurons in 1mM NEM, a myosin ATPase inhibitor, eliminated the writhing behaviour, suggesting that the cortical cytoskeleton participates actively to limit swelling.

Membrane tension

Membrane tension experiments were initiated to test the hypothesis that a change in membrane tension is the signal and effector used in *Lymnaea* neurons to regulate their surface area (Dai *et al.*, 1998). Membrane tethers were first pulled from neurons. Throughout the experiments, the tethers were kept at a constant length of 15μm, while changes in the membrane tether force were measured during swelling in 50%NS for 4 minutes followed by return to NS. Tether force measurements allowed for the calculation of membrane tensions. Membrane tension increased from 0.04 to 0.42mN/m after 30 seconds of swelling and then relaxed to a steady state swollen membrane tension of 0.12mN/m after several minutes. Upon shrinking the membrane tension dropped to 0.02mN/m, coincident with VLD formation (see below). Over time the tension returned to control levels as VLDs recovered. The swelling induced membrane tension increase from 0.04 to 0.12mN/m is about 2 orders of magnitude less than the known membrane lytic tension for *Lymnaea* neurons (ie. ranges from 5-12mN/m) (Morris and Horn, 1991; Wan *et al.*, 1995). Therefore the relatively low swollen neuronal membrane tensions and the C_m responses are consistent with the hypothesis that membrane tension gradients may be physical feedback signals used to bring about membrane area increases and decreases.

Vacuole-like dilations (VLDs)

Shrinking *Lymnaea* neurons invaginate membrane at their substrate adherent surface (Mills and Morris, 1998); these invaginations have been termed vacuole-like dilations or VLDs (fig 2.1) (Reuzeau *et al.*, 1995). VLDs were first observed when swollen *Lymnaea* neurons were shrunk by being placed in their normal culture media or normal saline (NS) (Reuzeau *et al.*, 1995). VLDs have also been observed in *Aplysia* bag cells, cultured rat hippocampal neurons and glia, dorsal root ganglia neurons (Reuzeau *et al.*, 1995) and skeletal muscle myotubes (see chapter 4 and appendix). VLDs begin to form at the neuron's substrate less than one minute after being placed in NS and expand into the cell interior, reaching a diameter of about 10μm. Whether VLDs enlarge from a pre-existing structure is unknown since VLDs suddenly appear during shrinking. The smallest VLDs that could be measured were about 0.5μm in diameter. It was calculated that for one VLD to grow from 0.5μm to 10μm in diameter, a minimum of 157μm^2 of membrane would be required, assuming the VLD is shaped like a sphere. VLDs are viewed as the excess membrane, that was at the surface, that has not yet been reincorporated back into the neurons' internal membrane stores. Exocytotic and endocytotic vesicles would be the natural assumptive structures which could explain how excess membrane is transferred to the surface and then retrieved. However, endocytotic vesicles are approximately 60 times smaller (Alberts *et al.*, 1989) than VLDs, therefore ruling this process out. Varying extracellular calcium concentrations had no affect on VLD formation, therefore eliminating the idea that VLD formation depends on an extracellular calcium influx. The possible role of calcium release from internal calcium stores, thereby mediating exocytosis, is examined in chapter 2.

The osmotic perturbations that were first used to elicit VLDs consisted of swelling the neurons in NS made hyposmotic by dilution in distilled water for a number of minutes, followed by shrinking the neuron in NS. The swelling time and the extent to which the NS was diluted was important. Swelling for only 1-2 minutes did not result in VLD formation upon shrinking unless the swelling solution was or close to distilled water. The longer the neurons were left in the swelling solution resulted in an increased number of VLDs. Initially solution exchanges were done in 35mm

Falcon dishes which required several solution changes to ensure the previous solution had been completely exchanged. It was with this apparatus that VLD characteristics were first described using distilled water as the swelling solution (Reuzeau *et al.*, 1995). However, it was later discovered that if the neurons were plated onto large, glass coverslips and assembled into flow through chambers, by adding and adhering another smaller top coverslip, that less solution and fewer solution changes were required to more efficiently induce VLD formation. VLD formation also occurred if the neurons were placed directly into 3.5xNS, a hyperosmotic solution made by the addition of sucrose. No VLD differences were observed whether neurons were 1) swollen then shrunk or 2) directly placed into a hyperosmotic solution. Chemical shocks such as changing or depleting ion concentrations in the swelling solutions had no effect on whether VLDs formed or not. Instead mechanical shocks that brought about shrinkage were necessary to induce VLD formation.

VLD reversal and recovery

Disappearance of VLDs (ie. VLDs no longer visible) occurred by two different mechanisms: VLD reversal or VLD recovery. VLD reversal causes VLDs to disappear by neuronal reswelling, whereas, VLD recovery allows the neuron's internal motors to reprocess the VLD membrane. Neurons undergoing VLD recovery are left in the shrinking solution which caused VLD formation, whereas VLD reversal entails reswelling of the shrunken, vacuolated neuron. VLD recovery ranges from 30 minutes to several hours and only during this time is VLD fusion observed between two or several closely positioned VLDs, thereby producing larger VLDs. As recovery progressed VLDs however underwent what was observed to be an intense period of turmoil or motor activity, which brought about smaller VLDs. VLDs were being kneaded, pushed, constricted and severed during this time. Pre-incubation of molluscan neurons in a variety of cellular inhibitors revealed that VLD recovery depended upon a number of different cellular structures, but had no effect on VLD formation or reversal. Incubation in brefeldin A (disrupts post-Golgi membrane trafficking), cytochalasin (inhibits actin polymerization), or NEM (inhibits myosin ATPases) had no effect on VLD formation or reversal. However, VLD recovery was inhibited in any neuron that has been pre-incubated in one of the above inhibitors. Coincident with inhibition of recovery was blocking or

impairment of the turmoil experienced by recovering VLDs. VLD formation, reversal and recovery were, however, independent of the microtubule network, as observed in neurons pre-incubated in the microtubule depolymerizing agent nocodazole.

Observations of repeated VLD formation, which occurs by reswelling and reshrinking of vacuolated neurons, revealed that VLDs form at the same discrete sites or substrate locations. Neurons reswollen and then reshrunk, 120 minutes into VLD recovery, likewise reformed VLDs at the same discrete sites. Repeated VLD formation and reversal was also observed in neurons that had underwent swelling and shrinking in low extracellular calcium (ie. 0.5μM).

During recovery some VLDs were able to pinch off from the substrate by constricting the invaginated membrane at their membrane-substrate adherent site, therefore becoming true vacuoles. The recovery of individual VLDs occurred in two ways: by fading away or shrinking in size (Reuzeau *et al.*, 1995). VLDs which faded were initially seen as discrete structures but over time slowly faded, whereas the shrinking VLDs over time became smaller in size. It has been postulated that it is the shrinking VLDs which may pinch off from the substrate (Reuzeau *et al.*, 1995; Mills and Morris, 1998). Confocal fluorescent microscope studies of VLDs retaining the fluorescent extracellular dye, rhodamine-dextran 3000, after the dye had been washed out, were defined as the VLDs which had pinched off from the substrate. VLDs without extracellular dye were therefore interpreted to be VLDs which had not pinched off from the substrate. Further confocal studies using rhodamine-dextran 3000 revealed that there were no initial VLD-like structures within these neurons. Rhodamine-dextran 3000, added to NS and to the swelling solution, was not taken up into the neuronal interior. Only upon shrinkage, which caused VLD formation, was the VLD lumen contiguous with the fluorescent extracellular solution.

Labelling of the neuron's plasma membrane with DiI, a fluorescent lipid dye, revealed that before and during swelling only the plasma membrane fluoresced. Upon shrinkage the plasma membrane and the VLDs, which formed due to shrinkage, fluoresced. This lead to the conclusion that the VLD membrane is surface membrane which has invaginated into the cell. Some DiI stained VLDs have been observed to pinch off from the substrate during recovery (Reuzeau *et al.*, 1995).

INTRACELLULAR CALCIUM, ACTIN AND THE SPECTRIN SKELETON'S INVOLVEMENT IN SURFACE AREA REGULATION

I have investigated three aspects of surface area regulation and membrane tension. It was first necessary to determine if the swelling and shrinking perturbations affected intracellular calcium in a way that could also directly affect exocytosis. The first hypothesis tested was: osmotic swelling and shrinking of *Lymnaea* neurons produces no change in intracellular calcium.

The last two sets of experiments were designed to determine if key elements of the membrane cytoskeleton were affected by osmotic perturbations in a way that might implicate them in surface area regulation. VLD formation and recovery was used here as an indicator that surface area regulation was occurring. In the first set experiments, F-actin was investigated. Since previous investigations using cytochalasin B (inhibits actin polymerization) implicated F-actin in VLD recovery (Reuzeau *et al.*, 1995), we tested the following hypothesis: the cellular distribution of F-actin changes during VLD formation and recovery.

The membrane skeleton was also studied with respect to VLDs. In order for the spectrin skeleton to play a role in VLD formation, it must have some association with VLDs. We, therefore, tested the hypothesis: that VLDs are lined by the spectrin skeleton.

CHAPTER 2: NEURONAL SWELLING AND SURFACE AREA REGULATION: ELEVATED INTRACELLULAR CALCIUM IS NOT A REQUIREMENT

INTRODUCTION

It is widely recognized that cells regulate their volume in response to osmotic perturbations, metabolic loads and cytomorphological changes. Much less consideration is given to the fact that cell surface area too must be continually regulated. Since surface area and cytoplasmic volume changes are not linearly related, we presume that regulatory mechanisms for surface area and for volume use distinct feedback systems. For surface area regulation, membrane tension changes may be the parameter that signals the need for changes in surface area (Zorec and Tester, 1993; Reuzeau *et al.*, 1995; Dai *et al.*, 1998). This would constitute mechanosensitive membrane disposition.

Molluscan neurons are well suited for studying mechanosensitive membrane disposition because their large size facilitates the monitoring of many parameters. We showed that osmotically swelling *Lymnaea* neurons are astonishingly compliant, increasing their apparent surface area threefold over an hour (Wan *et al.*, 1995). Robustness under osmomechanical stress thus relies partly on an ability to recruit membrane during swelling. It is likely that this compliance is normally used not to deal with osmotic stresses but for accommodating cell morphology changes in response to varying mechanical stresses (Chen *et al.*, 1997; Morris *et al.*, 1997; Van Essen, 1997).

The existence of mechanosensitive disposition of membrane between the cell surface and internal membrane stores is suggested by various lines of evidence (Zorec and Tester, 1993; Dai and Sheetz, 1995a; Wan *et al.*, 1995; Reuzeau *et al.*, 1995; Fink and Cooper, 1996; Dai *et al.*, 1998; Morris *et al.*, 1997). Calcium-mediated exocytosis (Okada *et al.*, 1992) and endocytosis, well-known processes by which cells alter plasma membrane area, may be modulated by tension. However, both rely on finely coordinated cellular chemistry and cytoarchitecture which could be compromised by stresses that create an urgent demand for surface area increase (ie. abrupt exposure to anisosmotic media or to large mechanical perturbations). Area increases triggered directly by the increased membrane tension might be more failsafe.

In osmotically perturbed molluscan neurons (fig 1.2), capacitance increases and decreases

are accompanied by apparent changes in surface area (assuming a specific membrane capacitance of ~0.7-1μFcm^{-2}). Moreover, swelling and shrinking not only alter total plasma membrane area, they cause measurable membrane tension increases and decreases (Dai *et al.*, 1998) and elicit visually dramatic rearrangements of membrane (Reuzeau *et al.*, 1995). Less than a minute after returning to isosmotic normal saline, previously swollen neurons develop vacuole-like dilations (VLDs) that can be 10μm across. In neurons made to reswell, the VLDs rapidly reverse (disappear), as if their membrane is drawn back to the general plasma membrane surface. Membrane tension variations in differentially adhesive regions of membrane are probably instrumental in VLD dynamics. VLDs are initially invaginations at the substrate but some become fully internalized as true vacuoles (Mills and Morris, 1998). We interpret eventual VLD vacuolation as a sign of particularly vigorous surface area regulation engendered by episodes of swelling then shrinking.

Swelling neurons may recruit lumenless infoldings of membrane to the surface. Electron micrographs of cultured *Aplysia* neurons reveal such infoldings (Fejtl *et al.*, 1995) that, by their ultrastructural appearance, are unlikely to contribute measurable capacitance except when opened out at the surface. Fejtl *et al.* (1995) postulated that these membrane invaginations constitute "hotspots" or sites of reserve membrane that could be used for surface area increases.

Osmotically-induced capacitance changes and VLD dynamics occur with equal facility in normal and in very low (0.5 μM) $[Ca]_{ext}$ (Reuzeau *et al.*, 1995; Wan *et al.*, 1995). Swelling neurons increase their capacitance even with EGTA in the cytosol (Wan *et al.*, 1995). While this does not rule out the possibility that swelling stimulates exocytosis, it suggests that membrane tension may trigger the surface area increases.

Vacuole-like membrane has been linked to cell surface area regulation in various other neuronal preparations (Cheng and Reese, 1987; Fujimoto and Ogawa, 1989; Dailey and Bridgman, 1993) and in skeletal muscle (Krolenko *et al.*, 1995). Cheng and Reese (1987) showed that lumenless membranous disks close to the plasma membrane in chick growth cones are part of an internal membrane pool for augmenting growth cone surface area. Dailey and Bridgman (1993) observed vacuole-like organelles confluent with the surface in rat superior cervical ganglia neurons;

they appeared spontaneously then disappeared several minutes later, as if they were participating in surface membrane recycling. Based on non-invasive capacitance measurements, Sukhorukov *et al.* (1993) postulated that internal membrane reserves are instantaneously available to the plasma membrane when myeloma, hybridoma and fibroblast cells swell osmotically. In frog muscle cells, Krolenko *et al.* (1995) observed vacuolar dilations which, like *Lymnaea* VLDs, formed in shrinking cells and readily reversed upon swelling.

Here our focus is on events during swelling. Specifically we ask if, over the time frame used to elicit VLDs, sustained swelling-induced cytosolic [Ca] increases occur which might be capable of driving exocytotic membrane area increases. We find that on average (but not in all neurons) swelling is accompanied by a small rise in cytosolic calcium, but never to a level sufficient to stimulate exocytosis. We also show that neurons can swell then shrink and make VLDs under various conditions of enforced low $[Ca]_{int}$. Swelling neurons need not, we conclude, rely on calcium-driven exocytosis as a means to avoid rupture. Membrane tension therefore continues to be a good contender as a primary signal for swelling-induced recruitment of membrane from internal stores. Beyond enabling neurons to adjust during osmomechanical perturbations, tension-mediated membrane disposition could be important during passive stretch of neurites and during their growth and retraction.

METHODS AND MATERIALS

Cells, solutions and flow-through chambers

Lymnaea stagnalis colonies were raised at the Loeb Research Institute Animal Care facility at the Ottawa Civic Hospital. They were kept in aquariums at a regulated water temperature of 26°C. Snails were feed romaine lettuce and fresh leaves were added every 2 days to the top of the water. Egg sacs which adhered to the sides of the aquarium were kept in the adult tank until the eggs hatched. Hatchlings were then removed from the adult tank and placed into a juvenile tank until becoming adults.

Circumesophageal ganglia were dissected from the adult snails by first removing the outer shell and pinning the snail body to a dissecting board. An incision perpendicular to the mouth was

first made, the mouth was then pulled out to reveal the circumesophageal ganglia. The ganglia were then cut away from its surrounding tissue and placed immediately into a plastic 35mm Falcon dish (Becton Dickinson, Lincoln Park, NJ) containing normal saline (NS). The NS solution contained (in mM) 50 NaCl, 1.6 KCl, 3.5 $CaCl_2$ (or 0.5μM $CaCl_2$for low Ca experiments), 2.0 $MgCl_2$, 5.0 HEPES, 5.0 glucose, pH adjusted to 7.6 with 1M NaOH. Gentamicin was added to 50μg/mL. Osmolarity was 126mOsm as determined by the Advanced MicroOsmometer (model 3MO).

Individual ganglion were separated and excess tissue was removed using a number 10 scalpel before being digested for 30 minutes in reduced calcium (0.5mM $CaCl_2$) NS with 0.25% type XIV protease (Sigma, St. Louis, MO). Ganglia were then washed twice in NS containing 3.5mM calcium. Ganglia were then either plated or stored in NS in the fridge for up to 1 week.

Neurons were plated on large sterile coverslips (24x60mm, VWR Scientific, Media, PA) and cultured for 2-3 days at room temperature as follows: sterile silicone grease (Dow Corning, Midland, Michigan) was pipetted by syringe into a large oval ring on the coverslip. NS was added and neurons from one ganglion were teased out with forceps and allowed to settle and adhere to the untouched glass surface. Coverslips were placed in large round glass petri dishes which were then placed into a square glass dish. Coverslips were kept moist and sterile due to wet paper towels had been placed at the bottom of the each petri dish which was then covered with crinkled aluminum foil. Two petri dishes were then stacked into one square glass dish, which had also been lined with wet paper towels, and covered with foil for the 2-3 days needed for the neurons to grow at room temperature.

Shortly before an experiment, 22x22mm glass coverslips (number 1) (VWR Scientific, Media, PA) were pressed on to the grease ovals on the larger coverslips, leaving a 100-150μm gap between coverslips. Excess solution and grease were removed and small dots of molten soft wax (equal parts lanolin, paraffin wax and petroleum jelly) were placed at the 4 corners of the small coverslip to secure the gap. This created a flow-through chamber which was operated by adding solutions (150-250μL) by pipette tip at one edge and wicking through the chamber using small strips of filter paper (Whatman, Maidstone, UK) at the other open edge. Solution changes were completed in about 30 seconds. Experiments were carried out at room temperature.

We previously determined (Dai *et al.*, 1998) that, with flow-through chambers, swelling for 4 minutes in 0.5xNS was sufficient to elicit VLDs in all neurons on return to NS and to generate measurable membrane tension changes. In the present experiments, we used even more extreme swelling conditions, namely 0.25xNS for 4 or 5 minutes (as noted), in order that $[Ca]_{int}$ changes, if any, would be exaggerated.

Swelling solutions were made by simple dilution of NS. The [Ca] of NS was varied, as noted, but usually contained 3.5mM or 0.5μM calcium, and the respective 0.25xNS solutions had 0.9mM calcium or 0.13μM calcium. The low (0.5μM) calcium NS was like NS except that 0.5mM calcium and 1mM EGTA (Sigma, St. Louis, MO) were used, yielding a free calcium concentration of 0.5μM (Reuzeau *et al.*, 1995).

When cells were loaded with 30μM BAPTA-AM (in a final concentration of 0.3% DMSO) (Molecular Probes, Eugene, OR) 0.5μM calcium NS was used. In some experiments, cells were simultaneously loaded in 30μM BAPTA-AM and 2μM FURA-2-AM; in this case 3.5mM calcium NS was used. Stock solutions for the FURA-2 calibration curve were (a) NS with 2mM EGTA and zero calcium and (b) 1M $CaCl_2$. Five 1mL aliquots of (a) were prepared; to the first, no calcium was added therefore yielding a 0μM calcium saline. To the second, 1.59 μL of (b) was added, yielding a free [Ca] of 0.1μM. To the 3rd, 4th and 5th aliquots were added 1.77, 1.90 and 2.00 μL, yielding 0.2, 0.5 and 5.0μM free calcium as determined by Fabiato and Fabiato (1979); the stability constant for EGTA at 20°C and pH 7.6 (3.819) was assumed.

Testing for VLD formation

Since the ratio imaging system did not allow simultaneous visualization of cell morphology (specifically, VLD formation and reversal) and measurement of $[Ca]_{int}$, at the end of the FURA experiments it was recorded if VLDs had occurred. VLD dynamics were checked in parallel experiments, using the test solutions on FURA-2-loaded, BAPTA-loaded and/or calcium-permeabilized cells. The flow-through chambers and the solutions were the same as for the $[Ca]_{int}$ measurements, and FURA-2-loading was identical (see below). What we took note of was whether VLD formation occurred, was reversible, and was repeatable at discrete locations (see fig 2.1), as

in previous work (Reuzeau *et al.*, 1995) without FURA-2.

In these experiments images were recorded with a Sony CCD video camera and JVC BR-S601 MU video recorder, using an Olympus IMT-2 microscope fitted with Hoffman modulation contrast optics (40x objective). Subsequently, taped videoframes were digitized by a Data Translations 3155 frame grabber using Image Tool software. Digitized images were processed in Corel Photo Paint and Corel Draw.

FURA-2 measurements of $[Ca]_{int}$

About 2 hours prior to an experiment, neurons in flow-through chambers were loaded for 45 minutes with 2μM FURA-2-AM (Molecular Probes, Eugene, OR) in 0.1% DMSO plus 0.02% Pluronic F-127 (Molecular Probes, Eugene, OR), a dispersing agent which facilitates -AM ester solubilization. At 45 minutes and again at 75 minutes chambers were washed with NS (5x50μL), enabling neurons to rid themselves of untransformed FURA-2-AM (intracellular FURA-2 is generated when endogenous cellular esterases cleave the -AM) either by hydrolysis to FURA-2 or by washout. A field with one or more neurons bearing a lamella was located (VLDs are easier to see in thin extensions than under the soma). The objective was focused not at the substrate, but at a rounded region of the cell body and the focal plane was maintained throughout. Unless noted, pairs of fluorescent images (at two excitation wavelengths - see below) of the field were generated every 30 seconds; each image was the average of 32 frames collected at 30 frames/seconds for a total duration of 1.07 seconds. A background image pair was taken at the end of each experiment in a field of view containing no neurons. Neurons exhibiting abnormally high resting $[Ca]_{int}$ were not used in the experiments.

$[Ca]_{int}$ was measured ratiometrically with a quantitative imaging fluorescence videomicroscopy system built around a Zeiss Axiovert inverted epifluorescence microscope. Fluorescence excitation was via a grating-type monochromator (Photon Technologies International, New Brunswick, NJ) with an electronic shutter (Uniblitz, Vincent Associates, Rochester, NY). Images were detected with a solid-state video camera (CCD72, Dage-MTI, Michigan City, IN) fitted with a Geniisys image intensifier (Dage-MTI). The emission wavelength was selected by a 510nm

bandpass filter. All of these were controlled by *Isee* and *dsp/os* software and imaging hardware (Inovision Inc., Durham, NC) running on a Silicon Graphics Indigo2 (R4400, Extreme Graphics) Unix Workstation (Silicon Graphics, Mountain View, CA). The excitation wavelengths were 350nm (for detecting calcium-bound FURA-2) and 380nm (for calcium-free FURA-2). For a circular area covering most of the soma of each neuron (preswelling), the ratio of the intensity at 350nm divided by that at 380nm was calculated pixel-by-pixel after background subtraction using the Inovision *Isee* software, and the mean ratio was recorded. A circular area just less than the neuron's diameter was chosen due to during solution changes the neurons position changes slightly. The quantitized areas were representative of the entire ratio images of the neurons, which were very homogeneous in appearance. Occasionally, however, it was evident from ratio images that a neuron had moved between data acquisition at 350 and 380nm; striking crescents of low and high intensity appeared at opposite edges of the neuron. Data from these neurons were discarded.

Calibration of FURA-2 as a free [Ca] indicator in *Lymnaea* neurons

Instead of calibrating by determining emission ratios only for extreme low ("zero-calcium") and extreme high (saturating) calcium levels as is normally done (Grynkiewicz *et al.*, 1985), we calibrated FURA-2 in neuronal cytoplasm (fig 2.2) over a range of extreme and intermediate concentrations. Thirty minutes before the experiment, 20μM of the calcium ionophore 4-bromo-A23187 (a non-fluorescent form which therefore does not interfere with the FURA-2 emission fluorescence) in 0.6% DMSO was added to the series of calibration solutions as described. Neurons were exposed to the 0μM calcium NS/A23187 solution for 25 minutes. Fluorescent image pairs were taken at the end of this time and then neurons were exposed for 10 minutes each to successively higher calcium/A23187 solutions, with image pairs obtained at the end of each incubation. Background fluorescent images taken at the end of each experiment were subtracted before analysis. The calibration curve for $[Ca]_{int}$ was constructed by plotting the fluorescence ratios versus free [Ca] and fitting to an arbitrary polynomial equation using a non-linear least squares fit. In essence, this is a computer-assisted "by eye" fit. The fitted line was used to read-off interpolated [Ca]s. To verify the accuracy of our *in vivo* calibration, the process was repeated months apart by

different workers, using newly made solutions. The *in vivo* half-maximal ratios for FURA-2 from the calibration curves of the two workers were at [Ca] 0.13 and 0.14μM.

Results are presented as mean values ± SE (n= number of experiments). Paired t-tests were used to test for statistical significance of changes in $[Ca]_{int}$ between experimental conditions. A p value of less than 0.05 was used to indicate statistical significance.

RESULTS

VLDs: a phenomenon that occurs at submicromolar Ca_{ext}

By demonstrating VLDs elicited in the same neuron for both normal and low calcium media (see methods regarding osmotic dilutions), figure 2.1 confirms that $[Ca]_{ext}$ does not affect the ability of neurons to form VLDs. Osmotic perturbations (swell, shrink, swell, i.e. 0.25xNS, 1xNS, 0.25xNS) were first done with normal calcium then repeated with low calcium solutions. VLDs formed when swollen neurons shrank (in NS) and reversed during the second swell (0.25xNS). During the low calcium repeat runs, VLDs formed at the same sites as previously, reversed with a second swelling and finally, reformed upon a second reshrinking (in low calcium NS).

Clearly, VLD dynamics - formation, reversal and reformation at discrete sites - are not dependent on $[Ca]_{ext}$ levels, but even when swelling in 0.13μM Ca_{ext}, free $[Ca]_{int}$ may become elevated as a result of swelling-induced release of calcium from intracellular stores. The following experiments address this possibility.

Does $[Ca]_{int}$ change during swelling and shrinking?

FURA-2-loaded cells were used to measure $[Ca]_{int}$ during swelling. In preliminary trials using Hoffman Modulation optics (which emphasize membranous structures) Ian Slotin confirmed that FURA-2-loaded neurons retain their ability to repeatedly make VLDs, as above. For the calcium-monitoring experiments below, inspection of the cells by transmitted light at the end of the experiment usually revealed the VLDs that had formed, but the optics were not set up for transmitted light, so during fluorescence image acquisition, only fluorescence imaging was done.

As shown in figure 2.3a, $[Ca]_{int}$ for *Lymnaea* neurons in NS prior to any osmotic insult was

96± 9nM (n=19), in keeping with values for other molluscan neurons (40nM in *Helix aspersa* (Kennedy and Thomas, 1996), 90nM in *Helix pomatia* (Kostyuk *et al.*, 1989), 10-100nM in *Helix pomatia* (Muller *et al.*, 1993)). Neurons were then swollen in 0.9 mM $[Ca]_{ext}$. Of 19 neurons tested, 11 showed a $[Ca]_{int}$ increase, 4 did not change and 4 decreased; the swollen neuron average was 105±11nM, amounting overall to an 11±0.5% increase over normal $[Ca]_{int}$ (p=0.016, n=19, within-neuron paired t-tests). After 5 minutes of swelling, neurons were returned to NS. At this point, they shrank, made VLDs and their average $[Ca]_{int}$ was 100±10nM, with 3 increased, 7 decreased, 9 unchanged (a 9±0.3% decrease which was not significant, p=0.08). Pairwise t-tests (n=19) also showed that $[Ca]_{int}$ in NS before swelling and in NS after the swelling episode were statistically indistinguishable (p=0.05). Thus, with $[Ca]_{ext}$ at 0.9-3.5mM during osmotic perturbations, there were at best marginal increases in Ca_{int}.

In the above experiments monitoring of the $[Ca]_{int}$ during the solution changes was not recorded. Solution changes took about 1 minute, so it was possible that a fast transient change was missed. To assess the likelihood of overlooked $[Ca]_{int}$ transients, we followed 3 neurons at 2 seconds intervals for about 1.5 minutes during solution changes (NS to 0.25xNS, with 3.5 mM calcium in NS). Care was taken not to mechanically disturb the chamber as solution was wicked off. As figure 2.3b shows, swelling neurons experienced no transient change in $[Ca]_{int}$ during the first 1.5 minutes of swelling, even though there was abundant external calcium. High frequency monitoring of this initial stage (which required two workers) was not, therefore, done on a routine basis. Since the $[Ca]_{int}$ was not monitored during the 1 minute of solution changes, the average of the $[Ca]_{int}$ value before the solution change and the first $[Ca]_{int}$ value after the solution change was calculated and was added as data points before constructing figures 2.3 and 2.4.

Trials were also run with $[Ca]_{ext}$ at 0.5µM and 0.13µM for 1xNS and 0.25xNS, respectively, collecting data as in figure 2.3a (fig 2.4). For these experiments neurons were pre-exposed to 0.5µM calcium NS for 5 minutes before the "control" part of the experiment (0-5 minutes in fig 2.4). $[Ca]_{int}$ before swelling was 53±7nM (n=11), whereas in swollen neurons it was 61±10nM and in NS after swelling it was 54±8nM. Of the 11 neurons tested, 6 showed a $[Ca]_{int}$ increase and 5 were unchanged. Overall this resulted in a significant 11±0.4% increase in $[Ca]_{int}$ during swelling

(p=0.04, within-neuron paired t-tests) followed by a significant (p=0.02) fall upon shrinking, with 7 decreasing and 4 unchanged. Again there was no difference between pre- and post-swelling $[Ca]_{int}$ (p=0.27).

Comparison of the $[Ca]_{int}$ in neurons which formed VLDs to the neurons which did not form VLDs, in normal extracellular calcium (3.5mM), did not reveal a statistically significant difference before, during swelling or during shrinkage (p=0.17, 0.06, 0.10). Likewise no difference existed between the neurons which formed VLDs to the neurons which did not form VLDs in low extracellular calcium (0.5μM) during either of the three osmotic perturbations (p=0.37, 0.33, 0.34).

In summary, about a 10% increase in $[Ca]_{int}$ was detected with swelling under both conditions of $[Ca]_{ext}$. This amounted to increases from 96 to 105nM calcium and from 53 to 61nM calcium in the normal and low extracellular calcium conditions respectively.

VLDs form with $[Ca]_{int}$ clamped to 0.1μM using a calcium ionophore

Having determined (fig 2.3a) that resting $[Ca]_{int}$ (pre-swell, 3.5 mM Ca_{ext}) for these neurons was ~0.1μM, the $[Ca]_{int}$ was clamped at equilibrium with this level then tested the neurons ability to form VLDs in response to osmotic perturbations. Under these conditions $[Ca]_{int}$ should be unable to fluctuate above 0.1μM calcium during perturbations.

After a brief wash in 0.1μM calcium NS, neurons were incubated for 25 minutes in 0.1μM calcium NS containing 20μM of the calcium ionophore, 4-bromo-A23187 (Molecular Probes, Eugene, OR) dissolved in 0.6% DMSO. While doing the FURA-2 calibration procedures, it was discovered that calcium-clamping with this ionophore requires ionophore to be continuously present in the medium. In the continued presence of the ionophore, therefore, neurons were swollen in 0.25xNS for 4 minutes then reshrunk in NS (note that for 0.1μM calcium NS this results in 0.025 μM calcium during swelling). The osmotic perturbation protocol was repeated to test if VLDs could reverse and then reform. Only about one-third of the neurons remained healthy during the 25 minute pre-incubation in 0.1μM Ca_{ext}. The other two-thirds retracted their processes and/or their soma became grainy in appearance. Nevertheless, those neurons with a tolerably normal appearance after the low calcium preincubation withstood the osmotic perturbation cycles and

formed then reversed VLDs. Figure 2.5 shows two such neurons with VLDs in a lamellar region. The important point here is that VLDs can form in neurons that are prevented from experiencing a calcium perturbation during the swelling stimulus.

Are VLD dynamics possible when Ca_{int} is held at very low levels by BAPTA?

To clamp the Ca_{int} to a lower level, cells were loaded with a membrane-permeant fast calcium chelator, BAPTA, by incubating them in 30μM BAPTA-AM in 0.3% DMSO for 1 or 3 hours. The ester (i.e. the AM form) freely crosses the lipid bilayer (Cohan *et al.*, 1987) and in the cytoplasm, non-specific esterases cleave the ester tail, trapping BAPTA in the cytoplasm. Although the cytoplasmic [BAPTA] is not known because loading is not an equilibration process, $[BAPTA]_{int}$ should have been at least as high at 3 hours as at 1 hour. After 1 or 3 hours, the neurons were swollen in low calcium 0.25xNS (0.13μM calcium) for 4 minutes then reshrunk in NS with 0.5μM calcium. All neurons formed VLDs, which were then reversed and reformed twice more with the same osmotic shock solutions. Figure 2.6a illustrates VLDs made by this swell/shrink protocol in a control neuron and figure 2.6b and c show neurons pre-loaded with BAPTA for 1 and 3 hours (respectively) before and after undergoing the swell/shrink protocol.

In another set of experiments, neurons were also loaded simultaneously with 30μM BAPTA-AM and 2μM FURA-2-AM to measure the neuronal $[Ca]_{int}$ upon swelling and shrinking, using the same data collection protocol as in figure 2.3a. To allow for adequate cellular processing of both of the esters, the following loading procedure was used: BAPTA-AM and FURA-2-AM (in a final concentration of 0.3% DMSO) were applied for 45 minutes, then cells were washed in NS (3.5mM Ca) and left to rest for 30 minutes, washed again in NS, allowed to rest for another 45 minutes, then experiments were begun. Experiments were completed over the next 60 minutes, so that a maximum of 3 hours elapsed since the beginning of load time. As figure 2.6d shows, BAPTA effectively buffered neuronal $[Ca]_{int}$ to 34.6±1nM (n=6) and upon swelling, no change in $[Ca]_{int}$ was evident. Since the BAPTA was loaded for only 45 minutes in these experiments, we assume that $[Ca]_{int}$ levels were at least as low after the previously mentioned 1 and 3 hour incubations.

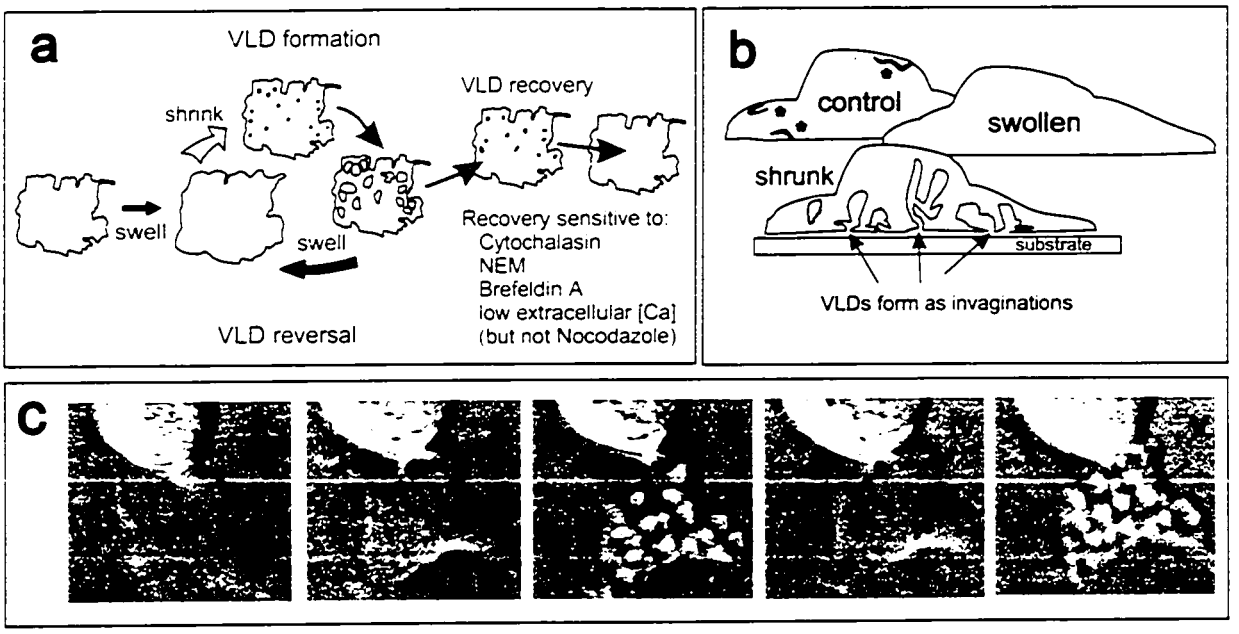

Figure 2.1 a: Protocol and terminology for vacuole-like dilation (VLD) formation, reversal and recovery. Repeated swell/shrink cycles cause VLDs to form and reverse repeatedly at the same sites. Neurons bearing VLDs undergo recovery (a process sensitive to the listed drugs) if left in normal saline (NS). b: A neuron sketched in dorsoventral section before swelling (control; asterisks indicate putative membrane stores), during swelling and then on return to NS (shrunk), illustrating the topology of VLDs. Some pinch off as true vacuoles. c: VLDs produced in a *Lymnaea* neuron with normal and then with low extracellular calcium. Control (i), swelling (ii) and shrinking (iii) in normal calcium media and swelling (iv) and shrinking (v) in low calcium conditions are shown. Arrows show that VLDs reappear at discrete sites. Scale: 10μm.

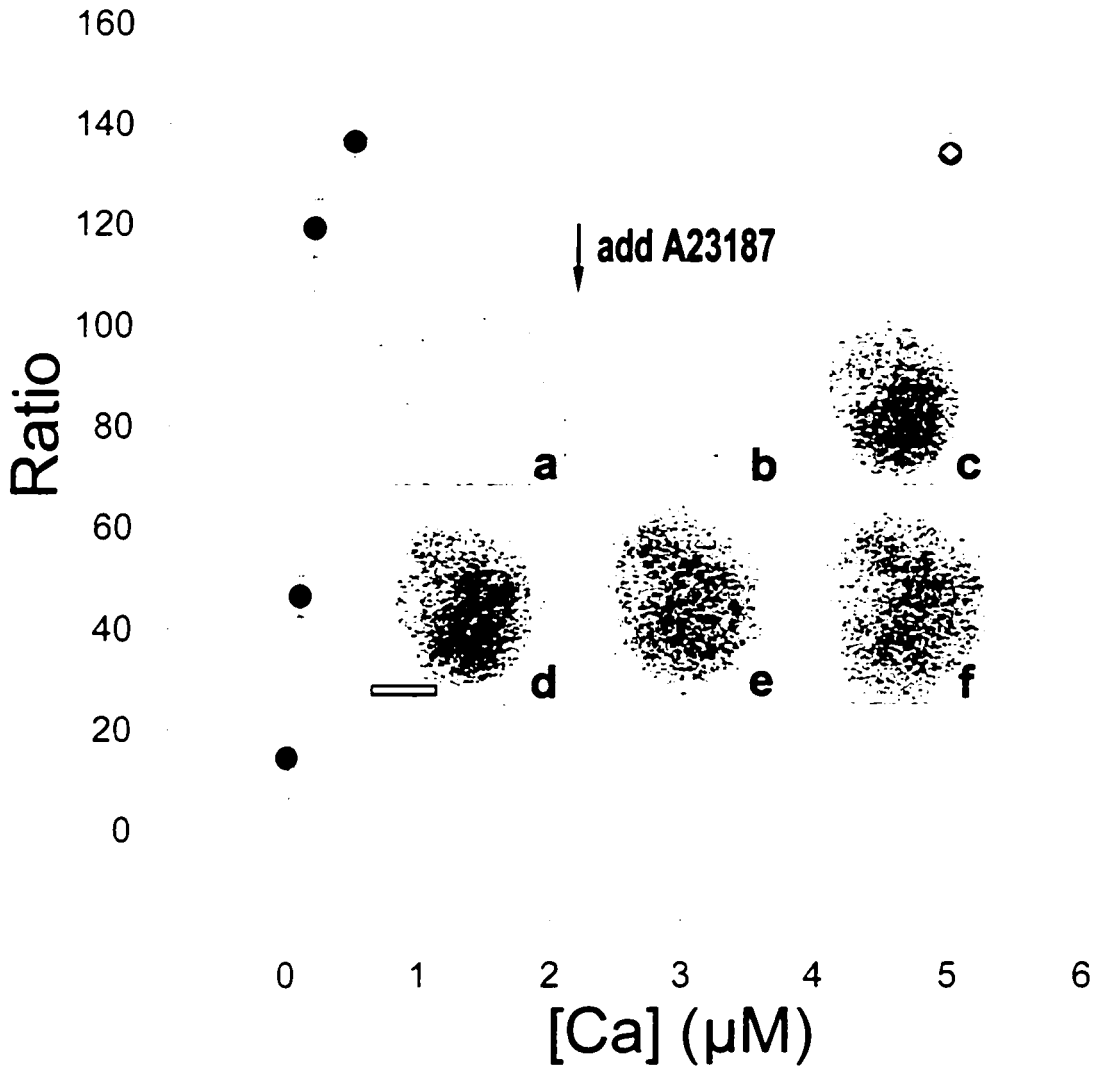

Figure 2.2 Intracellular calcium concentration ($[Ca]_{in}$) calibration curve(s) for *Lymnaea* neurons loaded with 2μM Fura-2, permeabilized to calcium using 4-bromo-A23187 and equilibrated to various calcium solutions. Two different symbols represent curves generated several months apart by 2 workers. Half-maximal ratio values were obtained at calcium concentrations of 0.13 and 0.14μM from the 2 curves. Inset: ratio images of a sample neuron in NS (a) and 0 (b), 0.1 (c), 0.2 (d) 0.5 (e) and 5.0μM calcium (f). Scale: 20μm.

Figure 2.3 FURA-2 measurements of $[Ca]_{int}$ in *Lymnaea* neurons at rest (0-5 minutes) and as they swell (5-10 minutes) in 0.25xNS then reshrink (10-20 minutes) in NS (a). Concentrations above traces are mean $[Ca]_{int}$ for 19 neurons during each phase; individual values are the average of readings taken every 30 seconds. Unlabelled sections between each phase indicate when solution changes were made; one 30 second time-point for $[Ca]_{int}$ was skipped during each change. For one trace (dashed line) representative ratio images for each phase are displayed above. Because the contrast between background and cell in the images was low (albeit readily visible on a computer monitor), the cell perimeter has been outlined by hand. Circles are the region from which ratios were averaged. When reshrunken cells were checked with transmitted light at the end of the experiment, VLDs were typically visible in the lamellar region. Scale bar: 22µm. $[Ca]_{int}$ of *Lymnaea* neurons during the first 1.5 minutes of swelling (b). For the first 10 seconds neurons were in NS then 0.25xNS was wicked through the chamber (about 15 seconds). Through the whole procedure image pairs were taken every 2 seconds. For runs at this speed, it was not possible to average image frames during real-time data acquisition (see methods), so ratios are calculated from pairs of single video frames (1/30s each).

a

neuron has VLDs at this stage

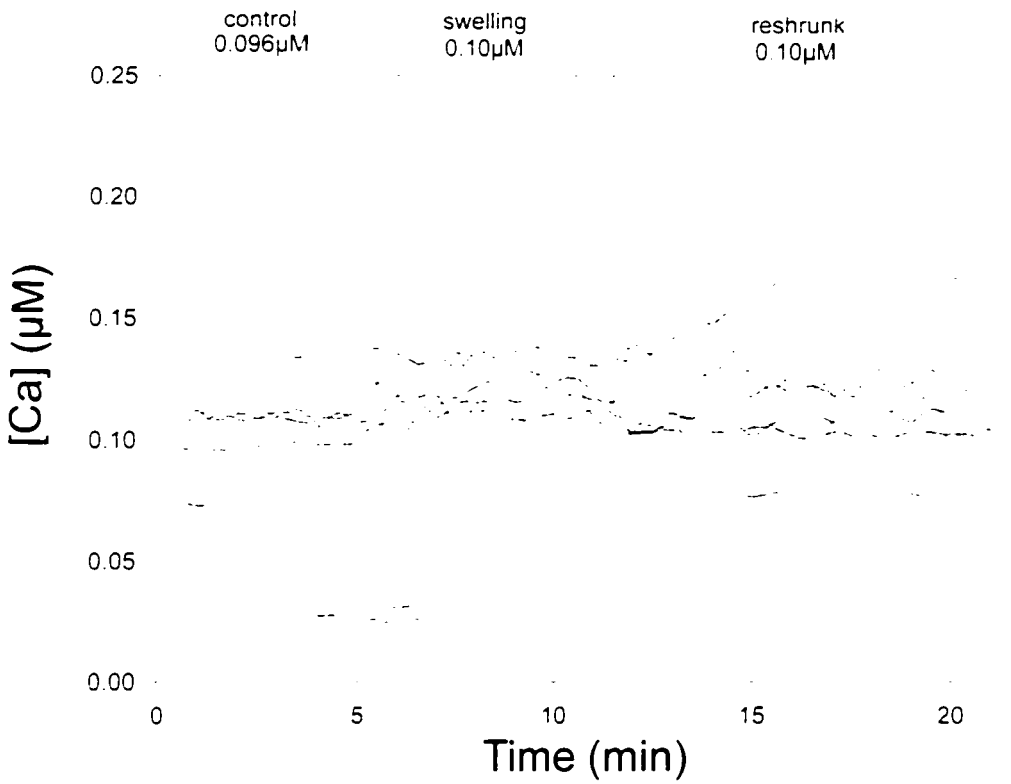

b

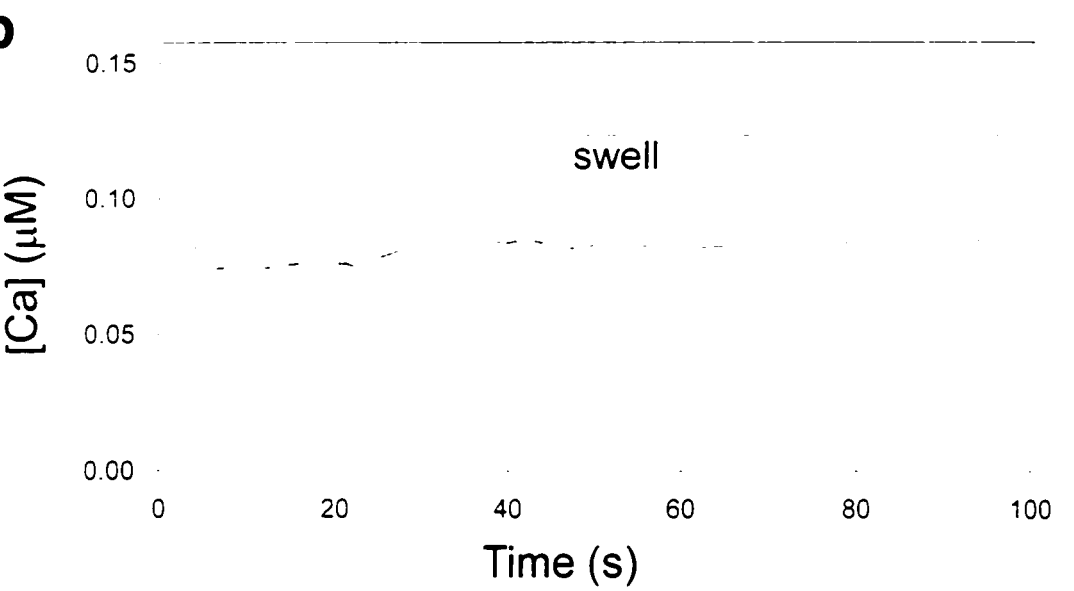

Figure 2.4 FURA-2 measurements of $[Ca]_{int}$ of *Lymnaea* neurons in low $[Ca]_{ex}$ media (0.5μM calcium) before swelling (0-5 minutes), during swelling (5-10 minutes) and during shrinkage (10-20 minutes). As in figure 2.3a, concentrations above traces are means for the 11 neurons during each phase and the dashed trace corresponds to the neuron displayed in each phase above the graph. A cell outline was generated as in figure 2.3; because swelling and shrinking occurred mostly in a vertical direction for this cell, little cross-sectional change is evident. Scale bar: 22μm.

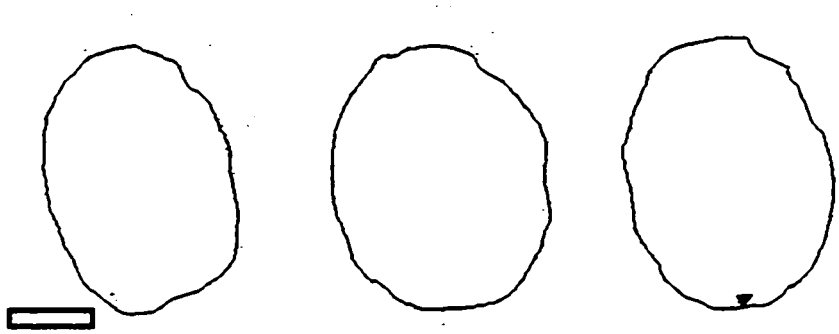

Cell has VLDs at this stage

control
0.053μM

swelling
0.061μM

reshrunk
0.054μM

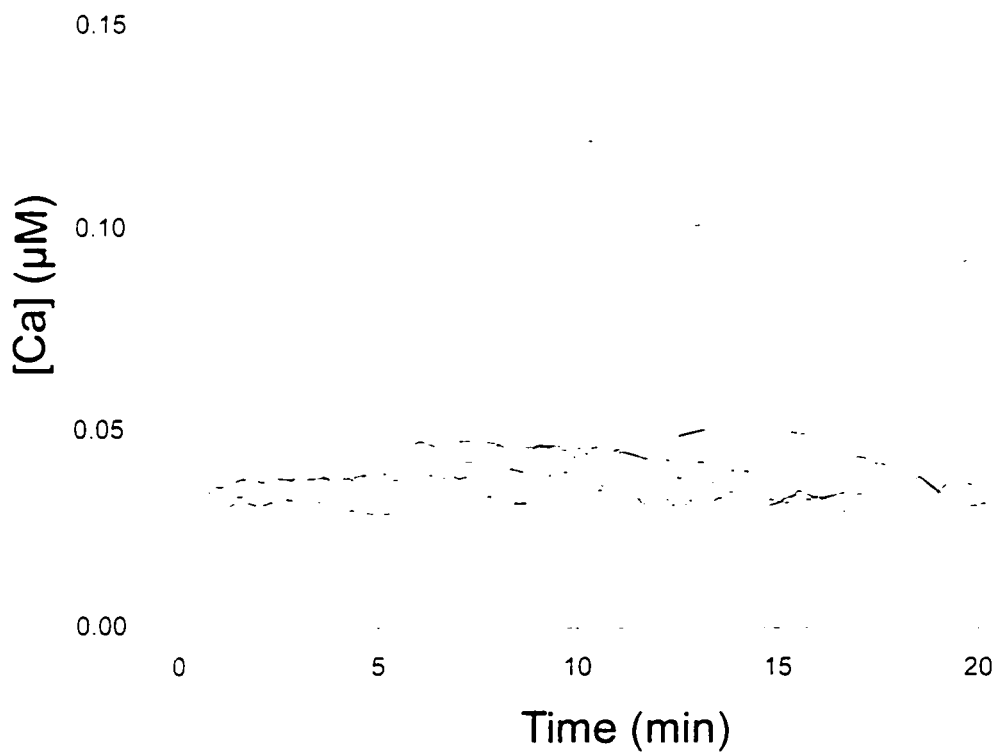

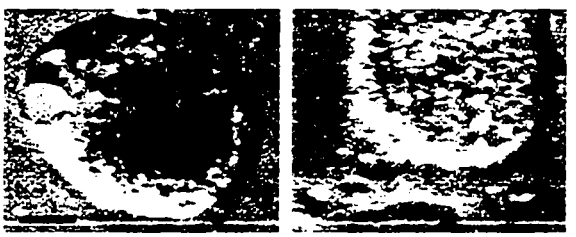

Figure 2.5: Examples of VLDs elicited in neurons with $[Ca]_{int}$ clamped at a $[Ca]_{ext}$ of 0.1μm by A23187. Scale: 10μm.

Figure 2.6 VLD formation in neurons loaded with BAPTA prior to a swell/shrink perturbation in low calcium media. Neurons swollen in 0.25xNS and subsequently (below image) in NS, showing VLDs in a control cell (a), a cell loaded with BAPTA-AM for 1 hour (b) or for 3 hours (c). Scale bar: 10 μm. FURA-2 measurements of $[Ca]_{int}$ of *Lymnaea* neurons loaded with BAPTA and FURA-2 show no change in $[Ca]_{int}$ from the control levels (0-5 minutes) upon swelling (5-10 minutes) or shrinking (10-15 minutes) (d). Also shows that BAPTA-AM loading is effective, buffering $[Ca]_{int}$ to less than half the resting $[Ca]_{int}$ measured in NS when no exogenous calcium chelator is present in the cytoplasm (compare to fig 2.3).

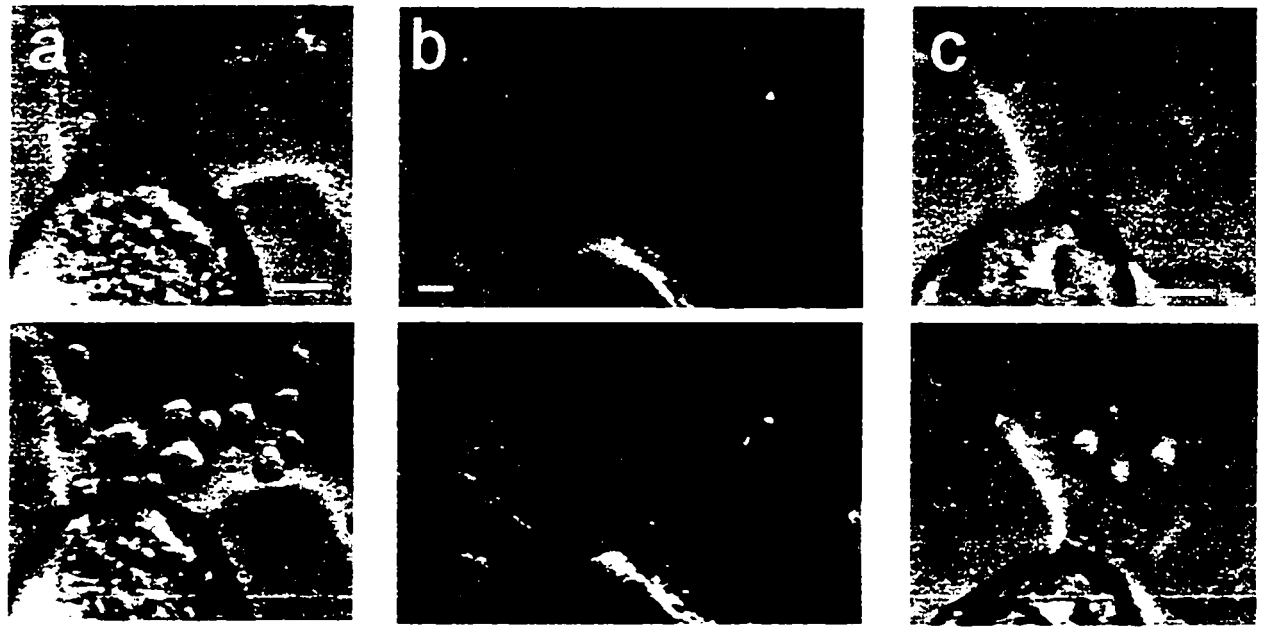
a
b
c

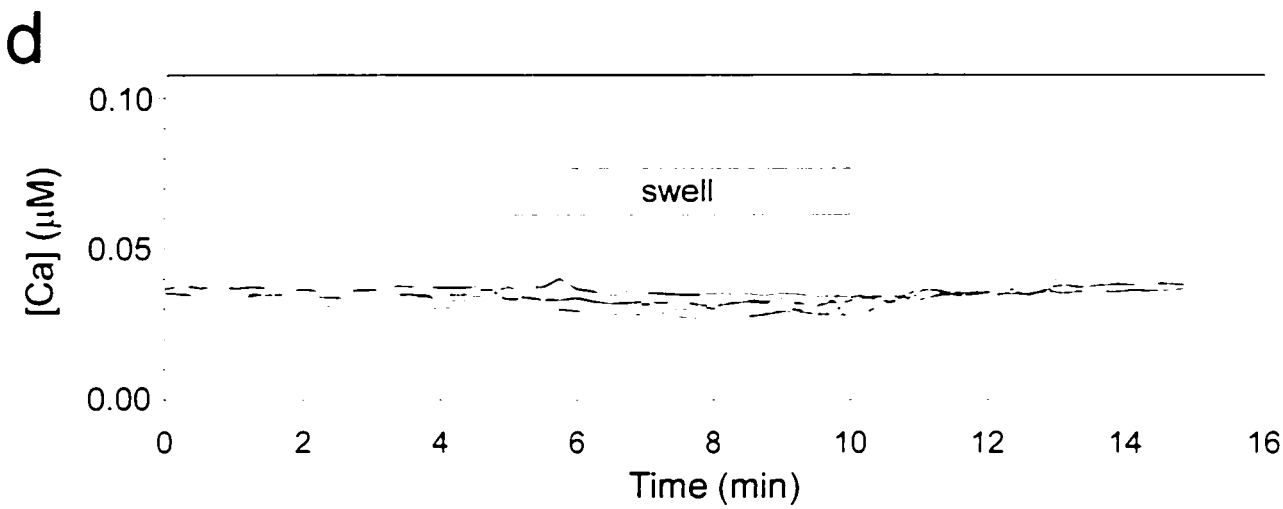
d
0.10
0.05
0.00
[Ca] (μM)
swell
0
2
4
6
8
10
12
14
16
Time (min)

DISCUSSION

Resting $[Ca]_{int}$ in *Lymnaea* neurons was about half the normal level when $[Ca]_{ext}$ was changed to 0.5µM instead of the normal 3.5mM (ie. 96nM in 3.5mM calcium and 53nm in 0.5µM calcium) (fig 2.3a and 2.4). Evidently, neuronal calcium-homeostasis mechanisms cannot effectively counteract extremely low extracellular calcium levels by drawing on internal calcium stores. Since submicromolar external calcium would not be experienced *in vivo*, this is unsurprising. It is, moreover, advantageous here because the induced low $[Ca]_{int}$ facilitates the study of putatively $[Ca]_{int}$ -independent events.

Swelling coincided with a small average increase in $[Ca]_{int}$ for media of both low and high $[Ca]_{ext}$. While they are statistically significant, these increases are not physiologically significant in the context of the calcium levels normally thought to drive exocytosis (see below). The increases - from 96 to 105nM and from 53 to 61nM for the 0.25xNS swelling solutions (0.9mM and 0.13µM $[Ca]_{ext}$ respectively) - amount to absolute changes of <10nM. Moreover, as seen in individual $[Ca]_{int}$ traces (see fig 2.3a and 2.4), some neurons experienced either no increase or even a decrease during swelling. The between-neurons variation in baseline $[Ca]_{int}$ is easily in the 10nM range, as is the noise level for some neurons. This noise is probably cellular rather than instrumentational, since BAPTA-loaded neurons (fig 2.6a) were markedly quieter.

Movement is inherent during swelling and shrinking of neurons. Swelling is most dramatic in the first minute after any osmotic perturbation in *Lymnaea* neurons (Morris *et al.*, 1989), as in any cell; movement artefacts would have been most problematic as solution changes were implemented, and in most experiments $[Ca]_{int}$ was not monitored over this period. Spatially, movement artefacts are most pronounced at the cell perimeter; as mentioned (methods), we discarded data if such artefacts were evident. The large size of *Lymnaea* neurons (~20-80µm diameter) should enhance the reliability of these measurements because the larger a cell, the smaller its perimeter-to-cross section ratio. Moreover, measurements were made not of the entire cytoplasm, but on a circular region slightly less than the minimum diameter of the soma, established for the control condition (ie. first image frame taken) then used throughout for the analysis of this one cell. This largely obviated problems at the perimeter of the cell related to inflation and deflation.

In future experiments, it would be desirable to monitor the immediate submembrane region but movements here will always introduce error. In any case, transmembrane influxes of calcium are not needed for cells to produce VLDs or to increase capacitance as they swell (Reuzeau *et al.*, 1995; Wan *et al.*, 1995), so a sustained calcium release into the bulk of the cytoplasm from internal stores is what was trying to be detected.

Our data do not rule out a minor release of calcium from stores in swelling neurons, but comparing the swelling-induced increases of $[Ca]_{int}$ in *Lymnaea* to the $[Ca]_{int}$ increases in various cells undergoing exocytosis puts the swelling-induced changes in perspective. Eosinophil $[Ca]_{int}$ rose from 240nM to 1.5μM on exocytotic stimulation with GTP-γ-S (Nusse *et al.*, 1990), a difference of ~1300nM. In squid giant nerve terminals, presynaptic $[Ca]_{int}$ rose from 100nM to 1000nM during trains of 250 action potentials (Augustine *et al.*, 1992), a 10-fold increase or, in absolute terms an increase of 900nM. Neher and Augustine (1992) measured the $[Ca]_{int}$ in chromaffin cells at rest to be ~100nM and upon depolarization to rise to ~550nM at the plasma membrane and 500nM deep in the cytoplasm. In the same preparation, Penner and Neher (1988) found levels in the range of 400-1500nM on stimulation. Others have confirmed these results, showing that the $[Ca]_{int}$ at rest ranged from 10-100nM and rose to an $[Ca]_{int}$ of 300-1000nM upon depolarization (Cheek and Barry, 1993).

Even in normal $[Ca]_{ext}$ the largest swelling-related $[Ca]_{int}$ increases in *Lymnaea* neurons should not have been able to drive calcium-dependent exocytosis. Nevertheless, membrane capacitance and area increases in swelling *Lymnaea* neurons (Wan *et al.*, 1995) and volume increases in swelling *Aplysia* neurons (Fejtl *et al.*, 1995) indicate that membrane is recruited by swelling. A simple possibility is that lumenless membrane folds or mechanically accessible membranous cisternae (Fejtl *et al.*, 1995) are drawn into the plasma membrane by elevated tension. We have measured membrane tension in swelling neurons using plasma membrane tethers pulled by optical tweezers (Dai *et al.*, 1998). Upon swelling in a 50% medium, *Lymnaea* neurons experience a tension transient that relaxes to a sustained 0.12mN/m, as compared to 0.04mN/m before swelling. This is consistent with acquisition of new membrane in response to swelling tension. The sustained 3-fold increase in tension is not dangerously high, since 0.12mN/m

is about two orders of magnitude below membrane lytic tension in *Lymnaea* neurons. In fact, 10-12mN/m has been determined as the lytic pressure in many biological membrane preparations (Nichol and Hutter, 1996a).

Nichol and Hutter (1996b) showed that 2μM but not 0.8μM Ca_{int} is mechanically treacherous; a sharp decline in membrane strength occurs between these concentrations. Because the "danger zone" of $[Ca]_{int}$ overlaps that of neurons undergoing calcium-driven exocytosis, it may be imprudent for a mechanically-stressed neuron to rely on calcium-driven exocytosis as a means of increasing membrane area. The small swelling-induced [Ca] elevations in *Lymnaea* neurons (even in the higher external [Ca]) are well below the danger range.

The specific capacitance of *Lymnaea* neurons prior to swelling is consistent with a relatively non-wrinkled membrane surface (Wan *et al.*, 1995) and fluorescent aqueous phase markers examined by confocal microscopy (Reuzeau *et al.*, 1995) reveal no dye-accessible infoldings. Thus, to prevent rupture, major options for a swelling neuron are a) retract processes and/or b) recruit new membrane. Brief swelling episodes elicit VLDs, yet seldom cause retraction of processes, so we assume recruitment of membrane occurs. In cell culture, some cell types (Wilkerson *et al.*, 1986; Menke and Jockusch, 1991) generate discrete spherical blebs as they swell. By contrast, swelling neuronal cells, including *Lymnaea* neurons and rat hippocampal neuron cultures (Dai *et al.*, 1998) seldom bleb. Neurons made unhealthy by overdigestion during isolation, by age in culture, or by calcium-loading generate large discrete blebs (unpublished observation) consistent with the availability of membrane in this form. Perhaps the subplasmalemmal reserves of Fejtl *et al.*, (1995) are the source of bleb membrane in weakened neurons. But, even swelling in near-distilled water (Wan *et al.*, 1995), healthy neurons remain bleb-free. Contractile resistance to hydrostatic stress may help protract the duration of swelling and of capacitance increase (Wan *et al.*, 1995). Overall, neurons seem to maintain good control of membrane reserves, playing them out only as needed to keep membrane tension low (Dai *et al.*, 1998). When stress is excessive, rupture, not blebbing, results. In initial trials for the present work, healthy *Lymnaea* neurons exploded as distilled water abruptly washed through the double coverslip chambers; previously (Reuzeau *et al.*, 1995) stepwise exchanges to distilled water were used, presumably allowing

sufficient time for augmentation of membrane area.

Any reserve membrane contiguous with the plasma membrane (Cheng and Reese, 1987; Dailey and Bridgman, 1993; Sukhorukov *et al.*, 1993; Krolenko *et al.*, 1995) could play a role in mechanosensitive membrane disposition. Additionally, cells undergo constitutive exocytosis and endocytosis; swelling-induced increase in exocytosis and/or decrease in endocytosis would result in net recruitment.

Holding $[Ca]_{int}$ constant does not prevent VLDs

Control neurons and BAPTA-loaded neurons were similar in appearance and produced VLDs. BAPTA liberated intracellularly has low membrane permeability, and so $[BAPTA]_{int}$ may have continued to increase during 3 hours of loading. Experiments with neurons loaded for 45 minutes with BAPTA plus FURA-2 showed that $[Ca]_{int}$ was buffered below ~40nM and that no $[Ca]_{int}$ increase was elicited by swelling. Therefore an $[Ca]_{int}$ ~40nM did not impair the ability of neurons to swell without rupturing or to form VLDs repeatedly at the same sites. Morán *et al.* (1997) also showed that BAPTA plus FURA-2 loaded cerebellar granule neurons exposed to 50% media for 90 seconds maintain a fixed $[Ca]_{int}$; no tendency for low-calcium neurons to rupture was reported.

In theory, the ideal experiment is to clamp $[Ca]_{int}$ and $[Ca]_{ext}$ to the resting $[Ca]_{int}$ level (0.1μM - see fig 2.3a) then attempt to elicit VLDs so that $[Ca]_{int}$ during swelling and subsequent VLD formation is known and invariant. However, calcium ionophores used to produce the clamp do not limit their effects to plasma membrane. Calcium released from intracellular stores (Itoh *et al.*, 1985) during A23187 treatment probably caused the general cellular trauma noted, since, in BAPTA experiments, low $[Ca]_{int}$ *per se* was benign. The A23187 may also have sufficiently increased the proton permeability of plasma membrane and/or endomembranes to alter the intracellular pH. The granular appearance of A23187-treated *Lymnaea* neurons echoes that of rat peripheral nerve (Schlaepfer, 1977) and dog spinal neurons (Emery and Lucas, 1995). Neurons which survived and withstood the first osmotic perturbations were fragile and recurrent shocks resulted in rounding up. Emery and Lucas (1995) noted, as did we, varying degrees of damage with A23187. As A23187 releases calcium from stores, the calcium may stimulate exocytosis.

BAPTA does not stimulate release of calcium from stores. Thus, even though we assume that A23187-treated neurons swelled then made VLDs with their cytoplasm clamped to 0.1 μM $[Ca]_{int}$, we consider the BAPTA experiments a better indication that neurons can swell (presumably recruiting membrane) and subsequently form VLDs with no change in $[Ca]_{int}$. In particular, the VLD formation experiments in low $[Ca]_{ext}$ using BAPTA-AM loaded neurons rule out the possibility that an undetected, fast, swelling-evoked, calcium transient produced a net increase in plasma membrane area, either through calcium-mediated stimulation of exocytosis or through calcium-mediated inhibition of endocytotic plasma membrane recycling.

$[Ca]_{int}$ and swelling in other preparations

In neurons, resting $[Ca]_{int}$ falls between 10-300nM (Kennedy and Thomas, 1996). This range easily encompasses all our findings, even those for swollen neurons. We did, however, reject at the outset, as potentially unhealthy, cells whose initial $[Ca]_{int}$ was abnormally high. O'Connor and Kimelberg (1993) measured $[Ca]_{int}$ in swollen astrocytes using FURA-2; $[Ca]_{int}$ increased rapidly to 600nM in about 25 seconds, then decreased to 250nM (over 5 minutes). The same pattern was seen without extracellular calcium. The astrocyte calcium transient is thought to be a component of the signalling pathway for regulatory volume decrease (RVD).

Like many vertebrate and invertebrate neurons (Fejtl *et al.*, 1995; Andrew *et al.*, 1997) *Lymnaea* neurons do not exhibit RVD (Morris *et al.*, 1989). By contrast, Pasantes-Morales and co-workers, using 0.2-0.5x media, observe partial RVD in isolated neurons (Sánchez-Olea *et al.*, 1993). Nevertheless, in their most recent work they show that RVD is not dependent on $[Ca]_{int}$. Cerebellar granule cells were loaded with FURA-2 and osmotic changes made at high time resolution. In 8 of 10 cells, swelling-induced changes were absent or inconsequential (Morán *et al.*, 1997). BAPTA buffered $[Ca]_{int}$ to levels comparable to what we observed and abolished any hint of swelling-induced effects. Swelling did not detectably release calcium from internal stores. In 0.13μM $[Ca]_{ext}$, the swelling associated increase of $[Ca]_{int}$ (53 to 61nM) of 0.008μM in *Lymnaea* neurons could have been supplied from the external medium or from stores.

The diminutive increases in *Lymnaea* neurons do not reflect insensitivity of the imaging

system; in the same set-up, mouse zygotes (which exhibit RVD) loaded with FURA-2 experience small swelling-induced increases in $[Ca]_{int}$ (Séguin and Baltz, 1997). As in the neurons, BAPTA clamped $[Ca]_{int}$ to a lower level.

In summary, swelling does not elicit in *Lymnaea* neurons a sustained increase in $[Ca]_{int}$ that could support membrane recruitment via calcium-driven exocytosis. Swelling-induced increases in surface area and capacitance may, therefore, be driven directly by elevated membrane tension. For a neuron changing shape in a manner that demands increased surface area, tension-induced recruitment could locally augment plasma membrane area independent of any cytoplasmic signal. *In vivo*, both calcium-mediated (Okada *et al.*, 1992; Steinhardt *et al.*, 1994) surface area regulation and a separate, tension-mediated, form of regulation may operate. Co-existing tension and calcium-dependent membrane recruitment may be widespread; plant protoplasts exhibit both calcium-mediated and (with ~30nM $[Ca]_{int}$ (Zorec and Tester, 1993)) pressure-stimulated capacitance increases and it is suggested that the membrane pools involved differ.

CHAPTER 3: F-ACTIN RESPONSES TO OSMOMECHANICAL PERTURBATIONS IN MOLLUSCAN NEURONS

INTRODUCTION

The idea of membrane tension as a coordinating signal for surface area, shape and volume adjustments has received much attention in plant cells (Wolfe and Steponkus, 1981; Wolfe *et al.*, 1985 and 1986; Kell and Glaser, 1993), but little in animal cells. Animal cells, including neurons (Van Essen, 1997), exhibit many tensegrity properties (Ingber and Folkman, 1989). Assuming that cellular form is governed by tensegrity, how does a dynamic tensegrity structure with a non-elastic skin (ie. the lipid bilayer) ensure that it has an appropriate amount of surface membrane at all locations as its volume and shape changes? We postulate that membrane tension is the signal and effector that brings about surface area regulation during volume and shape changes.

Developing neurons change shape and size continually and so require volume and surface area adjustments. How neurons coordinate their surface area and volume changes during outgrowth and retraction is not known. Large abrupt osmomechanical perturbations stimulate both volume and surface area changes (Wan *et al.*, 1995) and therefore can provide a useful approach to the study of surface area regulation. Diverse responses to osmomechanical perturbations suggest that local variations in membrane tension could act as sensor and as an effector for surface area adjustments (Reuzeau *et al.*, 1995; Dai *et al.*, 1996; Morris *et al.*, 1997; Herring *et al.*, 1998). If tension acts as both sensor and effector, the implication is that membrane tension increases would cause addition of membrane, whereas membrane tension decreases would cause membrane retrieval.

Abruptly shrinking neurons exhibit several phenomena which may be indicative of plasma membrane surface area decreasing to accommodate a smaller volume: 1) Their capacitance decreases at ~1μF per apparent cm^2 decrease in surface area (Wan *et al.*, 1995). 2) They rapidly invaginate substrate plasma membrane in the form of VLDs in a matter of minutes (Reuzeau *et al.*, 1995). 3) Their dorsal surface membrane tension, as opposed to their invaginating VLD membrane, falls slightly below control levels (Dai *et al.*, 1995a and 1998), thus facilitating the reinternalization of slack excess membrane as vacuoles (Morris *et al.*, 1997). Such observations

suggest that shrinking neurons undergo surface area regulation and that experimentally elicited VLDs may be exaggerated intermediary structures in this process. Since VLDs grow so rapidly, it is proposed that their membrane is initially at higher tension than adjacent membrane. The tension gradient would draw membrane bilayer from the general surface toward the VLD.

If neurons reshrinking in normal saline are left undisturbed, VLD recovery occurs. VLDs are therefore transient, although they will persist if neurons are treated with agents that interfere with actomyosin motility or active membrane reprocessing (fig 2.1). Whereas VLDs can not recover in the presence of these drugs, their osmomechanically-driven formation and reversal are not inhibited, consistent with the concept that VLD formation and reversal depend on membrane tension gradients generated by swelling and shrinking.

Cytochalasin blocks the recovery of VLDs. Since cytochalasin caps actin filaments, F-actin is implicated as necessary for the recovery process, and this suggests that the cortical cytoskeleton contributes to the regulation of surface area. However, F-actin's behaviour in neurons undergoing rapid surface area and volume changes has not been investigated. Therefore the first step in testing whether F-actin contributes to the process of surface area regulation, was to determine if a relationship existed between F-actin disposition and osmomechanically-induced VLDs during formation and recovery. Molluscan neurons were used to examine this relationship since their large size and spread-out morphology facilitates visualization of both VLDs (Reuzeau *et al.*, 1995) and of F-actin (Forscher and Smith 1988; Welnhofer *et al.*, 1997).

Osmotic swelling rapidly triggers F-actin depolymerization (Ziyadeh *et al.*, 1992; Cornet *et al.*, 1993 and 1994; Czekay *et al.*, 1994; Mills *et al.*, 1994; Morán *et al.*, 1996). For cell types that undergo fast regulatory volume decrease (RVD) in hypotonic media, it has been shown that the volume decrease phase coincides with actin repolymerization (Cornet *et al.*, 1994). RVD is, however, not detectable in mammalian neurons *in situ* (Andrew *et al.*, 1997) or in *Lymnaea* neurons (Morris *et al.*, 1989). Therefore, F-actin in *Lymnaea* neurons was examined by externally imposing swelling and shrinking osmolarity changes to bring about volume and surface area increases and decreases. To what extent the responses were driven by the primary physical stimulus or by secondary signalling cascades is open to question, but calcium signalling at least, is probably of

minimal relevance since swell/shrink cycles produce negligible calcium perturbations in both *Lymnaea* (Herring *et al.*, 1998), which do not exhibit RVD, and in other neurons where RVD is detectable (Morán *et al.*, 1997).

Images were initially obtained using conventional microscopy on fixed cells then extended and supplemented with high resolution video enhanced microscopy of live and fixed cells. Unidentified *Lymnaea* CNS neurons vary in their morphology, but because VLD formation and recovery is a robust phenomenon (Reuzeau *et al.*, 1995), neuronal heterogeneity was not a drawback.

METHODS AND MATERIALS

Cells and Solutions

Rearing and maintenance of *Lymnaea stagnalis* cultures were as described in the methods section in chapter 2.

Swelling solutions consisted of either 1) less than 0.05xNS for the conventional fixed microscopy samples or 2) 0.5xNS, by dilution of NS with an equal amount of distilled water for the high resolution live and fixed microscopy. A hyperosmotic solution of 3.5xNS was made by adding sucrose to NS to an osmolarity of 425mOsm. Normal saline (NS) was made as described in chapter 2.

Solutions changes were done in one of two ways: 1) for conventional microscopy with coverslips in 35mm dishes, the solution was exchanged 3x, using transfer pipettes to add and remove solutions. A thin layer of solution was always left covering the cells. 2) for high resolution microscopy, double coverslip flow through chambers were made, with silicone grease to hold the coverslips in place. A rectangular piece of plexiglass cut to fit the microscope stage slide holder was milled to hold a 22x22mm coverslip. Milled shelves and troughs allowed a second 22x22mm coverslip to be used as a cover and provided channels for solution changes. Solution exchanges were done by pipetting solution at one open edge of the top coverslip and then wicking it through the other open edge with filter paper as described in chapter 2. For each solution exchange, 3x 50µL of solution was wicked through the chamber.

The cytochalasin B (CB) experiments were carried out by pre-exposing the neurons to 10μM CB (Sigma, St. Louis, MO) in 0.5% DMSO for 20 minutes before VLDs were elicited, then maintaining this level through all steps until fixation. For control experiments, the same DMSO concentration was added to the solutions but with no CB. For the rhodamine 123 experiments neurons were exposed to 26μM rhodamine 123 (Sigma, St. Louis, MO) for 13 minutes prior to washout and viewing.

Fixation and Staining

Two different fixation procedures were used in the course of this study. Procedure 1: (for conventional microscopy, fig 3.1-3.4) Neurons were fixed in 0.25% glutaraldehyde (Fisher Scientific, Fair Lawn, NJ) in sodium cacodylate buffer. The fixation stock solution consisted of 0.13g $CaCl_2 2H_20$, 2.38g sodium cacodylate (BDH Ltd., Poole, UK) added to 180 mL H 0. Within less than 2 hours of fixing cells, 15mL of the stock was mixed with 1mL of a 4% glutaraldehyde solution, giving a final osmolarity of 179mOsm, pH 7.6. Saline was exchanged for fixative gradually over 2 minutes, cells were fixed for a further 10 minutes followed by washing 3x 5 minutes each, in phosphate buffered saline (PBS), extracting in 0.1% Triton X-100 (Sigma, St. Louis, MO) in PBS for 5 minutes, washed again in PBS 3x 5 minutes each, and reduced in 1% sodium borohydride in PBS, 3x 5 minutes each. Another PBS wash followed the reduction step, followed by staining of the neurons in 70μL of 0.44μM rhodamine-phalloidin (Molecular Probes, Eugene, Oregon) in PBS (methanol was evaporated from 1 volume of a 6.6μM rhodamine-phalloidin methanol stock solution and 15 volumes of PBS was added) for 30 minutes. After 30 minutes, the neurons were washed in PBS 3x 5 minutes each. Due to the high profile of molluscan neurons it was necessary to avoid compressing them upon mounting. Therefore, prior to mounting in 60μL of 2% n-propyl-gallate in PBS:glycerol (1:3), coverslip chips were positioned on a slide to elevate the 22x22mm coverslip. Silicone grease held the chips in place; a coverslip with mounting medium was inverted onto the chips. Coverslips were sealed with clear nail polish and slides were kept in the dark at -20°C until viewed, usually the next day. At least three slides of every experimental and control treatment were made and viewed.

Procedure 2: (done by Liz Welnhofer, University of Buffalo) (for high resolution microscopy, fig 3.6 and 3.7) Neurons were fixed in 0.5% glutaraldehyde in PHEM buffer (60 mM PIPES, 25mM HEPES, 2mM $MgCl_2$, 10mM EGTA, pH 6.9) for 2 minutes, post-fixed in 0.1% glutaraldehyde in PHEM for 20 minutes, rinsed for 5 minutes in PHEM, extracted in 0.5% Triton X-100 in PHEM for 5 minutes, rinsed in PBS 2x 5 minutes each, reduced in 0.5% sodium borohydride in PBS for 10 minutes, rinsed in PBS 2x 5 minutes each, incubated in 0.33μM Bodipy-phallacidin in PBS (1:20 dilution) (Molecular Probes, Eugene, Oregon) for 20 minutes, 2x 5 minutes rinses in PBS, dipped quickly in DW to remove any salts and mounted in Slow-Fade (Molecular Probes, Eugene, OR).

Viewing Cells

Procedure 1: Neurons were viewed within 2 days of staining, on a Zeiss Axiophot microscope fitted with a 40x (N.A. 0.75) phase contrast/neofluor objective and a filter set consisting of a 546nm excitation filter, a 580nm chromatic beam splitter and a 590nm barrier filter. Photomicrographs were taken on a Zeiss 35mm camera system using Ilford XP-2 400 ASA and Kodak TMY 400 ASA films. Phase contrast exposure times were automatic and fluorescence exposure times were manual and usually between 30-50 seconds. The negatives were processed by the Audio-Visual department at the Ottawa Civic Hospital. Photomicrographs from the negatives were enlarged on Ilford Multigrade III paper (Ilford Ltd., England) and mounted on heavy bristol board and rephotographed.

Procedure 2: (these experiments and the G-actin injection experiments were carried out in the lab of Dr. Chris Cohan, University of Buffalo) Neurons were viewed the same day on an inverted microscope equipped with a dry condenser (N.A. 0.85) and a 100x (N.A. 1.25) plan PH4 objective for phase contrast and fluorescence microscopy. Specimen irradiation was minimized by placing a shutter (Uniblitz, Rochester, NY) in front of the 100W halogen light and a green interference filter and infrared filter (Chroma Technology, Brattleboro, VT) were inserted into the light path. The shutter was controlled either manually or electronically triggered by a CCD camera controller.

Time-lapse movies were collected with a cooled CCD camera containing a back-illuminated

512x512 CCD (TEA/CCD-512, Princeton Instruments, Trenton, NJ) with 16 bit resolution. Microscopy images were projected either 2x, 2.5x, or 4x before acquisition. A computer (Power Macintosh 7100) with a nubus interface was used to control image acquisition. A "movie" script was written with IP Lab Spectrum software (Signal Analytics, Vienna, VA) to control exposure time, time intervals between image acquisition and number of frames in a movie. All image processing included background subtraction.

For video enhanced DIC microscopy, a 100x (N.A. 1.4) plan apo pol lens and an oil condenser (N.A.1.4) were used. Specimens were illuminated with light from a 100W mercury lamp that was passed through a fiber optic scrambler (Optiquip, MVI) before entering the transillumination pathway and were projected 4x. Video images were obtained with a Newvicon camera (Dage-MTI, Michigan City, IN) and converted to digital images using the computer (Power Macintosh 7100) with a frame grabber (Perceptics PixelPipeline). Time-lapse movies were made as described above.

All high resolution images were processed in Adobe Photoshop and assembled into figures in Adobe Illustrator in Ottawa.

Microinjection of G-actin

Tetramethylrhodamine-5-iodoacetamide labelled G-actin was prepared as outlined in Welnhofer *et al.* (1997). This rhodamine labelled G-actin (rh-actin) was diluted by 50% in injection buffer (2mM PIPES, 0.1mM ATP, 0.1mM DTT, 0.05mM $MgCl_2$, pH 7) to approximately 3mg/mL. Glass microelectrodes (AM Systems, Everett, WA) were back-filled with rh-actin and mounted onto a micromanipulator (Narishige). The cell bodies of the neurons were pressure injected with rh-actin. Pressure injection was controlled by a voltage activated valve (General Valve, Fairfield, NJ), triggered by an electronic stimulator. A small hyperpolarizing current was maintained during the injection period to inhibit action potentials produced by penetration of the cell membrane with the microelectrode. Neurons were incubated for at least 30 minutes after injection to allow for rh-actin incorporation into the growth cones. Fluorescent digital images were acquired as described above, except a 3 or 10% neutral density filter was inserted into the epifluorescence light path and a 500

millisecond exposure was used to reduce photobleaching and photodamage to neurons.

RESULTS

Fixation procedures

Before staining for F-actin, we ensured that fixation did not induce artefacts that might be confused with VLDs (ie. fixation induced vacuoles in Auer and Coulter, 1994). Previous monitoring of fixation procedures by Hoffman Modulation optics (40x objective) showed paraformaldehyde fixation to be unacceptably vacuologenic (Reuzeau, unpublished observation). Glutaraldehyde at 0.25% or 0.5%, however, produced no detectable morphology changes in *Lymnaea* neurons, but 0.5% was probably an upper limit since it is sporadically vacuologenic in other neurons (see fig 4 of Welnhofer *et al.*, 1997). In vertebrate neural tissue prepared for electron microscopy, glutaraldehyde (but not fast freeze) fixation disrupted endomembranes (Cheng and Reese, 1987). Such disruption might escape detection with transmitted light microscopy. But previous examination of neurons during fixation in 0.25% glutaraldehyde, at high resolution, revealed that tubular endoplasmic reticulum stained with the vital endomembrane dye diO, underwent no fixation-induced rearrangements (Morris, unpublished observations). Terasaki *et al.* (1984 and 1986) also found that 0.25% glutaraldehyde preserved the endotubular reticulum.

A drawback of glutaraldehyde, its autofluorescence, was substantially diminished by reducing with sodium borohydride, so that only neuronal somata fluoresced (fig 3.1A and B) and since the soma were also thick and pigmented, they were avoided. Lamellae and growth cones were therefore mostly imaged. Glutaraldehyde denatures proteins and then crosslinks the protein chains (Springall and Polack, 1995), causing high non-specific background fluorescence which interferes with detection of fluorescent labels (Weber *et al.*, 1978; Kosaka *et al.*, 1986). Reduction with 0.1% sodium metabisulfite (fig 3.1C and D) and up to 1% (not shown) was also tried but neuronal somata and neurite extensions fluoresced appreciably.

In all but one protocol (i.e. neurons hyperosmotically shocked), neurons were in normal saline just prior to fixation.

ACTIN AND VLDs: CONVENTIONAL MICROSCOPY

F-actin in fixed control neurons

Figure 3.2A is a survey image of a control neuron (no osmotic shock) focused near the cell-substrate contact plane, showing rhodamine-phalloidin fluorescence; figure 3.2B and C are phase contrast/fluorescence pair enlargements of the growth cone area. Typically, the most striking phalloidin positive structures were filopodia at the leading edges of growth cones (arrow in fig 3.2C) and along the lateral margins of neurites. Brightly fluorescent puncta (arrowhead in fig 3.2C) were scattered amidst diffusely stained background. Presumably, some of the diffuse fluorescence in the soma (fig 3.2A) was residual glutaraldehyde autofluorescence. Intense F-actin staining generally corresponded to phase dark material as expected (Letourneau, 1981; Glacy, 1983). The phalloidin staining pattern of this neuron was typical of *Lymnaea* neurons, regardless of variations in their neuritic morphology, and is similar to phalloidin staining in cultured vertebrate neurons also fixed in glutaraldehyde (Letourneau, 1981; Cornet *et al.*, 1994).

F-actin and VLDs: actipodia

F-actin was not imaged in swollen neurons, since glutaraldehyde was vacuologenic even at 0.25% in swollen neurons. Swollen neurons were, however, viewed live with conventional (Hoffman) and video enhanced optics. The swollen cytoplasm showed elevated Brownian motion absent in controls but comparable to that after cytochalasin treatment (Reuzeau *et al.*, 1995). Thus, swelling disrupted (presumably depolymerized) the cytoplasmic F-actin network. Whether this included F-actin immediately adjacent to the membrane could not be judged.

Figure 3.3A, B is a phase contrast/fluorescence pair of a neuron fixed 5 minutes after VLDs were elicited by a swell/shrink stimulus. VLDs first became apparent ~30 seconds after return to NS, enlarging from small points to fluid filled bubbles over the next 2-3 minutes. In this neuron, VLDs were particularly abundant and the fluorescent F-actin patterns exemplified the wide range of annular shapes and staining intensities observed in other neurons. Comparable annular F-actin configurations were absent in control neurons. VLD-bearing neurons, like controls, had filopodia (apparent on the right, though less intense than most of the annuli), an overall diffuse fluorescence

and scattered small puncta. The novel feature induced by the shrinking perturbation, the abundant F-actin annuli, aligned with the position of VLDs and were found at almost all VLDs. Because they were actin-rich and motile (see below), we termed these rings of F-actin "actipodia". The intensity of F-actin staining could differ dramatically among actipodia in a given cell. Moreover, the staining intensity could be radically different for two closely adjacent actipodia (fig 3.3B).

Thus less than 5 minutes after reshrinking of neurons in NS, actin was predictably reorganized as actipodia. Did VLD formation directly cause the preferential accumulation of F-actin in annuli, or were VLD and actipodial formation independent? If structures that could have be construed as pre-VLDs and pre-actipodia had been observed in control neurons, and if some actipodia had been observed without VLDs, then independent causation of VLDs and actipodia might be plausible. But such structures were not identified and so it is likely that actipodial formation was dependent on VLD formation.

Did F-actin annuli appear because randomly distributed cytoplasmic F-actin became compressed by enlarging VLDs? This is unlikely since compressive forces distribute isotropically through liquids and so would not preferentially compress peri-VLD cytoplasm. Furthermore, VLDs are initiated as point invaginations at the substrate (Mills and Morris, 1998); if enlarging VLDs acted as pistons with localized compressive effects, then small VLDs should have had faint actipodia, large VLDs intense actipodia, and adjacent similar-sized VLDs should have had actipodia of similar intensity. As is evident in figure 3.3B and D, this description does not hold. Not only were the brightest actipodia small, but very bright actipodia were frequently adjacent to very dim actipodia. The dynamics of actipodia in live cells (below) also argues that passive compression of cortical F-actin could not explain actipodial form.

Actipodial formation requires only a shrinking stimulus

VLDs were elicited using a swell/shrink stimulus, so that shrinkage, VLD formation and recovery occurred in normal saline (NS). The actual VLD-inducing stimulus is, however, not "swell/shrink", but shrinkage (Reuzeau *et al.*, 1995). With no preceding swell, large shrinking stimuli alone (i.e. from NS to hyperosmotic) also caused VLD formation.

It does not, however, follow that shrinkage alone would be sufficient to generate actipodia. Swelling induced depolymerization might be required to prime the redistribution of actin into actipodia. To determine if shrinkage alone could elicit F-actin-rich actipodia, VLDs were induced in 3.5xNS (sucrose added to NS) for 5 minutes. This induced multiple VLDs in all neurons tested (fig 3.3C). Fixation was identical to that used for VLDs formed in NS after a swell/shrink stimulus. As the actipodia in figure 3.3D demonstrate, prior swelling was not a prerequisite for actipodial formation. The VLDs plus their associated F-actin staining (i.e. ragged-looking actipodia) were indistinguishable from those in neurons that were made to swell and then to shrink in normal saline. Again, actipodia were always associated with a VLD, indicating that the actipodial configuration of F-actin was secondary to VLD formation.

Actipodia constrict VLDs at the substrate

VLD profiles were bubble-like in phase contrast images (Reuzeau *et al.*, 1995), whereas the associated actipodial profiles appeared ragged in fluorescent images, a discrepancy which stems from differences in the optics of the fluorescent and transmitted signals. In reality the membrane (i.e. its location prior to Triton X-100 extraction) and actipodial structures correspond precisely. The discrepancy arises because the fluorescent F-actin signal was consistently most intense at the substrate-contact plane whereas VLDs seen in phase contrast produced their strongest signal (the edge between VLD lumen and cytoplasm) above the substrate plane where the VLD was dilated. The phase contrast/fluorescent pairs (fig 3.3) were obtained by optimizing the fluorescent phalloidin image. No refocusing adjustments were made before obtaining the corresponding phase contrast images. Consequently, where F-actin stained as ragged annuli (fig 3.3D), same-focal-plane phase images of VLDs (fig 3.3C) were rounded and of greater diameter. Ragged phase contrast annuli (corresponding to the ragged F-actin) appeared on focusing marginally closer to the coverslip and likewise fluorescent F-actin annuli were rounder and larger when the focus was moved up slightly. Therefore actipodial and VLD profiles corresponded precisely. Both profiles were more ragged and more constricted at the substrate than above it.

Focusing through VLDs from the substrate to where they terminated in the cytoplasm

revealed that F-actin could cover the entire dilated VLD, though with conventional fluorescence microscopy, this was not evident on all VLDs. Thus, F-actin was not restricted to the substrate. However F-actin appeared to be most effective at constricting VLDs at the substrate. The presence of an F-actin coating over the cytoplasmic surface of some VLDs only 5 minutes after they were elicited is consistent with the dramatic cytochalasin-sensitive recovery dynamics (changing shape, splitting, shrinking) of VLDs (Reuzeau *et al.*, 1995).

Actipodia disappear when VLDs undergo reversal

When VLD-bearing neurons were made to reswell, VLDs reversed (shrank and disappeared); reversal is driven by mechanical forces and is distinctly different from recovery. Hyposmotically swollen neurons did not tolerate fixation procedures so instead, reversal was examined in normal saline. This was done by eliciting VLDs in 3.5xNS then reswelling the VLD-bearing neurons in NS (fig 3.3E, F). Full reversal of VLDs required ~4 minutes of reswelling in NS (as monitored by Hoffman optics). At this point, neurons were fixed, extracted and stained for F-actin. In these post-reversal neurons, no evidence of the former actipodial rings was detected. Neurons reswollen in normal saline exhibited a staining pattern like that of control neurons. A benefit of using this protocol (swelling in normal saline), as opposed to swelling in a hyposmotic medium, is that the disappearance of actipodia during reversal is clearly not the result of a generalized hypotonicity-induced depolymerization of F-actin. Note also the cell margin's abundant actin-rich filopodia. F-actin puncta were evident in these cells, as they were in the majority of neurons, regardless of the cell's osmotic history prior to fixation (fig 3.1F, 3.2A, C, 3.3B, D and F). As with the formation of actipodia during shrinkage, it seems most straightforward to relate the reversal of actipodia during swelling to mechanical forces acting in the immediate vicinity of VLDs.

Effects of cytochalasin

The effects of cytochalasin B (a 20 minute preincubation and throughout the osmotic perturbations, all at 10μM CB) were tested on control neurons and on neurons in which VLDs were elicited. Neurons maintained their adhesion during CB treatment. In CB-treated no-shock controls

(fig 3.4A, B), CB had two major effects. There was extensive depolymerization and/or collapse (fig 3.4A) of the F-actin associated with filopodia and the appearance of F-actin puncta just behind the leading edge (fig 3.4B). As in controls, CB-treated neurons (fig 3.4C, D) rapidly produced abundant VLDs, but these VLDs were smooth-edged at the substrate, instead of ragged, as seen in neurons not exposed to CB. Correspondingly, in CB-treated neurons the peri-VLD region lacked phalloidin-positive material. Presumably, the lack of the F-actin rich actipodia accounted for the smoothly rounded VLD profiles.

In CB-treated neurons viewed in phase contrast, the strikingly phase dark regions were not phalloidin positive; neither the collapsed material from the filopodia nor the peri-VLD region was fluorescent yet both were phase dark. By contrast, the intensely phalloidin positive puncta were not phase dark. These staining patterns and the lack of peri-VLD F-actin, despite the persistence (after the osmotic perturbation) of the large CB-induced puncta, indicates that actipodial F-actin was more akin to filopodial F-actin than to the phalloidin positive material in puncta. Phalloidin staining adjacent to VLDs (inset) was either absent or exceedingly faint. For instance, the phalloidin staining adjacent to the VLDs was less intense than the stained disorganized strands seen in the neurite. Neurons not shocked (not shown) or osmotically shocked to induce VLDs (fig 3.1E, F), but not incubated in CB, confirmed that 0.5% DMSO, used to dissolve CB, did not cause the phalloidin staining patterns attributed to CB.

VLDs under conditions akin to regulatory volume decrease

In the experiments above, VLDs were rapidly elicited by imposed shrinking. However, we noted earlier (Reuzeau *et al.*, 1995) that prolonged hyposmia also elicits small VLDs. Hyposmotic VLDs may reflect surface area retrieval as neurons adjust to a new osmotic regime. Though *Lymnaea* neurons do not exhibit regulatory volume decrease, they limit their rate and extent of swelling (Morris *et al.*, 1989; Wan *et al.*, 1995). To confirm that VLDs form during prolonged hyposmia, we subjected neurons to 50% hyposmia for 2 hours. Hyposmotic VLDs appeared in neurons after ~15-60 minutes in 50% medium and were typically small (less than 5µm in diameter) (fig 3.5). Note in figure 3.5B and C that the membrane edge has begun to retract, as if the neuron

is slowly accommodating to its new environment. This was observed in 3 of 3 neurons monitored continually during prolonged hyposmia.

HIGH RESOLUTION MICROSCOPY

F-actin in association with VLDs

High resolution images of actipodial F-actin fixed 5 minutes after shrinking previously swollen neurons in normal saline and stained with phallacidin (fig 3.6 and 3.7) revealed more vividly than conventional microscopy, the following points: 1) VLD F-actin at the substrate had the same form as leading edge F-actin. 2) F-actin coated the entire cytoplasmic surface of VLDs. 3) For individual actipodia, F-actin intensity around the perimeter could be non-uniform. 4) For immediately adjacent actipodia, F-actin intensity could vary dramatically.

Figure 3.6A and B are a phase contrast/fluorescent image pair of a control neuron (not osmotically shocked) stained with bodipy phallacidin. These were typical high resolution images of control neurons, which revealed, as the conventional microscopy images had, that *Lymnaea* neuronal filopodia are actin-rich and the neurons exhibit small fluorescent puncta throughout their cytoplasm, which is above the overall cytoplasmic background staining.

Three neurons osmotically swollen in 50% NS for 5 minutes, shrunk in NS and then fixed 5 minutes after being shrunk to cause VLD formation exhibited different actipodial structures (fig 3.6C-E). All osmotically shocked and fixed neurons had actin-rich filopodia, small puncta, general cytoplasmic staining and actin-rich actipodia, but interestingly, actipodia and filopodia from each neuron appeared to be structurally similar (ie. frequency and length of filopodia in each neuron appeared to be reflected in that neuron's actipodia).

VLDs are shown from 3 neurons (fig 3.7A-D, E-G, H-J) which were fixed 5 minutes after VLDs first formed. Phase contrast images, either at the substrate (fig 3.7 A,E,H) or above (fig 3.7C), show the location and shape of the VLDs (lumen is light, cytoplasm is darker). For the fluorescence pairs, the F-actin signal was optimized with averaging and contrast adjustments.

Fluorescence images above the substrate illustrate that where VLDs dilated to bubble-like structures (fig 3.7D,G), their membrane became covered in a smooth layer of F-actin with some

thickened patches. The dilated fluorescence profiles were continuous with actipodial profiles at the substrate (fig 3.7B and F). The small VLDs in B and D, though dilated in the cytoplasm (D), appear pinched off at the substrate (arrow in B). Likewise, a larger VLD (arrow in E-G) has actipodia that almost occlude the substrate. Over the VLDs, the F-actin coating was well delineated and distinct from the cytoplasmic background. Therefore whatever the initial state of the invaginating VLD membrane, by 5 minutes (the time of fixation) VLD membrane had been able to acquire F-actin in a form that could contribute to a supportive membrane skeleton. Were some VLDs not F-actin coated at 5 minutes? It appeared so, but, because of the wide range of F-actin intensity surrounding the VLDs and the possibility of photobleaching, signal optimization may not have always have been achieved. The ensemble of profiles unequivocally confirmed that while the most dramatic F-actin staining was associated with actipodial processes at the substrate level, F-actin extended up over the VLDs as well. Therefore whatever the initial state of the invaginating VLD membrane, at 5 minutes post-initiation, most VLDs were not naked bilayer but plasma membrane, made up of lipid bilayer plus a F-actin membrane skeleton.

Sharp demarcations in the F-actin densities of immediately adjacent VLDs suggests that individual VLDs organize their own F-actin (fig 3.7 H-J). Phase contrast image H and fluorescence images I and J were all from the same focal plane (ie. at the substrate). In J, 3 small intensely F-actin positive VLDs appeared to be giant F-actin puncta, not actipodia. However when the same area was "underexposed", actipodial details emerged (I), but other F-actin structures disappeared or appeared fainter. Even one of the 3 intense VLDs became almost undetectable. Note the close proximity of the several small round VLDs on the left; although 3 had actipodia, two lacked detectable F-actin entirely (compare images H and J). What the highly localized instructions might be is unknown. One possibility is that the earliest invaginations compete best for the G-actin and/or F-actin pool. Another is that highly localized F-actin nucleating signals exist at the membrane surface. A third possibility, that the amount of F-actin acquired by any given VLD depends on the general region in which the VLD forms, is not consistent with the patterns seen. Evidently, some VLDs compete far better than others for the pool of G-actin and/or F-actin.

Actipodia in live neurons at high resolution

If there is any question that the larger actipodia consist of filopodia and lamellipodia, it is dispelled by monitoring live neurons by time-lapse video enhanced DIC (fig 3.8). In essence, new leading edge was rapidly created at all these sites. It is dramatically apparent that the information for making "regular" filopodia is not lost even after a severe osmotic perturbation. Figure 3.8 shows that above the substrate, actipodia are not observed (A), however, focusing on the substrate revealed the actipodia (B) and how they changed over time (C and D). DIC movies of actipodia demonstrated how actipodia projected and swept across VLD openings over a number of seconds. Some regions of actipodia moved faster than others but measurements from the DIC movies revealed that during filopodial extension the rate of outgrowth approximated 3µm/minute (fig 3.8 graph). This outgrowth is comparable to filopodial outgrowth, in other invertebrate neuronal preparations: filopodial outgrowth in embryonic grasshopper Q1 neurons has been measured at 1.3-1.7µm/minute (Myers and Bastiani, 1993), 0.22-0.31µm/minute in *Helisoma* B19 and B5 neurons (Haydon *et al.*, 1985; Mattson and Kater, 1987) and 1.2-1.7µm/minute in *Aplysia* neurons (Wu and Goldberg, 1993). Filopodia were not observed in smaller VLDs. This does not eliminate the idea that smaller VLDs form filopodia, only that smaller VLDs were constricted and therefore harder to study.

Fluorescent G-actin accumulates at actipodia

To establish whether the peri-VLD region was enriched in F-actin, live *Lymnaea* neurons were injected with rhodamine-labelled rabbit muscle G-actin (fig 3.9). Figure 3.9 is one example of the many movies made of neurons injected with G-actin. The signal-to-background ratio in some neurons was adequate to reveal a filamentous actin web and puncta in pre-shock controls (fig 3.9A). But in swollen neurons and in the immediate post-swelling period, there was little more than a fluorescent glow in the cytoplasm. Presumably this was the result of swelling induced release of G-actin from previously polymerized F-actin. However by 5 minutes post-swelling (ie. on return to normal saline), labelled G-actin had reorganized in a non-homogeneous manner and was particularly concentrated in the peri-VLD regions (B). A reasonable interpretation of this timecourse

is that G-actin repolymerized into filaments in actipodia. As seen by comparing figure 3.9A and B, there is also evidence of F-actin polymerization at the margins of the neuron. Actipodia were dynamic and 10 minutes later (C) about half the VLDs present at 5 minutes (B) had disappeared. At 80 minutes (D), all but 2 large VLDs had disappeared and rhodamine G-actin was, as in the preswell neuron, mostly associated with puncta and again as a fine F-actin web.

There was a tendency for the rabbit actin to polymerize with itself (bright spicules formed at but perpendicular to the periphery of some neurons, not shown). However, this staining pattern was never observed in the fixed samples stained with rhodamine phalloidin or bodipy phallacidin. This staining pattern could not be eliminated in all cells and it was therefore ignored with respect to actin's dynamics during the osmomechanical perturbations.

The live, injected experiments corroborated the fixed tissue data and revealed other aspects of actin dynamics during shrinkage. As VLDs and actipodia formed (fig 3.9B and inset), puncta reappeared (fig 3.9B-D). As recovery progressed more puncta appeared throughout the neuron. These puncta therefore must contain newly repolymerized F-actin. Therefore the punctate structures seen in fixed neurons (fig 3.1F, 3.2A, C, 3.3B, D, F, 3.4B, D, 3.6B-E, 3.7F) are real F-actin structures. These experiments also corroborated the observations that the phase dark structures encircling VLD peripheries colocalized to F-actin (fig 3.9C inset).

Mitochondria and endoplasmic reticulum around VLDs

Mitochondria, however, also appeared dark in phase contrast microscopy, but the phase dark material associated with VLDs was not mitochondria. This seemed evident from many phase contrast movies, but to be sure that the dark worm-like structures seen in the phase contrast movies were mitochondria, neurons were incubated in rhodamine 123 (a fluorescent dye which accumulates in live mitochondria as a result of their large electrical potential), to vitally stain the mitochondria and follow them over time (fig 3.10A, B). Mitochondria randomly encountered VLDs, but clearly did not cluster around the VLD peripheries.

With video enhanced DIC it was sometimes possible to visualize large expanses of the tubular endoplasmic reticulum in large flat lamellae (fig 3.10C, D). No evidence was observed that

this membranous reticulum was contiguous with VLD membrane. However VLDs not fully recovered displaced the entire reticulum upwards. When the tubular reticulum was seen in live and unstained in this fashion, its physical resilience was apparent. Where the reticulum was anchored was not observed, but multiple anchorages must have existed to enable the reticulum to keep its integrity as it was displaced upward and as it subsequently subsided upon full reversal of the VLDs.

Figure 3.1 Reagent control micrographs showing how different agents reduce the autofluorescence of glutaraldehyde fixed neurons. A and C are phase contrast images of neurons fixed in 0.25% glutaraldehyde with either 1% sodium borohydride (A) or 0.1% sodium metabisulfite (C) used as a reducing agent. The fluorescent images (B, D) show that sodium borohydride was more effective. The neuron shown in C and D was osmotically shocked to elicit VLDs. The neuron in micrographs E and F was pre-incubated and osmotically shocked in NS containing 0.5% DMSO. Scale: 40µm A-D, 50µm E and F.

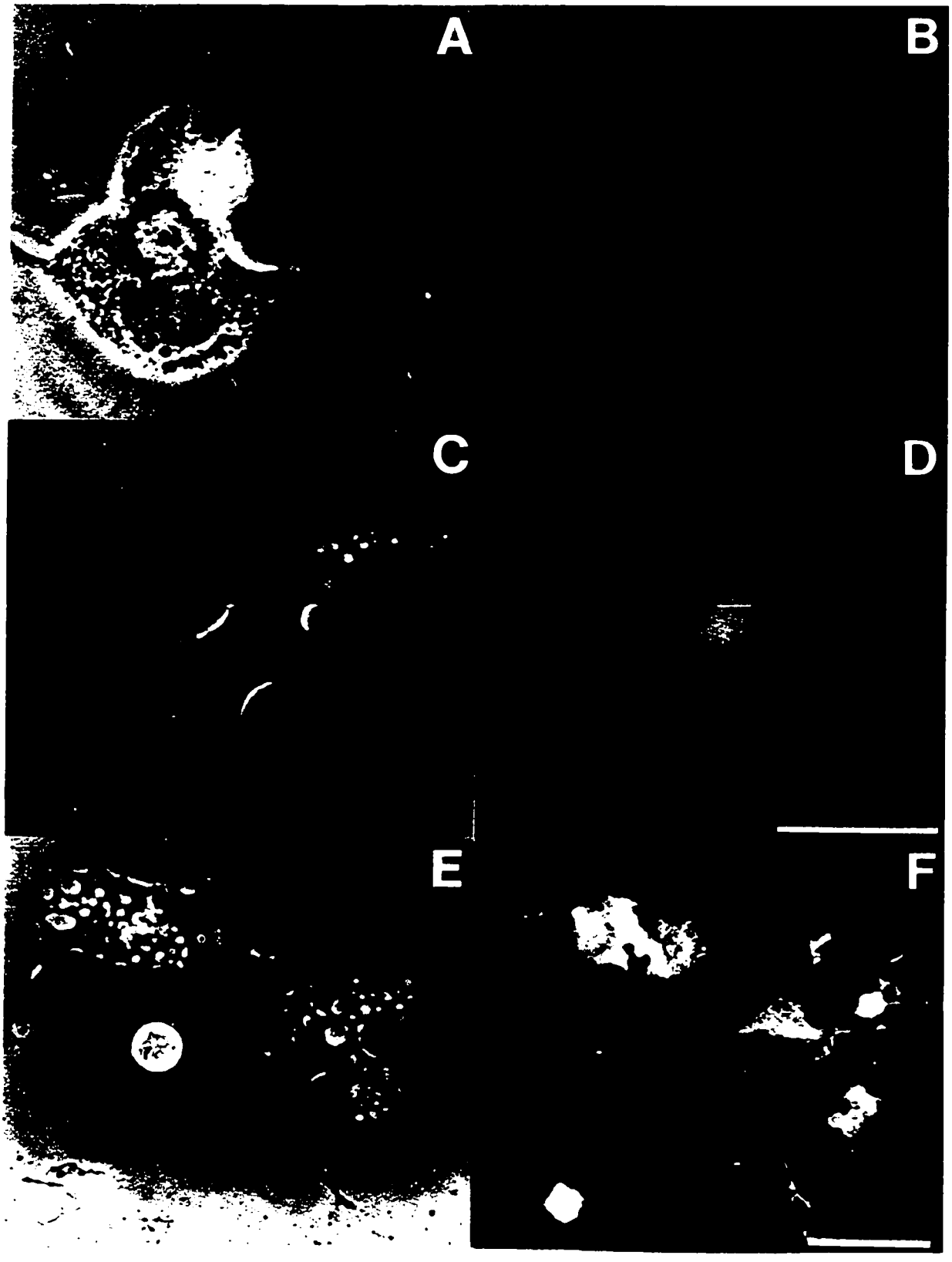
A
B
C
D
E
F

Figure 3.2 A neuron stained for F-actin with rhodamine-phalloidin. The focus was near the substrate in A and in enlargements of this neuron's growth cone in phase contrast (B) and fluorescence (C). Filopodia (arrow in C) at the leading edge of the growth cone were intensely stained for F-actin. Also bright puncta scattered throughout the neuron and diffuse fluorescence in the soma was common in all *Lymnaea* neurons, osmotically and not osmotically shocked. Scale bar: 33 µm in A. 15µm in B and C.

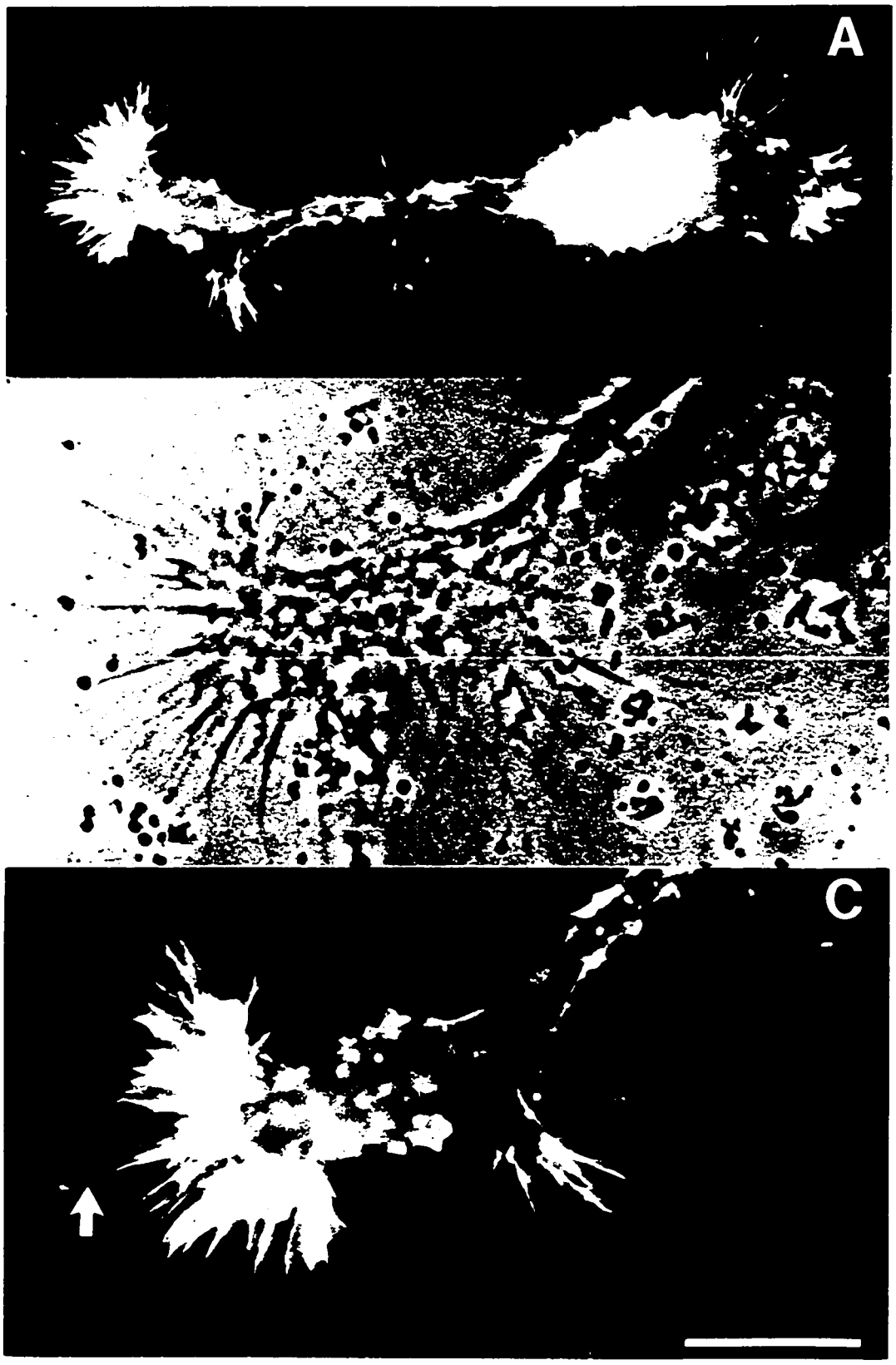
A
C

Figure 3.3 VLD-bearing neurons stained with rhodamine-phalloidin. Comparison of the phase image (A) to the corresponding fluorescent image (B) shows that F-actin surrounds the VLD membrane. The intensity of staining differs around different VLDs (arrow: VLD with bright staining; arrowhead: VLD with less staining) and that VLD-bearing neurons had filopodia, puncta and an overall diffuse fluorescence, as exhibited by the control neurons. A substrate view of a 3.5xNS hyperosmotically shocked neuron (C). Hypershocking also causes VLDs to form which are surrounded by F-actin rich actipodia (arrowhead in D). Reswelling previously hyperosmotically shocked neurons in NS causes VLD reversal (E). But also caused F-actin to rearrange into filopodia upon VLD reversal (F). Scale bar: 33μm in A, B, 11μm in C, D and 30μm in E, F.

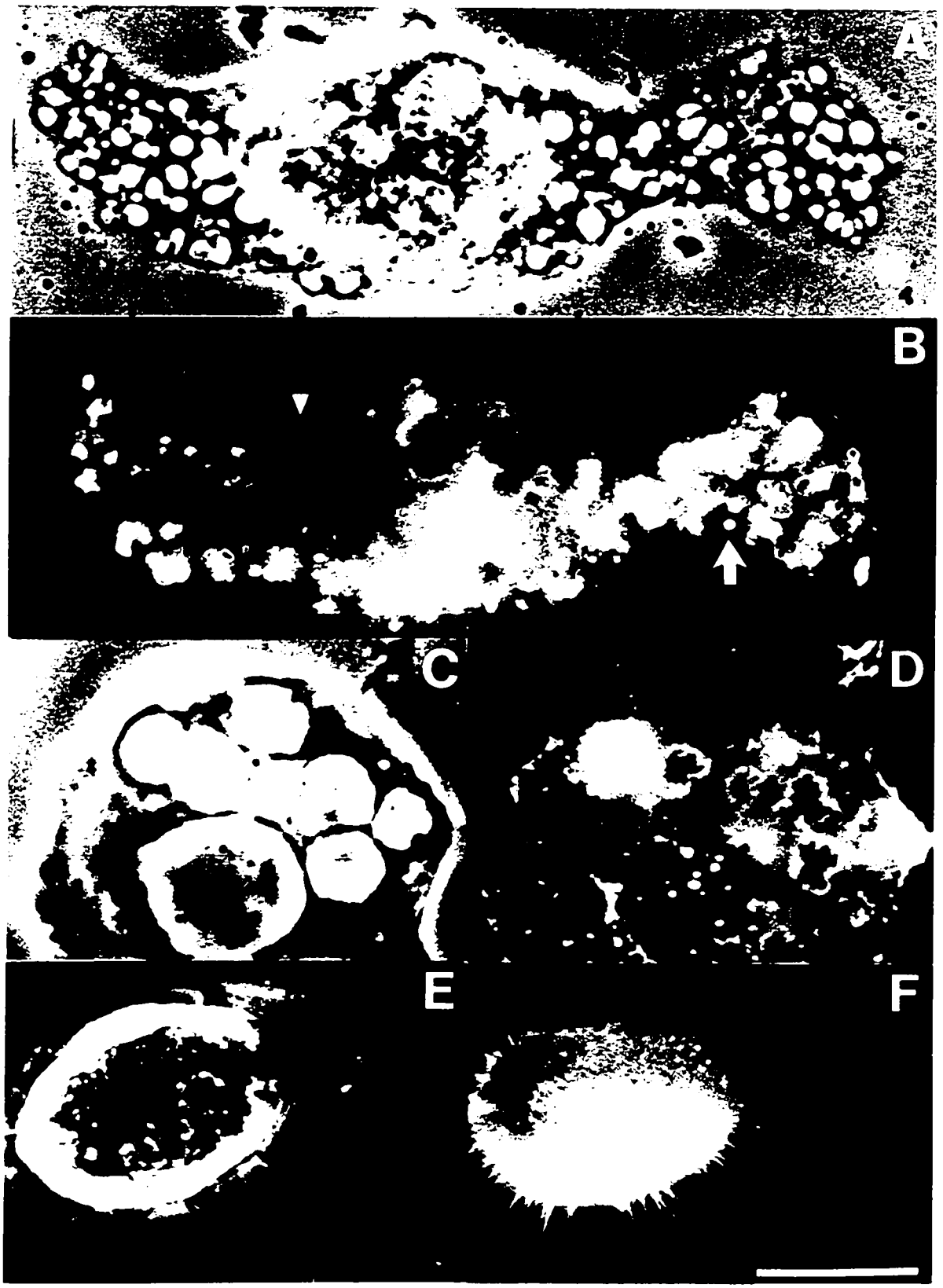
A
B
C
D
E
F

Figure 3.4 The effects of cytochalasin B. A neuron (A) after a 20 minute incubation in 10μM CB. CB had no effect on the morphology or appearance of the neurons in phase contrast (A), however. F-actin associated with filopodia were absent (B) and CB resistant puncta were noted (arrow in B). Neurons likewise treated with CB for 20 minutes produced abundant VLDs (C). These VLDs were not, however, associated with actipodia at the substrate but large CB resistant F-actin puncta persisted (D). The inset to D, an enlargement of VLDs from the mid growth cone region, show that peri-VLD staining was faint and no greater than the background. Scale bar: 24μm in A, B. 20μm in C, D and 14μm in inset.

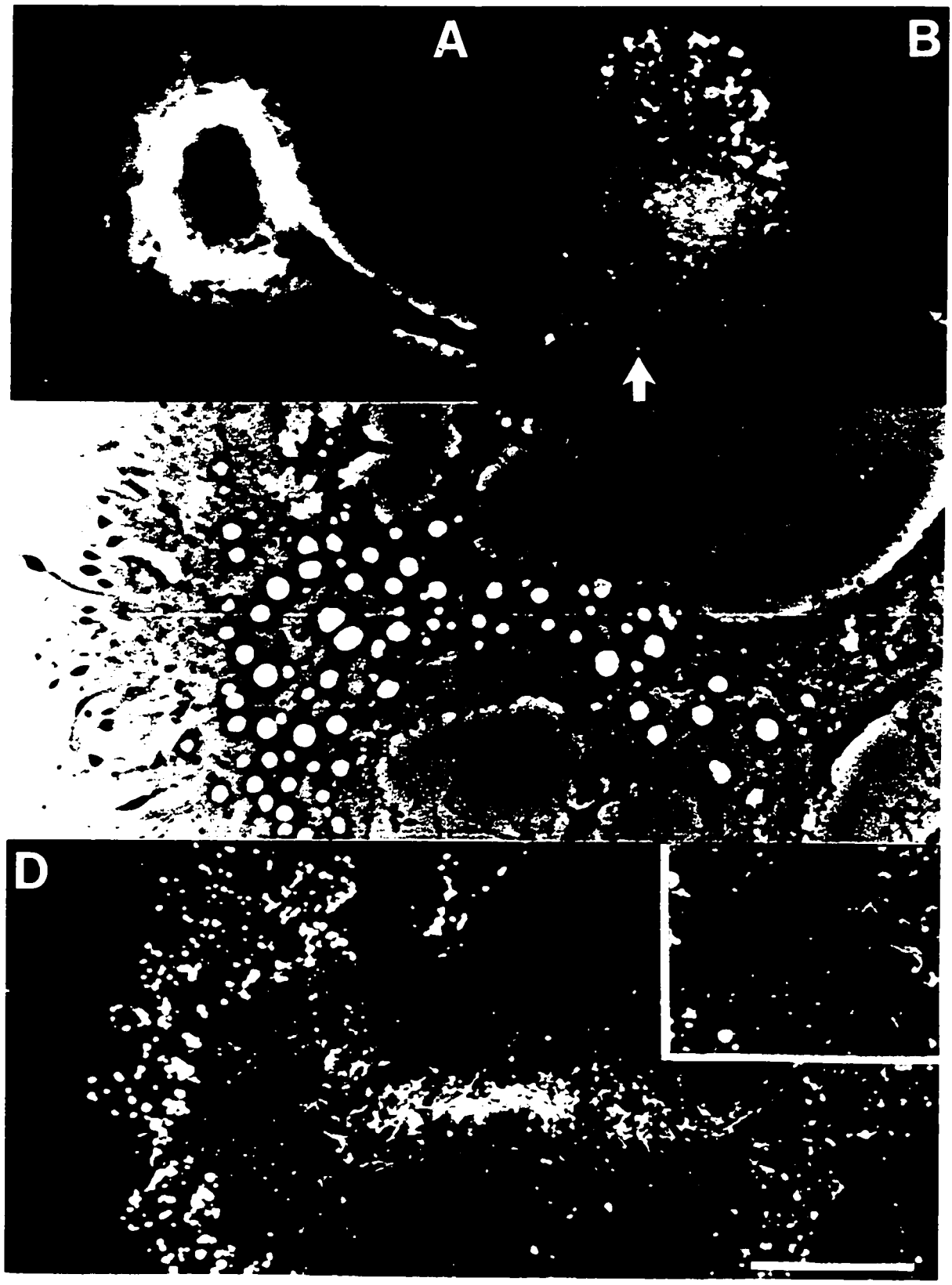
A
B
D

Figure 3.5 Prolonged exposure to hyposmotic medium. This neuron (A in NS, B in 50% NS for 60 minutes, C in 50% NS for 70 minutes) illustrates that VLDs appear in neurons exposed to hyposmotic conditions. By 70 minutes, the neuron not only has VLDs but is retracting its swollen lamellar process (arrows). Such behaviour has the hallmarks of slow regulatory volume decrease, though measuring the volume is not feasible. Scale bar: 10μm.

Figure 3.6 High resolution microscopy images of neurons stained with bodipy phallacidin. Typical F-actin staining of a neuron not induced to form VLDs (A, B). Comparison of A and B show that filopodia at the neuron's edges (A) are F-actin rich and that puncta are normal F-actin structures (B). Three different neurons (C-E) induced to form VLDs, fixed 5 minutes after being placed in NS. Actipodia in each neuron had similar characteristic features exhibited by that same neuron's filopodia. Scale: 5μm.

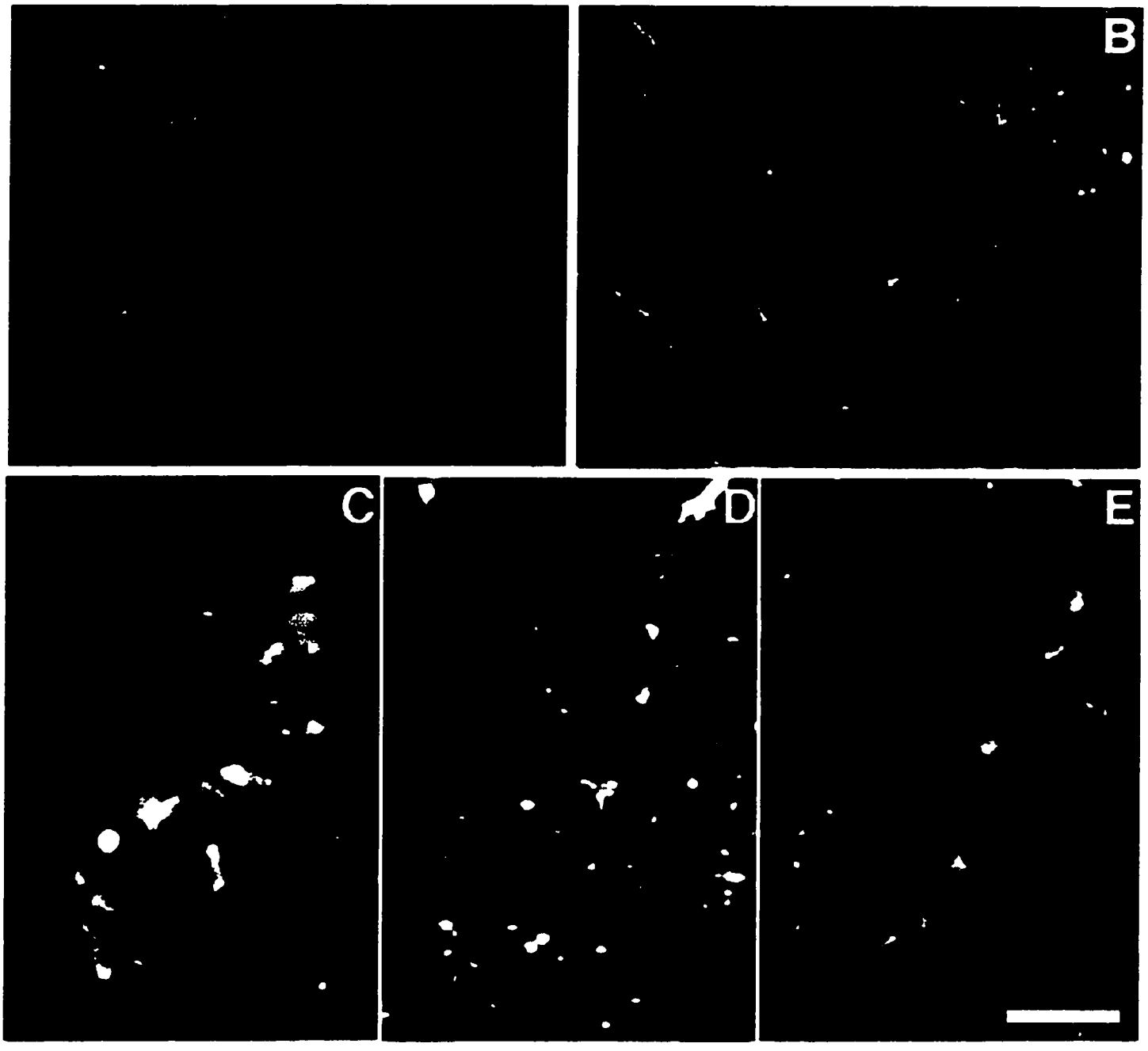
B
C
D
E

Figure 3.7 F-actin associated with VLDs. VLDs from 3 neurons (A-D, E-G, H-J) that had undergone a swell/shrink stimulus and were fixed 5 minutes after being shrunk. The phase contrast images taken at the substrate (A, E, H) or above (C) show the location of the VLDs, whereas the fluorescent images (B, D, F, I, J) showed the F-actin staining pattern colocalized around VLDs. Many small VLDs at the substrate (B) were either surrounded by F-actin rich actipodia (arrowhead) or were close to pinching off (arrow). Above the substrate, VLDs had a more rounded appearance (C) and were still surrounded by F-actin (D). E-G further illustrate VLDs (E) with actipodia at their substrate (F) and F-actin extending upward (G). In F, actin filaments or bundles are evident at the substrate. H illustrates how large and small VLDs close together can have extreme F-actin density differences. Modifications to the contrast settings allowed for visualization of actipodia at smaller VLDs (I), whereas no modifications did not (J). Scale: 5μm.

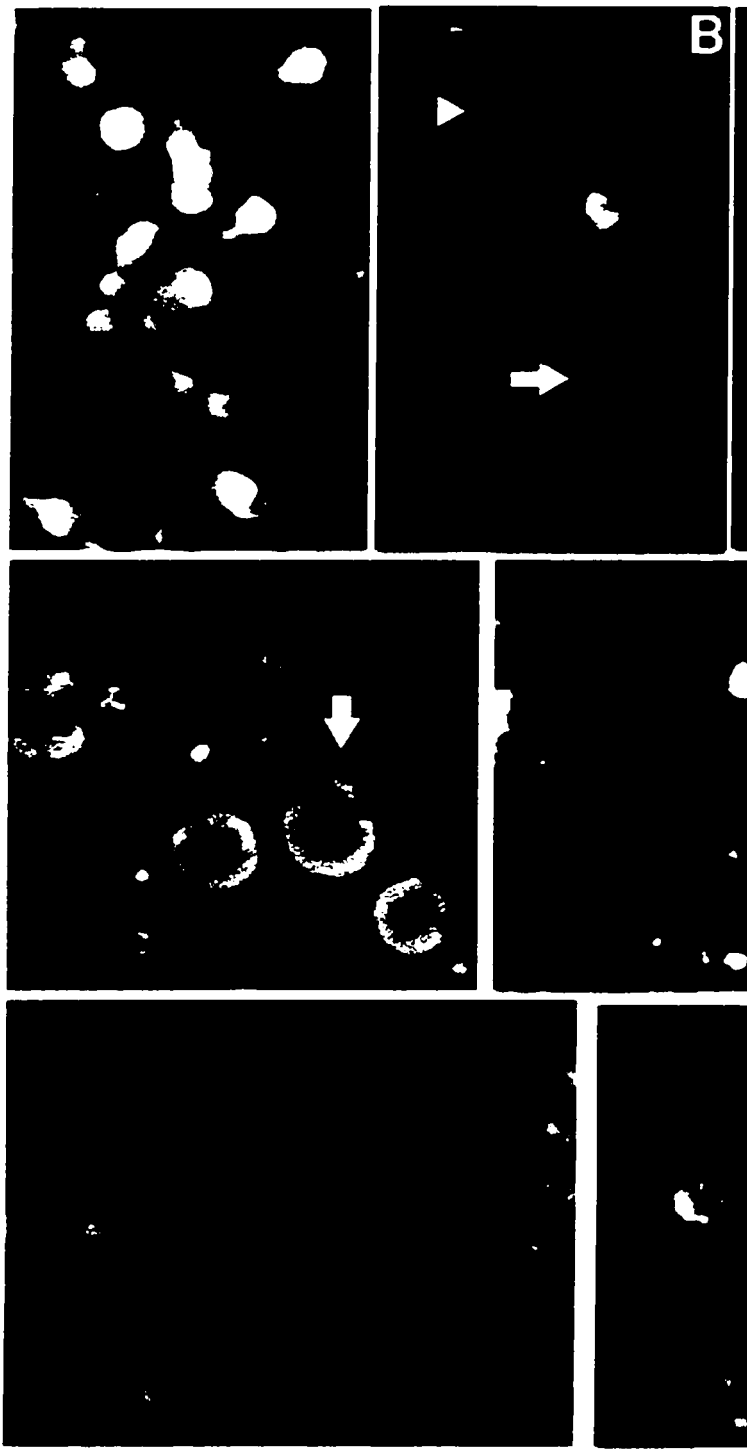
B

Figure 3.8 Neuronal actipodia in live time-lapse video-enhanced DIC microscopy. Above the substrate (A) no actipodia were observed but were evident upon refocusing at the substrate (B). In another cell at the substrate, actipodia consisted of filopodia and lamellipodia-like structures (C). Three minutes later (D), many more actipodia were evident sweeping across the VLD opening. The graph of actipodia cycling between outgrowth and retraction was made from measurements of 3 VLDs with actipodia, from 2 different neurons, revealing that actipodia elongate at a maximum rate of 3μm/minute. VLDs in A-D are shown about 1 hour after the VLDs first formed. Scale: 10μm.

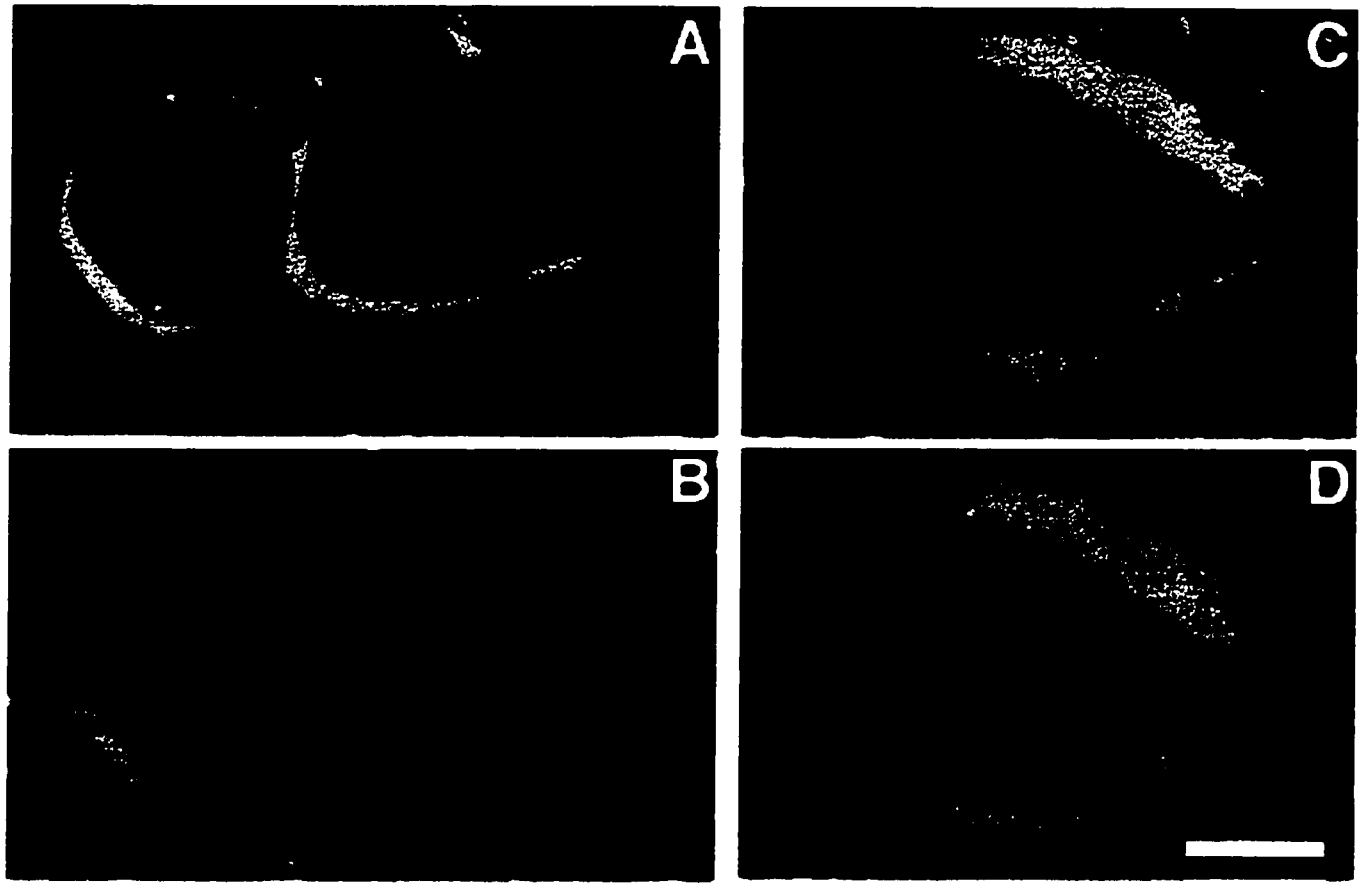
A
C
B
D

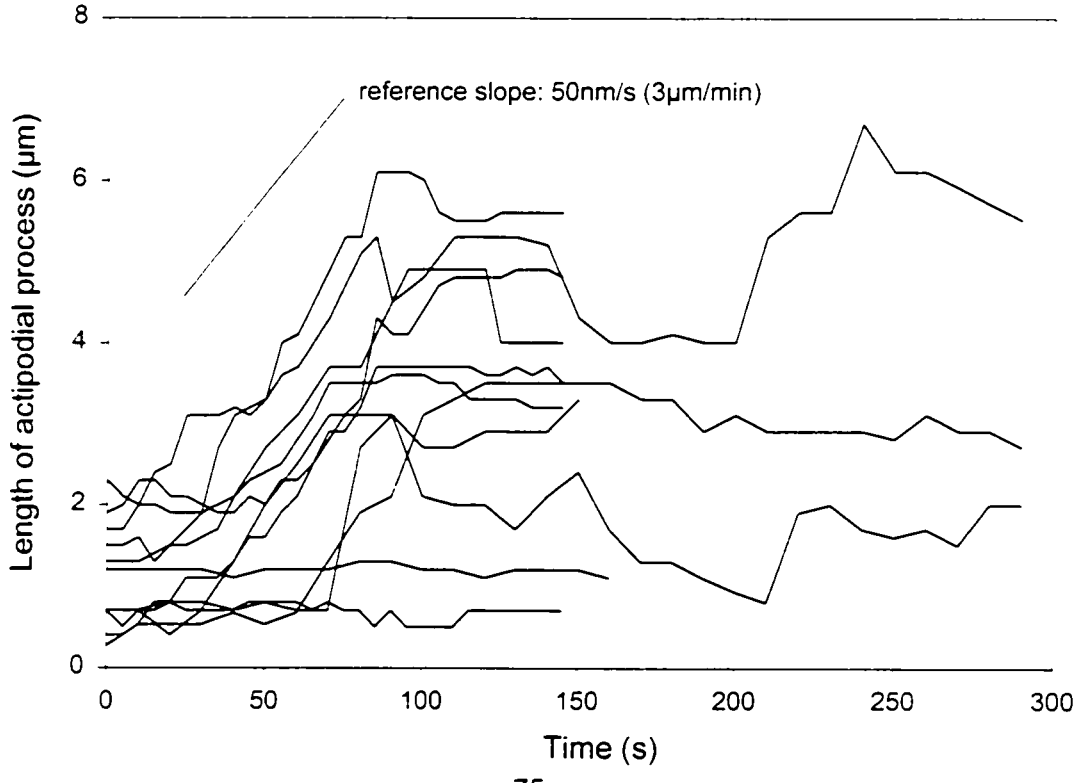
reference slope: 50nm/s (3µm/min)
Length of actipodial process (µm)
Time (s)
0
2
4
6
8
0
50
100
150
200
250
300

Figure 3.9 Fluorescent G-actin is incorporated into actipodia. Live neurons injected with rh-actin after a swell/shrink perturbation to induce VLDs (A-D). G-actin was incorporated into actin filaments and into puncta before being swollen (A). Five minutes after VLD formation, F-actin was localized around the VLD peripheries (B). Inset to B shows one VLD's association with F-actin. Fifteen minutes later, F-actin was still associated with the VLD peripheries and small actipodial structures became evident (C). Inset in C shows that F-actin staining around VLDs is phase dark. Eighty minutes after the neurons were first induced to form VLDs, two large VLDs were still associated with F-actin (D). Puncta and an overall F-actin staining pattern was likewise reappearing during this time (D). Scale: 10μm (5μm in inset to B, 8μm in inset to C).

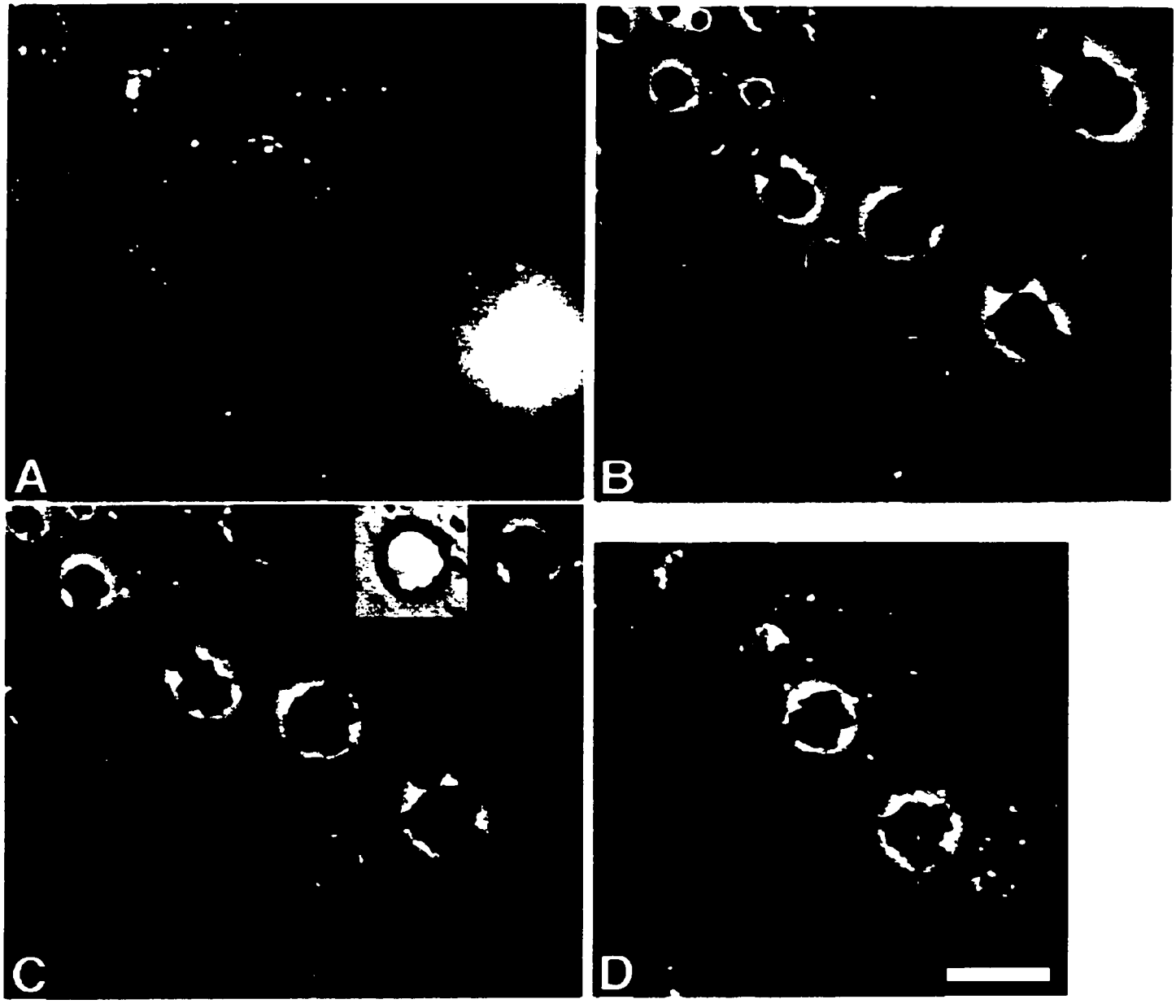
A
B
C
D

Figure 3.10 VLDs association with mitochondria and endoplasmic reticulum. Phase dark mitochondria (A) sometimes appeared to localize around the VLD peripheries, therefore to distinguish if mitochondria or F-actin were the phase dark material that surrounded VLDs, neurons were stained with rhodamine 123 (a mitochondrial stain) (B). Mitochondria sometimes encountered the VLD peripheries but were not the phase dark material that surrounds VLDs. Visualization of tubular endoplasmic reticulum was observed sometimes with video-enhanced DIC microscopy (C and D). VLD formation appeared to displace the reticulum upwards but there was no indication that these structures associated with the VLD membrane and upon VLD recovery, the reticulum was still evident (D). Scale: 10μm A, B and 5μm C, D.

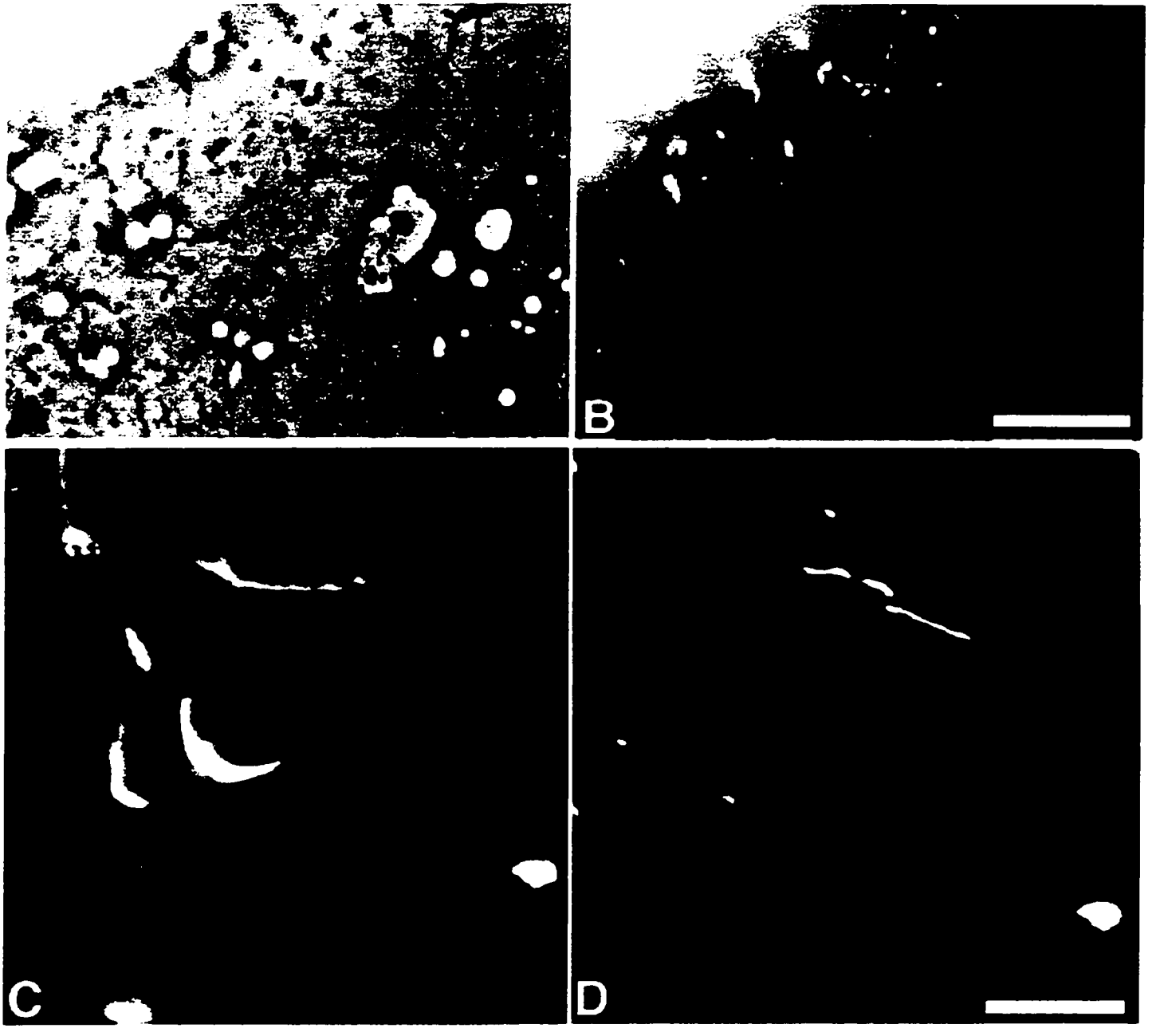
B
C
D

DISCUSSION

We have shown using *Lymnaea* neurons that VLDs, shrinking induced plasma membrane invaginations at the substrate-adherent surface, become surrounded by F-actin within minutes of formation. Using conventional and high resolution light microscopy we found that at the substrate, adjacent to VLDs, F-actin reorganizes into a ring of leading edge, which we have termed actipodia. Above the substrate, F-actin is organized as a continuous coat over the VLD membrane. Since F-actin is depolymerized upon swelling (Ziyadeh *et al.*, 1992; Cornet *et al.*, 1993 and 1994; Czekay *et al.*, 1994; Mills *et al.*, 1994; Morán *et al.*, 1996), we assume that in the shrinking neurons F-actin did not just reorganize, but actually repolymerized *de novo* around the VLD peripheries, as actin-rich actipodia. The tight coupling between VLDs and actipodia suggests that F-actin may organize into actipodia by responding to a signalling system that is activated by the same mechanical forces that drive VLD formation.

Actipodial formation was dependent on a shrinking perturbation. Neurons formed actipodia whether the neuron had been swollen then shrunk or hyperosmotically shrunk. In live neurons, actipodial formation and dynamics were only clearly observed in the larger VLDs. Smaller VLDs had continuous F-actin coats, but at the substrate their actipodia were more difficult to resolve because the smaller size and because some were constricted. Previous observations revealed that smaller VLDs tended to pinch off (Reuzeau *et al.*, 1995). Perhaps then the smaller F-actin rich VLDs that we observed here, pinched off more readily and are therefore better constrictors. However, this needs to be tested by monitoring the internalization of VLDs filled with bath dye while also monitoring how the VLD associated actin responded during VLD recovery. Regardless of the VLD size, F-actin repolymerization occurred around the VLD peripheries and since we know that cells incubated in CB do not undergo VLD recovery (Reuzeau *et al.*, 1995), F-actin is therefore required for this process to ensue. Since the dilating membrane that VLDs arise from behaves as if it is under higher tension than membrane elsewhere in the cell (and therefore acts as a sink for lipid bilayer material at lower tension), repolymerization of F-actin, as actipodia, may ultimately lead to the pinching off and reinternalization of VLD membrane.

Actipodia-like structures were also not seen during short term exposures to hyposmia and

the VLDs seen in long term exposures have not yet been examined for actin. Had we viewed the prolonged hyposmotic exposed neurons (ie. fig 3.5) by high resolution microscopy or developed a protocol to fix and stain these neurons, we predict that actipodia would have been observed.

Fixed and live experiments both indicated that actipodia were always associated with a VLD. No actipodia were ever observed without a VLD and actipodia persisted until VLDs had recovered in normal saline. We therefore suspect that as VLDs are beginning to form, elevated tension at the VLD initiation sites simultaneously communicates to and stimulates actin polymerization machinery adjacent to VLD membrane, therefore making this a preferred site of actin repolymerization. Even though actipodia represented the preferred sites for actin polymerization, individual actipodia were not uniformly stained, some appeared to be actin free at the time of fixation and neighbouring actipodia could be vastly different in their F-actin content. Evidently some actipodia were substantially better at recruiting actin than others. Presently we can suggest no explanation for this.

In all the fixed *Lymnaea* neurons stained for F-actin, small fluorescent puncta were observed whether the neuron had been osmotically perturbed or not. It is not likely that these were an artefact of the fixation procedure because the live microinjected cells also exhibited fluorescent puncta (fig 3.9). Previous researchers have microinjected G-actin into a variety of cell types (Taylor and Wang, 1978; Kreis *et al.*, 1979; Glacy, 1983; Amato and Taylor, 1986; Okabe and Hirokawa, 1989 and 1991) and from these studies it was discovered that the injected G-actin enters the endogenous actin pool, undergoes protein turnover (Kreis *et al.*, 1979), behaves like native actin and is incorporated at the membrane associated ends of pre-existing filaments (Okabe and Hirokawa, 1989). Therefore we are confident that the fluorescent puncta in the fixed and live neurons are real actin structures.

Lymnaea neurons with or without VLDs also exhibited F-actin puncta after incubation in CB. CB induced puncta are commonly seen in a variety of cell types (Norberg *et al.*, 1975; Weber *et al.*, 1976; Letourneau *et al.*, 1981; Schliwa, 1982; Forscher and Smith, 1988; Cornet *et al.*, 1993; Levina *et al.*, 1994). The relation of CB-induced puncta to punctate F-actin in control neurons and non-CB neurons with VLDs is unknown. Forscher and Smith (1988) hypothesized that punctate aggregates remaining after CB incubation may become areas of actin repolymerization after CB

washout.

F-actin associated with surface membrane in other cell types

Observations of filamentous actin surrounding membrane invaginations are not unprecedented. Actively growing yeast exhibit finger-like plasma membrane invaginations surrounded by actin filaments (Mulholland *et al.*, 1994). It was proposed that because cell wall material is deposited locally within the membrane invagination, the invaginations enable yeast to insert new cell wall in the face of osmotic (turgor) pressure.

Macrophages reorganize their F-actin into actin-rich phagocytic cups around *Toxoplasma gondii* during phagocytosis of this protozoan parasite (Morisaki *et al.*, 1995). Within 2-4 minutes the host cell invaginates its plasma membrane into a phagosome and reorganizes its F-actin.

Inductopodia, comet tail-shaped structures rich in F-actin, form behind polycationic beads applied to the extracellular surface of cultured *Aplysia* bag cell growth cones (Forscher *et al.*, 1992). Inductopodia form immediately upon bead binding and grow to about 5µm in 1 minute. Negatively charged beads or beads treated with blocking proteins (albumens) do not stimulate inductopodia formation. Inductopodia formation was due to bead-induced actin filament assembly since CB reversibly inhibited inductopodia elongation. It was concluded that positive charges on the bead surfaces might sequester or recruit endogenous actin nucleating proteins thus stimulating actin filament assembly. This rapid site-directed actin filament assembly at a new adhesive zone may share some mechanisms with the rapid induction of actipodia.

Membrane tension and the reconfiguration of F-actin

The 50% osmotic perturbations used here to generate VLDs produced only minor changes in intracellular calcium (Herring *et al.*, 1998). Therefore *Lymnaea* neurons were useful for studying tension's possible role in surface area regulation, independent of any calcium responses. We hypothesized that changes in membrane tension, brought about by swelling and shrinking, were a likely candidate to instruct neurons to regulate their surface area, and by extension, their membrane-associated cortical actin cytoskeleton. Shrinking neurons formed new leading edge-like

structures, actipodia, at VLD substrate openings. If the membrane tension hypothesis for VLD formation is correct, then these leading edges may have formed in response to high tension signals.

Present models of how neurons grow and elongate incorporate tension (Bray *et al.*, 1991; Zheng *et al.*, 1991; Lin *et al.*, 1995; Dai and Sheetz, 1995a and b). In a seminal paper entitled "Direct evidence that growth cones pull", Heidemann and colleagues first reported that a direct and linear relationship existed between neurite force and growth cone advance (Lamoureux *et al.*, 1989). Pulling of chick sensory neuronal somata caused increases in neurite tension, which resulted in advance of the growth cone and net neurite elongation. No increase in neurite tension occurred in neurite growth cones that failed to advance. This was followed up by observations that membrane tension increases in pulled chick sensory neurons at cell body margins without existing neurite outgrowths, caused initiation of new neurites (Zheng *et al.*, 1991). Pulled neurites had growth cones capable of motility, axons capable of elongating and microtubular arrays, all characteristics of "normal" neurite development. Next they compared the rates of elongation of pulled chick sensory neuronal growth cones in osmotically diluted saline to isotonic saline (Lin *et al.*, 1995). They observed that neurons pulled in a 50% osmotically diluted saline elongated 50-300% faster than neurons pulled in isotonic saline. Therefore neurons appeared to respond to membrane tension increases by producing new outgrowth or elongating previously formed extensions; which would be consistent with our hypothesis of membrane tension increases eliciting membrane addition. By analogy, dilating VLD membrane can be viewed as growth cone membrane experiencing a membrane tension increase. In the same way that growth cones respond to tension increases by forming or elongating leading edge, we postulate that VLD initiation sites experience increased membrane tensions so that VLD enlargement should likewise stimulate formation of new leading edge (ie. actipodia).

Actipodia form regardless of whether neurons shrink in hypertonic saline or shrink in isotonic saline after a swelling perturbation. Bray *et al.* (1991) observed that filopodial outgrowth in embryonic chick sensory neurons was stimulated upon shrinkage. We only observed actipodia, which we interpret to be new leading edge, upon shrinking. This adds to our confidence that cellular tensions associated with shrinking may be the signal which stimulates the formation of new

leading edge.

CHAPTER 4: THE SPECTRIN SKELETON LINES OSMOTICALLY INDUCED VACUOLE-LIKE DILATIONS

INTRODUCTION

Spectrin and fodrin are filamentous, dimeric cytoskeletal proteins which form a network that lines and, it is assumed, supports the plasma membrane. Spectrin was first discovered in erythrocytes and was for many years thought to be an erythrocyte specific protein (Hiller and Weber, 1977). Later, Goodman *et al.* (1981) discovered spectrin-like proteins in embryonic chicken cardiac myoblasts and another term, fodrin, was used to distinguish these 2 proteins (Levine and Willard, 1981). Fodrin was subsequently found in almost all cells studied and it was proposed that the spectrin family name be changed to fodrin, due to fodrin's more general cellular expression (Glenney and Glenney, 1983a and 1983b), but this never gained acceptance. Confusion was compounded when it was shown that the "erythrocyte specific" protein, spectrin, is also expressed in brain and muscle cells.

The mammalian spectrin/fodrin proteins are derived from 4 genes: one for each α-fodrin, β-fodrin, α-spectrin and β-spectrin (Porter *et al.*, 1997). An initiative to reorganize spectrin family nomenclature has been proposed (Winkelmann and Forget, 1993) but there is still confusion as many researchers continue to use the term spectrin when in fact they are studying fodrin, or do not specify which protein, erythroid-like or non-erythroid, is being studied in cells that express both classes. In this thesis spectrin refers to the erythroid-like gene products found in erythrocytes and several other cells, while fodrin refers to everything else; ie. the gene products of the homologous non-erythroid gene which are expressed in all cells except erythrocytes. "Spectrin skeleton", however, we use to refer collectively to whichever spectrin family constituents and associated proteins happen to be present in whichever membrane skeleton is being discussed.

In erythrocytes, spectrin is a heterodimer of α-spectrin and β-spectrin subunits which associate head-to-head, yielding a 100nm dimer of approximately 460kDa (Speicher and Marchesi, 1984) (fig 4.1). Two heterodimers then associate in an anti-parallel manner, yielding a 200nm tetramer. Both the α and β subunits are composed of homologous 106 amino acid repeat segments, a distinguishing feature of the spectrin protein family. Each 106 amino acid segment

is folded into triple helical segments and connected to the next 106 amino acid helical segment by flexible non-helical regions (Speicher and Marchesi, 1984). Spectrin is attached indirectly to the plasma membrane by two protein linkages (fig 4.1). One occurs between a β-spectrin carboxy (C) terminal region and ankyrin, a globular protein connected to the cytoplasmic domain of the transmembrane integral protein, band 3 (Dhermy, 1991). A second linkage occurs between the β-spectrin amino (N) terminus and protein 4.1, which is thought to bind to transmembrane glycophorins (Dhermy, 1991), small erythrocyte specific glycoproteins that carry 90% of the surface carbohydrates found in erythrocytes (Alberts *et al.*, 1989). The β-spectrin N terminus also has an F-actin binding site, which binds short F-actin strands (about 15 monomers in total) cross-linked by spectrin tetramers.

Spectrin and fodrin belong to a common protein family with extensive cDNA homology (Winkelmann *et al.*, 1990a), whose distinguishing characteristics include: 106 amino acid repeat segments in the α and β subunits, heterodimers that form head-to-head associations resulting in tetramer formation, ankyrin binding sites on β-subunits, formation of junctional complexes with actin and band 4.1 and similar molecular weights (Dhermy, 1991).

Spectrin's function in erythrocytes is to support or to stabilize the plasma membrane (Burridge *et al.*, 1982; Goodman and Shiffer, 1983; Bennett, 1985; Marchesi, 1985). While circulating, erythrocytes undergo elastic deformations and their ability to preserve their integrity, shape and elasticity is due to the flexible spectrin and actin cytoskeleton (Gratzer, 1981). The spectrin-actin cytoskeleton creates a membrane associated scaffold or framework beneath the erythroid plasma membrane (Burridge *et al.*, 1982; Goodman and Shiffer, 1983; Bennett, 1985; Marchesi, 1985). The low intrinsic rigidity and linearity of erythroid spectrin underlies its overall flexibility (Coleman *et al.*, 1989). This flexibility allows the spectrin network to reversibly deform by elongating or unfolding when faced with perturbations (Goodman *et al.*, 1988; McGough and Josephs, 1990; Ursitti and Wade, 1993; see fig 4.1Bi and Bii).

Muscle β-spectrin refers to the products of the erythroid-like gene expressed in muscle cells, whereas muscle α-fodrin and muscle β-fodrin refers to the products of the non-erythroid gene, also expressed in muscle cells. The only feature that distinguishes the muscle β-spectrin protein from

the erythrocyte β-spectrin protein is that the muscle β-spectrin C terminus amino acid coding sequence is different and longer (Winkelmann *et al.*, 1990b; see fig 4.1A). This difference arises from alternate splicing (Winkelmann *et al.*, 1990b) which yields different β-spectrin pre-mRNA and structurally different β-spectrin isoforms in erythrocytes, skeletal muscle and brain (Winkelmann *et al.*, 1990b). Muscle β-spectrin evidently combines with α-fodrin in muscle; there is little evidence for an erythroid α-spectrin isoform in muscle cells (Winkelmann *et al.*, 1990b).

Little is known about the function of spectrin and fodrin in non-erythrocytes. It is has been assumed that spectrin and fodrin supports the bilayer in non-erythroid cells (Porter *et al.*, 1992; De Bleecker *et al.*, 1993; Vita *et al.*, 1994; Pumplin, 1995), as they do in erythrocytes. In erythrocytes, however, spectrin makes up 75% of the cytoskeletal protein mass in erythrocytes, far more than in other cells (Glenney and Glenney, 1983a), so functional differences are to be expected.

Spectrin and/or fodrin have been shown to line vacuoles and vesicles in various cells (Bonder *et al.*, 1989; Fujimoto and Ogawa, 1989; Fishkind *et al.*, 1990a and b; De Bleecker *et al.*, 1993; Vita *et al.*, 1994). In line with this we propose that the spectrin skeleton supports the plasma membrane, not only at the surface, but also when membrane is invaginated. As such, it may play a role in the retrieval or reinternalization of VLD membrane. As discussed in the thesis introduction, VLDs are membrane invaginations which grow up to 10μm in diameter as a swollen cell is reshrinking. In order to account for what appears to be a new flow of surface membrane towards the cell interior, it is postulated that surface membrane in shrinking cells has a decreased membrane tension compared to the invaginating membrane. Therefore low tension lipid bilayer flows to high tension regions. More specifically, it is hypothesized that in shrinking cells, membrane at certain invagination points along the substrate experiences high tensions, so that excess surface membrane flows to these points which, as invagination ensues, form VLDs.

If VLDs are spectrin and/or fodrin lined, this membrane skeleton network may be drawn in by the shrinking cytoplasm. If so, it might provide a mechanism whereby the invaginating VLD membrane tension is kept at a higher level than surrounding membrane. Also given the inherent instability of large membrane vesicles (expanses of unsupported lipid bilayer tend to break into small higher curvature structures (Lipowsky, 1991; Porter *et al.*, 1992)), extensive spectrin-

membrane interactions could stabilize invaginating membrane. On the other hand, it may be that VLDs invaginate where the plasma membrane is at its weakest because it is unsupported by the membrane skeleton. Whereas the proteolytic breakdown of the spectrin/fodrin skeleton in metabolically traumatized cells is receiving much attention (Saido *et al.*, 1994; Morimoto *et al.*, 1997), surprisingly little is known of the mechanical status of membrane skeleton in mechanically perturbed cells. Erythrocytes are the exception and there the skeleton is highly extensible and hence robust (Hitt and Luna, 1994). If newly invaginated skeletal muscle membrane (ie. VLDs) proves to have a membrane skeleton, this may indicate that in non-erythrocytes, too, membrane skeleton rapidly adjusts to accommodate cell shape changes.

Ideally the molluscan neuron preparation used for the calcium and actin experiments, would have been our first choice for investigating the spectrin skeleton in conjunction with VLDs. However, available anti-spectrin and/or fodrin antibodies recognize mammalian isoforms and would probably not cross react with invertebrate spectrin. Others have used mammalian anti-spectrin antibodies to probe protozoan and plant Western blots (Kwiatkowska and Sobota, 1990; de Ruijter and Emons, 1993; Sikorski *et al.*, 1993) but immunocytochemical results with these antibodies were either lacking or generally unsatisfactory (Kwiatkowska and Sobota, 1990; Hemphill *et al.*, 1991; de Ruijter and Emons, 1993). Since VLDs form in many cell types, it was preferable to use a cell line for which good spectrin/fodrin antibodies were available. An antibody (Porter *et al.*, 1992) against a peptide representing the 16 amino acid C terminal sequence of the human skeletal muscle isoform of β-spectrin (Winkelmann *et al.*, 1990b) was used in these experiments (gift of Dr. Robert Bloch, University of Maryland). This polyclonal antibody, called 4I12, recognizes the C terminal oligopeptide sequence of both muscle β-spectrin and muscle β-fodrin (Porter *et al.*, 1997) (fig 4.1). In adult rat muscle, it recognizes β-spectrin immunocytochemically (Porter *et al.*, 1992) and β-spectrin and β-fodrin by Western blotting (Porter *et al.*, 1997). For convenience, therefore, L6E9 rat skeletal muscle myotubes were used for eliciting VLDs. Experiments performed by Jenni McNally, a summer student in our lab, showed that skeletal myotubes of this cell line, formed VLDs via swelling and then shrinking (fig A.1A, B, and C), that the VLDs reversed upon reswelling, forming repeatedly at the same sites (fig A.1D and E), and recovered (fig A.2) as molluscan

neuronal VLDs do (relevant methods and figures are presented at the end of this thesis in the appendix). Jenni used a 4 minute/50% swelling perturbation and found that 3-4 minutes after myotubes had been shrunk, on average 8 VLDs formed per myotube. The average diameter of the measured VLDs was 2μm. However this is probably an overestimate. If the data are plotted as a frequency distribution of VLD sizes (fig A.3) and fit with a single exponential, an exponential decay constant of 1μm is obtained. Myoblasts, the mono-nucleate muscle cell precursors that fuse together to form multi-nucleate myotubes, did not form VLDs. Why only multi-nucleate myotubes were competent to form VLDs was not investigated further. Unlike *Lymnaea* neurons, rat skeletal muscle myoblasts and myotubes bleb during swelling (fig A.1B). The blebs were retrieved during shrinkage and VLD formation. Damaged, spreading or swelling cells often bleb (Wilkerson *et al.*, 1986; Cunningham, 1995). Blebs are plasma membrane that has become separated from the underlying cortical cytoskeleton (Dai and Sheetz, 1995b). In particular, bleb formation occurs when the rate of cell membrane expansion exceeds the rate of actin polymerization (Cunningham, 1995). Jenni prepared Western blots on myoblast cultures and mixed myoblast/myotube cultures using the 4I12 antibody. This antibody labelled one protein of at least 235kDa in L6E9 myoblasts and myotubes (fig A.4). In adult rat skeletal muscle cells, the 4I12 antibody labelled two proteins of 265 and 275kDa, muscle β-spectrin and muscle β-fodrin, respectively (Porter *et al.*, 1997). Previous investigations into chicken and rat muscle myogenesis revealed, however, that embryonic myotubes, such as L6E9 cells, contain muscle β-fodrin and very little muscle β-spectrin (Nelson and Lazarides, 1983 and 1985; Zhou *et al.*, 1998). Upon adult muscle differentiation muscle β-fodrin is replaced with muscle β-spectrin (Zhou *et al.*, 1998). The protein recognized by the 4I12 antibody in the rat myoblast and myotube Western blots may have been muscle β-spectrin and/or muscle β-fodrin since our antibody was specific for both proteins. We, therefore, use the term spectrin skeleton to refer to both proteins. The next step, immunocytochemically localizing the spectrin skeleton in L6E9 myotubes in relation to the VLD membrane, using the 4I12 antibody, is presented here.

METHODS AND MATERIALS

Cells and Solutions

Rat embryonic skeletal muscle (L6E9) cells (provided by Dr. Micheline Paulin-Levasseur, University of Ottawa) were cultured in 75cm^2 Falcon tissue culture grade flasks (Becton Dickinson, Lincoln Park, NJ) containing 50mL of α-minimum essential medium (α-MEM) (Gibco BRL, Grand Island, NY) composed of 10% fetal bovine serum (FBS) and 1% streptomycin/penicillin in a tissue culture incubator (37°C, 5% carbon dioxide) until reaching sub-confluency. The α-MEM solution was then removed and 10mL of PBS was added to washout any remaining FBS. PBS was removed and 1mL of 0.05% trypsin-EDTA in PBS (Gibco BRL, Grand Island, NY) was added briefly to detach the cells. Once the majority of cells had detached, 5mL of α-MEM was added to stop the trypsin's action. This solution was pipetted out of the flask, an aliquot was put on a hemocytometer and the rest in a 15mL centrifuge tube and centrifuged for 5 minutes at 1000rpm. During centrifugation a cell count (cells per 10^4 mL) was done. After being centrifuged the α-MEM supernant was pipetted off and the cells were resuspended in the same volume of fresh α-MEM. To another 15mL tube containing 10mL of α-MEM, a volume of resuspended cells was added to give $1x10^5$ cells per mL. One mL of this cell suspension was added to each well of a 24 well Falcon tissue culture dish (Becton Dickinson, Lincoln Park, NJ). Autoclaved 12mm round glass coverslips (VWR Scientific, Media, PA) had been previously placed in each well. The cells were cultured to confluency, approximately 2 days, then α-MEM was replaced with 1mL of fresh α-MEM containing 2% FBS and 1% streptomycin/penicillin. Lowering the serum concentration initiated membrane fusion between adjacent, touching myoblasts. This medium was changed every 2-3 days. After about 2 weeks in the lowered α-MEM serum, the majority of the cells had become large multi-nucleate myotubes and were used for immunocytochemistry.

Fixation and immunocytochemistry

Cells were washed in L6 normal saline (L6NS) to remove culture media. L6NS was composed of (in mM): 150 NaCl, 2 KCl, 2 $CaCl_2$, 1 $MgCl_2$, 5 HEPES, 11 glucose; pH 7.4, 312mosM as determined by the Advanced MicroOsmometer (model 3M0). To increase the yield of VLDs per cell, a longer, larger swelling stimulus was used than in Jenni's experiments. All solution changes

were done 3 times. VLDs were elicited by swelling in 30% L6NS (made dilute by the addition of distilled water) for 10 minutes and then shrinking in L6NS for 3 minutes. Controls were maintained in L6NS with no osmotic perturbation. To preserve antigenicity and cell morphology, fixation was done on ice by adding -20°C methanol for 5 minutes (fixation in paraformaldehyde was first tried but not used as it induces VLD-like structures during fixation). Fix was added approximately 3 minutes after myotubes were restored to L6NS. Coverslips were then removed from the plastic culture dish and placed into a glass petri dish on ice and extracted by adding -20°C acetone for 1 minute (Czar *et al.*, 1996). Only 4 coverslips were fixed and extracted at any one time. The coverslips were transferred to 60mm round plastic Falcon dishes (Becton Dickinson, Lincoln Park, NJ) for 1 hour preincubation in blocking solution (blocking minimizes non-specific binding of the primary and secondary antibodies) containing 0.1% bovine serum albumin (BSA)(Gibco BRL, Grand Island, NY) in PBS. Coverslips were inverted onto 30µL of the primary polyclonal rabbit anti-human antibody 4I12 (diluted 1:500 in 0.1% BSA in PBS) for 1 hour at room temperature. The antibody drops were on parafilm in a humid chamber. Cells were washed 3 times, 10 minutes each, in 0.1% BSA in PBS, then inverted onto 30µL of the secondary goat anti-rabbit antibody conjugated to Cy2 (diluted 1:50 in 0.1% BSA in PBS) (Jackson Labs, Mississauga, ON) again in a humid chamber for 1 hour. Cells were washed 3 times, 10 minutes each, in 0.1% BSA in PBS, quickly dipped into a beaker of double distilled water to remove any salts, air dried for about 1 minute and then mounted in mowiol on glass slides. All slides were processed as above except some control cells were not incubated in the primary antibody but only in the secondary antibody to see if the secondary antibody fluorescence was producing a background signal. At least three slides of every experimental and control treatment were made and viewed.

Viewing of fixed cells

Cells were viewed and imaged with a Bio-Rad MRC 1024 laser scanning confocal microscope (Hemel Hempstead Herts, UK) fitted with a Krypton-Argon laser. A 60x oil immersion PlanApo objective (N.A. 1.4) and a universal dry condenser (N.A. 0.85) was fitted onto an Olympus IX70 inverted microscope. Each field of view was simultaneously captured in phase-contrast and

fluorescence microscopy using Lasersharp acquisition software (Bio-Rad, Hemel Hempstead Herts, UK). The 488nm laser line was used to excite the Cy2 secondary antibody using a laser power of 3% unless otherwise stated. A 522nm emission/barrier filter was used and all fluorescent images were Kalman filtered online (essentially this procedure averages multiple replicates, thereby enhancing resolution; 6 were generally averaged). A survey view of the myotubes was always taken to localize the VLDs and to compare the spectrin skeleton staining pattern to the VLD locations and then zoomed images were obtained from selected regions. Z series were routinely done using the system's focus motor to investigate the staining differences in the spectrin skeleton throughout the myotube, beginning at the substrate.

Image Processing

Images were digitally processed in Confocal Assistant 4.02 (free software written by Bio-Rad for handling their proprietary ".pic" image files). The digital filters used in Confocal Assistant were brightness, contrast, gamma and sharpen. These filters were used to adjust the phase contrast and fluorescent images to optimize important cellular features associated with the plasma and VLD membranes with respect to the spectrin skeleton staining. To view z series stacks as single images, Confocal Assistant's "projection" was used either in the average pixel or maximum pixel mode. All images were then assembled in Corel Photo Paint and Corel Draw. Magnifications were obtained directly using image-specific scale bars from Lasersharp processing software (Bio-Rad, Hemel Hempstead Herts, UK) transferred into Corel Draw at the same time as the image.

RESULTS

The multinucleate L6E9 myotubes were very flat cells, approximately 2-3µm thick. By contrast the majority of published spectrin and/or fodrin immunocytochemistry deals with muscle biopsy tissue (De Bleecker *et al.*, 1993; Vita *et al.*, 1994) or acutely isolated adult rat muscle (Porter *et al.*, 1992 and 1997), preparations in which the cells have a larger cross-section than L6E9 myotubes. The thinness of the L6E9 myotubes affects the staining profiles obtained since, with only 2-3µm from substrate plasma membrane to the top of the cell, immunopositive structures often

passed tangentially or obliquely (rather than perpendicularly) through the image plane. The 4I12 antibody was appropriate for L6E9 cells in that it was able to detect, by Western blotting, strong single bands in the molecular weight range expected for the spectrin skeleton in L6E9 myotubes and myoblasts (fig A.4). This antibody was likewise able to detect the spectrin skeleton immunocytochemically. Controls without the primary antibody (fig 4.2A and B) showed very little non-specific binding of the fluorescent secondary antibody, only enough to faintly distinguish cell from non-cell. Figure 4.2A is a phase contrast image of a control (no osmotic perturbation) myotube or possibly 2 recently fused myoblasts.

Myotubes and myoblasts incubated in the primary and secondary antibodies but not osmotically perturbed to form VLDs, showed distinct plasma membrane staining at the cell margins and also a variable amount of diffuse intracellular staining (fig 4.2C and D). This view was focused closer to the substrate than to the top surface of the cells. Myotubes incubated in the secondary antibody only showed minimal background staining and absolutely no tendency to stain preferentially in the regions where plasma membrane would be expected, whereas myotubes stained with the secondary antibody plus the 4I12 antibody were much brighter than the controls. It seems certain, therefore, that the staining pattern observed represents the muscle spectrin skeleton. Staining was most distinct at the myotube margins, which is what is expected for the spectrin skeleton, a protein that is an integral part of the plasma membrane cytoskeleton, and that locates at the cell margins via attachments to membrane proteins (Winkelmann and Forget, 1993).

Immunostaining of VLD-bearing myotubes revealed that the spectrin skeleton colocalizes with the VLD plasma membrane (fig 4.3). The focal plane for this view is similar to that in figure 4.2C and D, closer to the substrate than the top of the cells. Figure 4.3A and B illustrate a myotube in which large and small (arrows) VLDs, visible in phase contrast, are seen in the fluorescent pair to be lined by the spectrin skeleton. In the control cells which had not been subjected to the swell/shrink protocol, there was no evidence of either VLDs (as seen in phase contrast) or of fluorescent rings. The intensity of stain associated with VLDs did not correlate with how large the VLDs were. Figure 4.3C and D illustrate a myotube with a particular large VLD and with bead-like strings of phase bright structures (arrows). These structures were commonly seen in both control

(fig 4.3E) and experimental (VLD) myotubes and are neither a fixation artefact nor small VLDs. They were not positive for the spectrin skeleton (fig 4.3E and F). Thus circular spectrin skeleton profiles localized at VLDs is a pattern dependent on the formation of VLDs: it is not explained by pre-existing spherical or tubular cellular structures.

Spectrin skeleton staining was also investigated in confocal sections of various distances from the substrate, to determine if the spectrin skeleton colocalized around the VLD membrane as it pushed deeper into the cell interior (fig 4.4). Confocal z series were obtained, beginning at the substrate and stepping up to the top of the VLD or to the top of the myotube. Figure 4.4A is a fluorescent image generated from a z series projected as a single image to give a three-dimensional effect. Figure 4.4B and C are individual sections from the same myotube but shown at different levels above the substrate. Arrows locate the same points in A, B and C. B is near the top of the myotube, 2.4μm above the substrate, whereas C is closer to the bottom, 0.8μm above the substrate. Notice that some VLDs were evident near the substrate but were not evident farther up (eg. VLD at arrow). Likewise some VLDs evident higher up in the myotube were not evident closer to the substrate (eg. VLD at arrowhead). Assuming that VLDs were stained over their entire surface, this suggests that some of the VLDs had become pinched off at the time of fixation. The VLD identified by the arrow was open near the substrate (C) but did not extend deeper into the myotube's interior (B), whereas the VLD identified by the arrowhead appeared to be pinched off at the substrate (C) but was clearly evident farther up into the myotube interior (B).

The projected image (fig 4.4A) also confirms a point made earlier, on the basis of individual confocal sections, namely that spectrin skeleton staining intensity is not a function of VLD size. Figure 4.4A is a maximum pixel projection; an averaged pixel projection (not shown) gave the same impression of size independence. Although overall intensity was not a function of VLD size, within-VLD staining did seem more uniform in smaller VLDs, but this may be by simple reason that they are both smaller and more numerous. Viewing z series, such as those in figure 4.4, as movies left the impression that large VLDs are lined over their entire surface but that some of them had become internalized.

Figure 4.4D is an individual section from another z series. In this case the section was

1.2μm above the substrate. Figure 4.4D illustrates that when VLDs touched, they could maintain a septum of spectrin skeleton between them. A "doublet" VLD (indicated by a double arrowhead) and a less well defined "triplet" VLD occur in this image. If VLDs were just naked bilayer (ie. not supported by the membrane skeleton) then they would more easily fuse together but, at the stage shown here, at least, they had not coalesced. This image also illustrates that the other major planar membrane in myotubes, the nuclear envelope membrane, was not immunopositive for the spectrin skeleton.

Figure 4.4 E-G shows three sections from another z series revealing that VLDs are lined above the substrate. At 0.4μm above the substrate (E) a "rosette" of spectrin skeleton is evident (arrow). This rosette evidently represents a cluster of pinched off VLDs since in successive confocal sections (not shown) VLDs dilate and at 1.2μm above the substrate (F), the VLDs in the cluster are full blown (arrow). At 2μm above the substrate (G) one VLD is still dilated but the other VLDs appear to have terminated; the aggregate of staining presumably corresponds to spectrin skeleton lining the top of the VLDs. Notice in F the distinct plasma membrane staining for the spectrin skeleton (as well as distinct VLD staining); as was typical for the confocal slices, plasma membrane staining was not equally apparent in all sections (see E and G).

Overall, VLD membrane spectrin skeleton staining had the characteristics of plasma membrane spectrin skeleton staining. The intensity of staining around the VLDs did vary both among and within VLDs, but not more so than staining at the plasma membrane. The fact that no correlation between VLD size and staining intensity was noted indicates that enlarging VLDs did not acquire stain simply by pushing aside non-specifically stained background material (in any case, background staining was minimal) or the diffuse immunopositive material in the cytoplasm.

In neither the control (ie. no osmotic perturbation) nor in the VLD-induced myotubes was the spectrin skeleton plasma membrane staining as vivid as in some of the published *in situ* myotube and muscle fiber images (De Bleecker *et al.*, 1993; Vita *et al.*, 1994; Porter *et al.*, 1992 and 1997). This is not surprising given that many of these images represent muscle biopsy tissue imaged in cross-section, whereas very flat myocytes in 2D cultures were imaged here. The structures that we could image in cross-section, namely the VLDs, did stand out vividly as being

positive for the spectrin skeleton. Figure 4.5 is an interpretive cartoon suggesting why even a uniformly thick spectrin skeleton network associated with sarcoplasmic and VLD membrane in myotubes could produce confocal images in which spectrin skeleton appeared non-uniform around the circumference of individual VLDs and over the surface of the cell. Membrane (sarcoplasmic or VLD) passing perpendicularly through the confocal section (asterisks) would appear as intensely stained lines, whereas membrane parallel (double arrowhead) or membrane cutting obliquely through the confocal section (arrowheads) would be less intensely stained and blurred. Membrane running parallel to the confocal section would generate the weakest fluorescent signal and could be mistaken for diffuse background staining. As shown in the top confocal slice, large VLDs might be brightly and well-defined on one side (asterisks) but less distinctly delineated elsewhere (single arrowhead) due to the angle at which the membrane goes through the confocal section. At a confocal section closer to the substrate, the largest VLD depicted would be a faintly stained blur on the right hand side (double arrowhead) but brightly stained line on the left hand side. Furthermore sarcoplasmic membrane from 2 touching myotubes (two asterisks in bottom confocal section), both perpendicular to the confocal section, would generate a particularly bright fluorescent line. This could explain why some myotube margins were exceptionally brightly stained or "distinct" in comparison to other myotube margins where the membranes were oblique and not doubled up.

Figure 4.1 Schematic diagrams depicting the best known protein of the spectrin/fodrin family, erythrocyte spectrin along with its association with other cytoskeletal proteins, the membrane bilayer and its extensibility. The homologous location of the muscle β-spectrin C terminal sequence against which the antibody 4I12 was made, is indicated on the erythrocyte β-spectrin protein though that sequence is absent in erythrocyte β-spectrin. The two bottom cartoons are a "model in which changes in the inter- and intramolecular interactions between spectrin oligomers provide elasticity. Bi: schematic of the interactions between spectrin chains in the native membrane skeleton before application of tension in the direction of the arrows. Bii: an extended spectrin meshwork after tension-induced disruption of lateral interactions between spectrin oligomers" (Hitt and Luna, 1994). This model is based on a publication by Ursitti and Wade (1993).

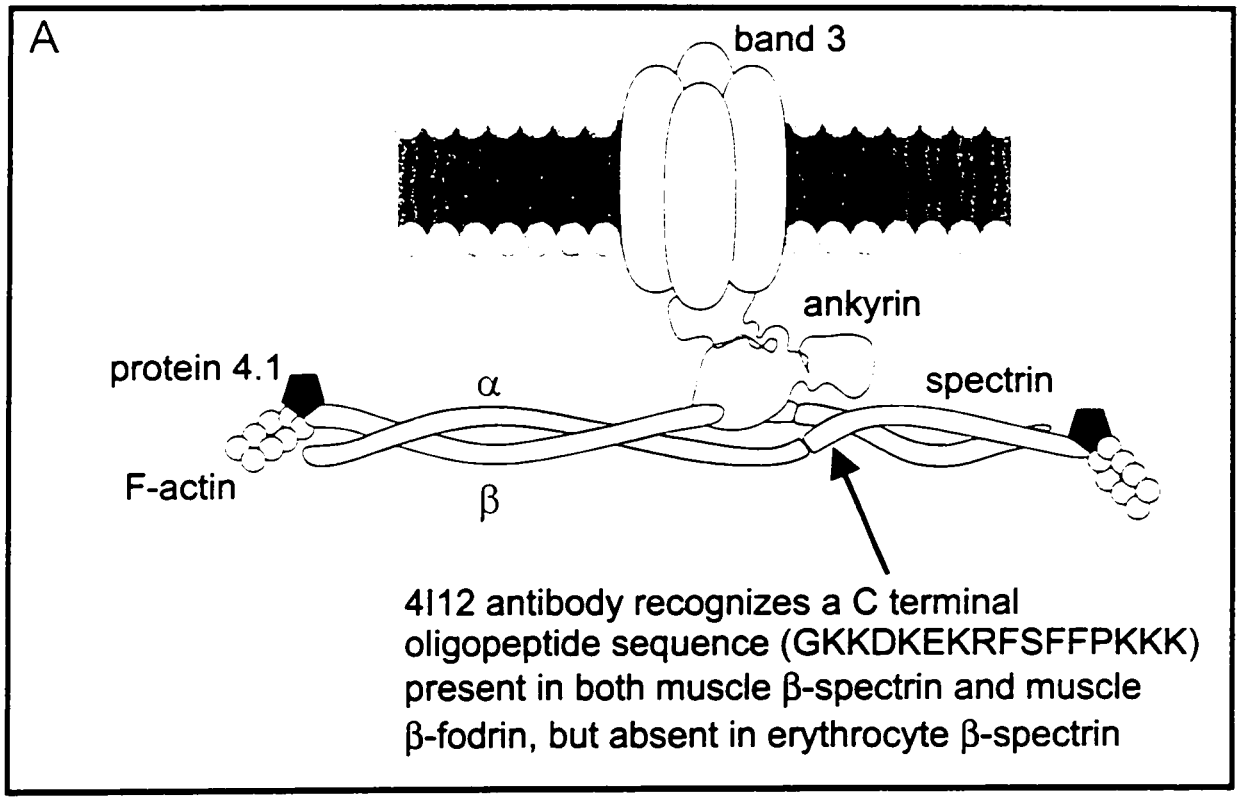
A
band 3
ankyrin
protein 4.1
α
spectrin
F-actin
β
4I12 antibody recognizes a C terminal oligopeptide sequence (GKKDKEKRFSFFPKKK) present in both muscle β-spectrin and muscle β-fodrin, but absent in erythrocyte β-spectrin

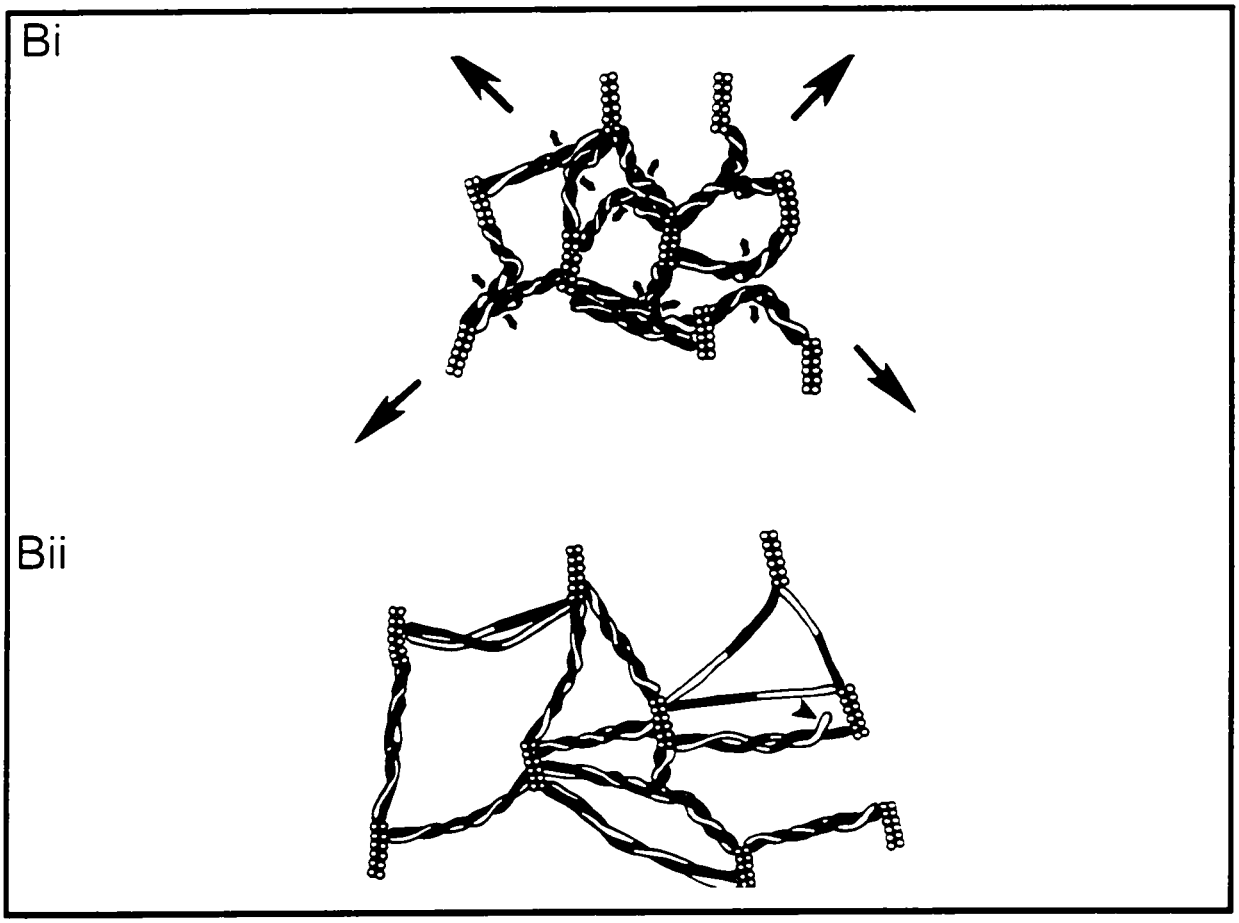
Bi
Bii

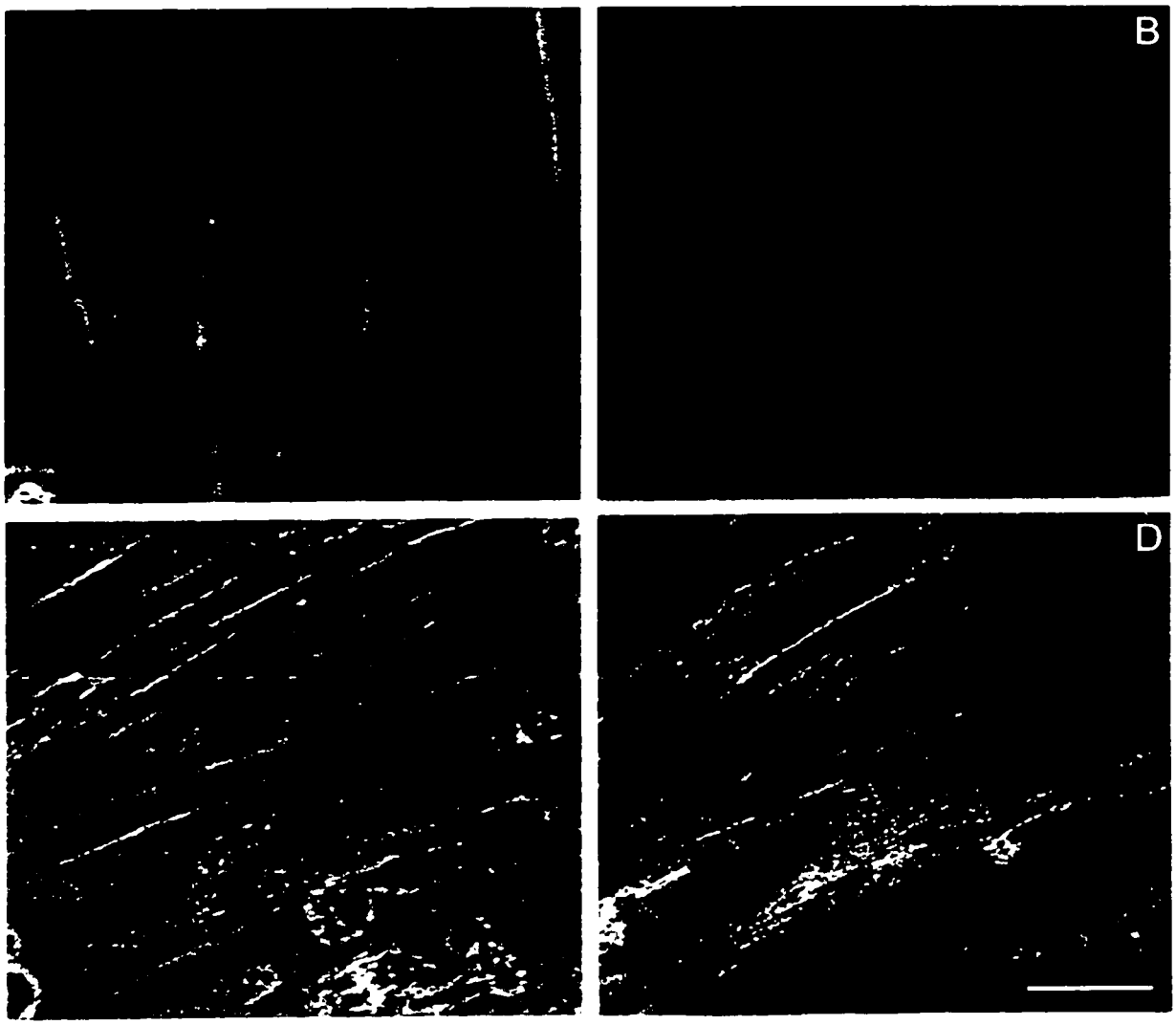

Figure 4.2 Phase contrast and fluorescent pair control images of L6E9 myotubes. A, B was treated with the Cy2-conjugated secondary, whereas C, D was treated with both the primary (4I12) and secondary antibodies. A, B show that the fluorescent secondary antibody did not appreciably bind non-specifically in myotubes or myoblasts. C, D show the typical 4I12 antibody staining pattern of myotubes and myoblasts not induced to form VLDs. Notice the distinct plasma membrane staining at the cell margin and the diffuse, slightly punctate cytoplasmic staining. Scale: 10μm for A, B and 40μm for C, D.

Figure 4.3 Phase/fluorescence pairs showing that the muscle spectrin skeleton lines osmotically induced VLDs in rat myotubes. A, B show that the spectrin skeleton colocalizes with the periphery of both small and large VLDs. In C, D, a large VLD completely lined with the spectrin skeleton is located adjacent to bead-like phase-light strings (arrows) often seen in both control (E, F) and osmotically perturbed myotubes. Scales: 30μm A, B and 10μm C, D and E, F.

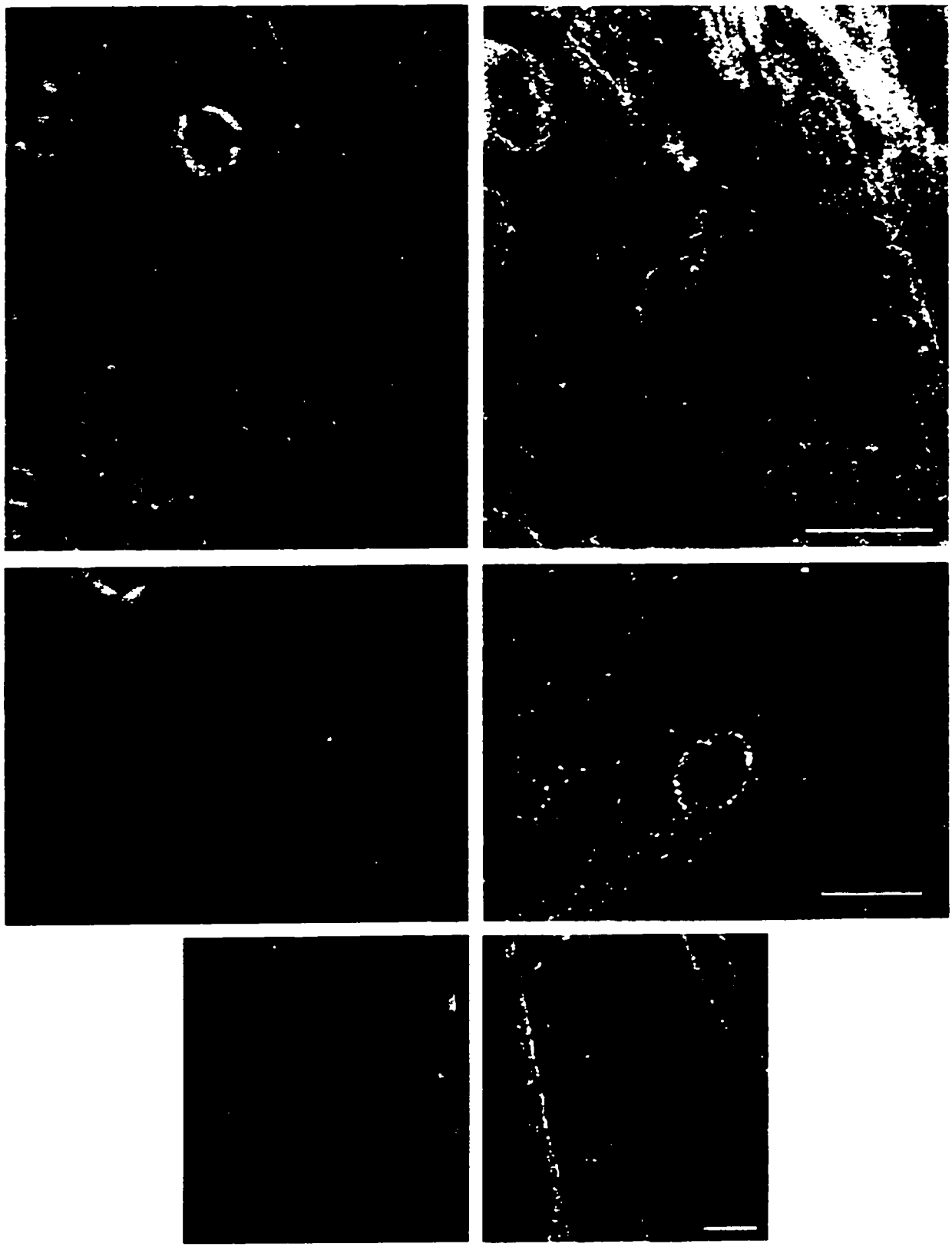

Figure 4.4 Fluorescence images of VLDs lined with the spectrin skeleton at various levels above the substrate. A projected image (using maximum pixel intensity) of a z series with 20 sections taken 0.2μm apart shows the variability of VLD sizes and intensity of their spectrin skeleton staining (A). B, C are sections from the same myotube as shown in A, but at 2.4μm and 0.8μm above the substrate respectively. Some spectrin skeleton lined VLDs were evident near the substrate but did not extend right through the myotube interior (arrows provide location markers). By contrast, some other VLDs not evident at the substrate appeared higher up in the myotube. D is a section from a z series at 1.2μm above the substrate. The two, large dark regions close to the VLD pair indicated with a double arrowhead are nuclei (evident in phase contrast, but not shown). Nuclear envelope membrane showed almost no evidence of staining for the spectrin skeleton. E-G are 3 confocal slices from another z series, showing a cluster of small spectrin skeleton lined VLDs that have pinched off from the substrate. E, F and G are 0.4, 1.2 and 2μm above the substrate respectively. Scale bars: 10μm.

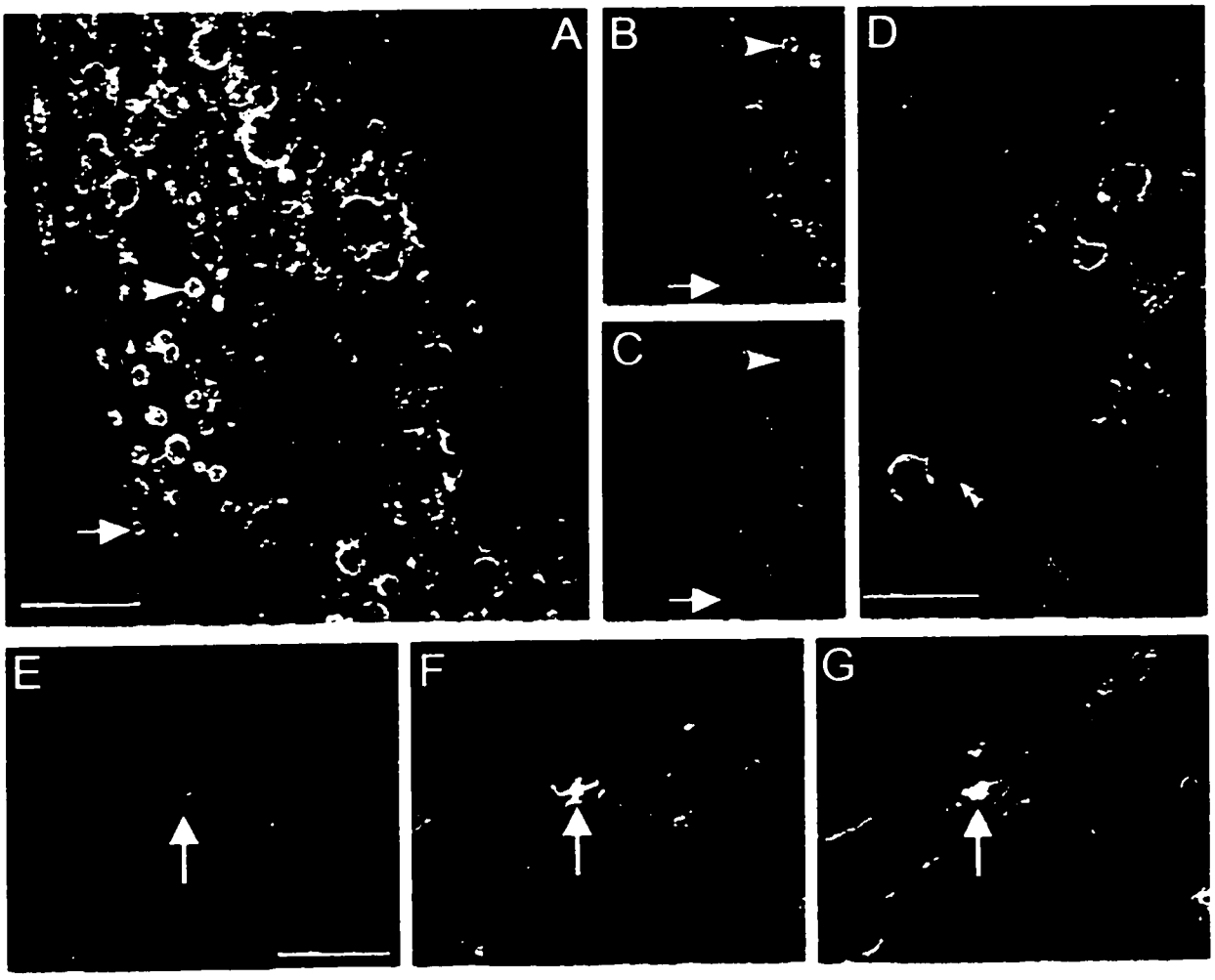
A
B
C
D
E
F
G

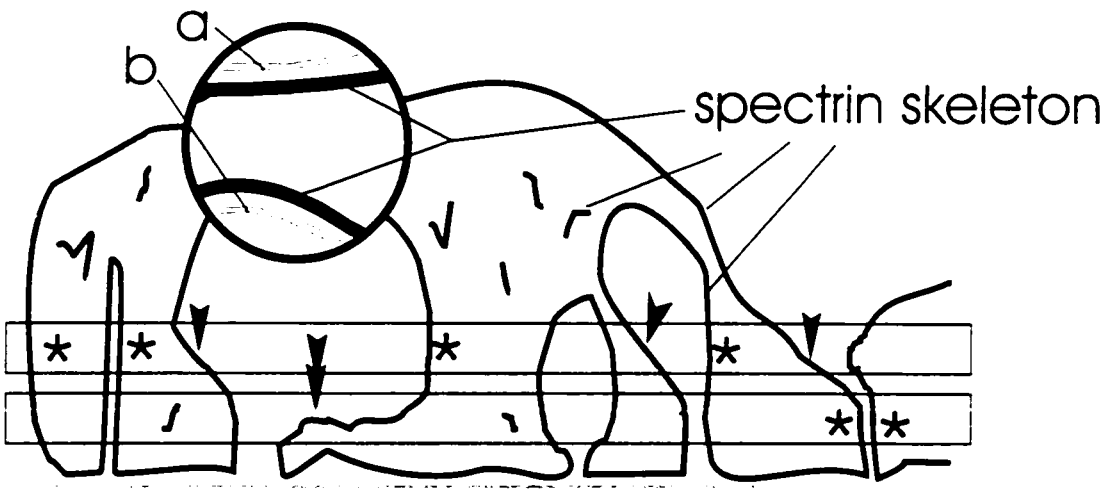

Figure 4.5 Interpretive cartoon of spectrin skeleton staining patterns observed by confocal microscopy in rat L6E9 myotubes. The rectangles represent confocal slices. The magnified area shows the topological relation of sarcolemma (a) and VLD (b) lipid bilayer (prior to detergent extraction) to spectrin skeleton. Asterisks and arrows are explained in the text.

DISCUSSION

L6E9 myotubes were a suitable cell type for determining if VLD membrane is lined and therefore, perhaps supported by the spectrin skeleton. Like neuronal VLDs, myotube VLDs were reversible and repeatable. The 4I12 antibody detected the spectrin skeleton in these cells by Western blotting and by immunocytochemistry; it stained the plasma membrane of control cells as expected.

Comparison of phase contrast and fluorescence images showed that shrinking-induced VLDs in the myotubes were lined by the spectrin skeleton. Myoblasts, which did not form VLDs, did not exhibit circular spectrin skeleton profiles like those in VLD-bearing myotubes. Thus the profiles were not present in any shrinking cell, only in cells where shrinking also triggered invagination of VLDs. VLDs form as surface membrane invaginations (Mills and Morris, 1998); in myotubes this resulted in internalization of the spectrin skeleton lined surface membrane. Whether the spectrin skeleton network is continuously in intimate contact with the surface membrane or whether it rapidly reorganizes after the osmotic perturbations remains to be determined.

In L6E9 myotubes, VLD membrane appeared to originate from the substrate adherent plasma membrane, as was also observed in molluscan neurons (Reuzeau *et al.*, 1995). The plasma membrane origin of the L6E9 VLDs makes them correspond most closely to the "type 1" vacuoles classified by De Bleecker *et al.* (1993) for human vacuolar myopathies. In these skeletal muscle myopathies (De Bleecker *et al.*, 1993), type 1 and type 2 membrane originates from the sarcolemma. Vacuolar membranes and surface membranes were all immunopositive for β-spectrin and for another membrane skeleton protein, dystrophin. Because the T-tubule system was not immunopositive for either of these proteins it was unclear whether T-tubule membrane contributes to the vacuoles. The question of T-tubular involvement in vacuolation is complicated by the fact that in frog skeletal muscle (Krolenko *et al.* 1995) reversible, discrete shrinkage-induced vacuoles (ie. essentially, VLDs) form by dilation of T-tubule membrane. This was shown by live confocal microscopy using a membrane dye.

A feature that L6E9 VLDs share with both types 1 and 2 vacuoles (De Bleecker *et al.*, 1993) is that they have membrane skeleton. The VLDs become more akin to type 2 vacuoles in the cases

where they seem to have become internalized as true vacuoles; according to De Bleecker *et al.* (1993), type 1 vacuoles are, in fact invaginations, not pinched off vacuoles, whereas type 2 vacuoles evidently are not connected to the surface. How these type 2 vacuoles acquired their membrane skeleton was not known, and it was not ruled out that T-tubular membrane might contribute bilayer material.

Spectrin supports and stabilizes erythrocyte plasma membrane (Burridge *et al.*, 1982; Goodman and Shiffer, 1983; Bennett, 1985; Marchesi, 1985) and it has been generally assumed that spectrin and/or fodrin serve similar functions in non-erythrocytes (Porter *et al.*, 1992; De Bleecker *et al.*, 1993; Vita *et al.*, 1994; Pumplin, 1995). Alternatively, Morrow (1989) proposed that since spectrin and/or fodrin are not detected at some plasma membrane areas (eg. spectrin occurs in the cytoplasm of mouse lymphocytes (Black *et al.*, 1988)) and since its expression can be highly polarized (eg. fodrin in kidney cells is polarized at basolateral domains (Nelson and Veshnock, 1986)), they may serve not for mechanical support but in receptor organization, membrane topographical assembly and membrane trafficking. These ideas are not mutually exclusive. In various human vacuolar muscle myopathies (De Bleecker *et al.* 1993; Vita *et al.*, 1994) it has been postulated that β-spectrin support of vacuolar membrane would be especially important in mitigating further problems during muscle contraction.

A role for spectrin and/or fodrin in membrane trafficking is suggested by observations in a variety of cells. In goldfish retinal ganglion cells, α-spectrin lines axonal varicosities, aggregations of tubular, smooth endoplasmic reticulum, thought to be cytomembranes involved in membrane recycling (Koenig *et al.*, 1985). Vesicles thought to be involved in trafficking in mouse lymphocytes are α-fodrin lined (Black *et al.* 1988). Immuno-electron microscopy and immunocytochemistry of sea urchin eggs revealed that cortical granules, endoplasmic vesicles, acidic vesicles, pigment granules and yolk platelets are all spectrin lined (Bonder *et al.*, 1989, Fishkind *et al.*, 1990a and 1990b). After hyperstimulation of secretion in rat chromaffin cells, Fujimoto and Ogawa (1989) observed fodrin lined retrieving vesicles. They postulated that these vesicles may be connected to the extracellular space and pinch off from the substrate giving rise to vacuoles. Moreover, they hypothesized that the fodrin lined retrieving vesicles could be part of a membrane response system

that retrieves excess membrane from the surface, a role also postulated with respect to VLDs (Reuzeau *et al.*, 1995; Mills and Morris, 1998). We found that in L6E9 myotubes and myoblasts, the spectrin skeleton was not limited to the plasma membrane. Diffuse cytoplasmic staining for α and β-spectrin have also been observed in adult differentiated muscle fibers (Repasky *et al.*, 1986; Porter *et al.*, 1992; De Bleecker *et al.*, 1993; Vita *et al.*, 1994), aneurally cultured mouse and human skeletal myoblasts and maturing myotubes (Kobayashi *et al.*, 1995). Some level of cytoplasmic staining for the spectrin skeleton in L6E9 cells is to be expected if the spectrin skeleton participates in membrane turnover. Additionally, there may have been some unpolymerized spectrin skeleton in the cytoplasm. Immunoprecipitation teamed with immunocytochemistry using the 4I12 antibody in adult rat skeletal muscle revealed that muscle β-spectrin paired with α-fodrin results in plasma membrane staining, whereas unpaired muscle β-spectrin results in cytoplasmic staining (Porter *et al.*, 1997).

Spectrin integrity and the effects of hypotonicity

Spectrin deficiencies cause reduced stability, increased mechanical fragility, loss of supported plasma membrane (Goodman and Shiffer, 1983; Palek, 1987) and loss of membrane elasticity in erythrocytes (Lux *et al.*, 1979). Spectrin mutations that impair spectrin dimer-dimer self association result in fewer spectrin tetramers, decreased expression of the spectrin protein at the membrane (Liu *et al.*, 1990) and defective spectrin binding to other cytoskeletal proteins, such as protein 4.1 (Goodman and Shiffer, 1983). Spectrin tetramers are oriented parallel to the membrane plane and any dimer-dimer self association defects lead to mechanically weakened cytoskeletons unable to maintain their role as membrane supports (Liu *et al.*, 1990). Spectrin deficient erythrocytes lose membrane surface area (Palek, 1987; Liu *et al.*, 1990); lack of sufficient spectrin to support the membrane bilayer may explain the membrane vesiculation common in the deficient erythrocytes. The band 3-ankyrin-spectrin interaction is likewise critical in maintaining the structural integrity of the membrane (Low *et al.*, 1991). At physiological ionic strength and temperature, tetramers are the favoured spectrin unit *in situ* for erythrocyte membrane and only tetramer rich membrane skeletons are stable to mechanical stress (Liu and Palek, 1980). Tetramer formation

problems are the primary reason membrane skeletons are not stable when faced with a mechanical stress.

Human erythrocyte spectrin tetramers convert to dimers in hypotonic buffers and reversed to tetramers on return to isotonic buffer as demonstrated by gel filtration analysis (Liu and Palek, 1980). In isotonic buffer the majority of the spectrin protein was in the form of tetramers but the tetramer/dimer ratio decreased with decreasing NaCl concentrations, reaching 60% tetramers in the buffer of 7% normal tonicity.

Hypotonically treated membrane skeleton ghosts exhibited a diminished mechanical stability (Liu and Palek, 1980) that is a direct consequence of loss of tetramers. This was shown by assessing the extent of skeleton disintegration after either swelling (7% of isotonic) or swelling then reshrinking erythrocyte ghosts (plasma membrane still present), detergent extracting the plasma membrane, then vigorously shaking the resulting membrane skeleton ghosts for 40 minutes in either the 7% or 100% buffer. Swelling alone did not produce disintegration but swelling plus shaking resulted in disintegration of about 90% of the membrane skeletons.

Spectrin and membrane tension

Based on measured erythrocyte membrane lytic tension, Gruen and Wolfe (1982) postulated that in osmotically swollen erythrocytes, macroscopic membrane tensions up to 20mN/m may be sustained by the crosslinked spectrin cytoskeleton. Since spectrin accounts for about 75% of the erythrocyte cytoskeletal protein mass (Glenney and Glenney, 1983a), it is the best candidate to sustain such membrane tensions.

Because we hypothesize that VLD formation indicates that an adherent cell is undergoing large membrane tension changes, we wished to know the disposition of membrane skeleton with respect to VLD membrane. Our first question was: does the membrane skeleton line VLD membrane? We showed that the spectrin skeleton does line VLDs. This indicated that VLDs have membrane skeletons and leads to the possibility that the VLD membrane is mechanically stabilized by the spectrin skeleton network. We hypothesize that VLDs enlarge and accrue membrane because they are under high tension during their dilation phase, and that membrane skeleton could

be instrumental both in creating that tension and in preventing bilayer disruption as plasma membrane rapidly invaginates. Our findings are consistent with this possibility, however, we are not yet certain if the spectrin skeleton network rearranged itself over the VLDs or if the spectrin skeleton network was continuously present during VLD formation. If there was a major depolymerization (during 10 minutes in 30% swelling medium) followed by repolymerization of the membrane skeleton (during the 3 minutes in isotonic medium prior to fixation) it was a tremendously efficient feat of reorganization. Background staining did not appear higher in VLD-bearing cells compared to controls, as might be expected if there had been a major breakdown of the spectrin skeleton network upon swelling and shrinking. If the spectrin skeleton remained intact at the surface membrane during the osmotic perturbations then the spectrin skeleton could have lined the VLDs during their entire time of formation; invaginating along with the bilayer. The network would need to be extensible as well as continuous to have behaved this way.

Conversion of spectrin from dimers and back to tetramers was characterized in erythrocytes using 15 minutes swelling and 15 minutes reincubated in isotonic medium (Liu and Palek, 1980). We used 10 minutes swelling and 3 minutes between shrinking before fixing the myotubes. Whether spectrin skeleton tetramers were converted from dimers then back into tetramers remains to be determined. However, even if the myotube spectrin skeleton network did partially dimerize, its mechanical stability and integrity may not have been severely compromised; in erythrocytes, membrane disintegration occurred only in cells that underwent both swelling and vigourous shaking for 40 minutes (Liu and Palek, 1980).

VLD formation suggests that osmotically perturbed cells may regulate their surface area. The finding that the spectrin skeleton lines VLDs therefore suggests that the membrane skeleton may contribute to surface area regulation mechanisms. Interestingly, this function could encompass both of the major roles suggested by others for the spectrin/fodrin network - providing mechanical strength and stability to the lipid bilayer and involvement in the disposition of membrane between the surface membrane and internal membrane stores.

CHAPTER 5: GENERAL DISCUSSION

This thesis centers around the general idea that cells regulate their surface area in response to membrane tension changes. Accordingly, in-plane membrane tension increases would cause addition of membrane, whereas tension decreases would cause membrane retrieval. Studies of how cells grow, elongate and respond to membrane tension changes (Bray, 1984; Zheng *et al.*, 1991; Lin *et al.*, 1995; Dai and Sheetz, 1995a and 1995b; Sheetz and Dai, 1996; Fink and Cooper, 1996; Nichol and Hutter, 1996a) have provided support and further insight into how cells may regulate their surface area during osmomechanical perturbations (Reuzeau *et al.* 1995; Dai *et al.*, 1998).

Shrinking cells invaginate membrane at their substrate-adherent surface, pinch off vacuoles and lower their membrane capacitance. Taken together, these responses suggest that cells regulate their surface area. To further investigate this issue, I studied how intracellular calcium, F-actin and the spectrin skeleton responded to swelling and shrinking perturbations in neurons and in muscle cells. Intracellular calcium concentration changes were monitored during swelling by ratiometric microscopy to investigate if calcium mediated exocytosis could be the mechanism that brings about membrane addition at the cell surface. Neuronal intracellular calcium concentrations did change upon swelling but not enough to elicit calcium dependent exocytosis.

Actin and the spectrin skeleton were next investigated to study how the cytoskeleton responds to osmotic perturbations. Previous observations of swollen molluscan neurons reshrinking in normal saline revealed that neurons form vacuole-like dilations (VLDs). VLDs grow from membrane invaginations at the cell substrate (Reuzeau *et al.*, 1995; Mills and Morris, 1998) and recover by processes sensitive to actomyosin inhibitors (Reuzeau *et al.*, 1995). One such inhibitor of VLD recovery is cytochalasin. Molluscan neurons do not undergo recovery in the presence of this drug. These observations lead to the hypothesis that the F-actin network is required for VLD recovery. Neurons were stained with fluorescent phalloidin or phallacidin to investigate the different staining patterns associated with VLD formation in neurons incubated and not incubated in cytochalasin B. F-actin rings of newly constituted leading edge (filopodia and lamellipodia), which we termed actipodia, were observed sweeping and projecting into VLDs at the

substrate and support the hypothesis that actipodia are the structures that help VLDs pinch off from the substrate in order to bring about VLD recovery.

Spectrin is a cytoskeletal protein known to stabilize erythrocyte surface membranes. Since spectrin and/or fodrin line cytoplasmic vacuolar structures in a variety of cell types (Bonder *et al.*, 1989; Fujimoto and Ogawa, 1989; Fishkind *et al.*, 1990a and 1990b; De Bleecker *et al.*, 1993; Vita *et al.*, 1994) and since VLD membrane originates from surface membrane, the possibility that they are supported by membrane skeleton was investigated. Rat skeletal myotubes were stained with an antibody specific for muscle β-fodrin and muscle β-spectrin, to determine if VLD membranes are lined by this cytoskeletal network. The spectrin skeleton was observed lining VLDs.

Model of how VLDs form in response to membrane tension changes

VLD formation provides an experimentally accessible, albeit exaggerated indicator of surface area regulation. The presence of the spectrin skeleton on VLDs suggests that invaginating VLDs are stabilized by the membrane skeleton. Calcium mediated exocytosis is not a player in membrane addition to the general surface during cellular swelling or to the dilating VLDs during cellular shrinking. The simplest explanation for VLD enlargement is that VLD membrane is initially under high tension and therefore can act as a sink for membrane at low tension elsewhere on the cell (fig 5.1). It is known that membrane tension is lowered at the upper surface in shrinking neurons (Dai and Sheetz, 1995a; Dai *et al.*, 1998), so this is plausible. As the first illustration in figure 5.1 depicts, before the swelling perturbation is initiated, plasma membrane and any contiguous internally stored membrane is in in-plane membrane tensile equilibrium. Upon swelling (middle illustration in fig 5.1), tension increases in the upper plasma membrane (ie. not attached to substrate) (Dai *et al.*, 1998), therefore creating a relative tension difference between this membrane and contiguous internal stores. The stores may therefore flow to the surface and provide the increased capacitance observed in swollen neurons (Wan *et al.*, 1995).

Upon shrinking, membrane tension of previously swollen cells decreases (Dai *et al.*, 1998) and therefore according to our hypothesis, the excess plasma membrane accrued during swelling could flow to membrane areas under the highest tension. Why the substrate sites at which VLD

invagination is initiated would be under increased in-plane membrane tension is not understood. One possibility is that the shrinking cytoplasm draws membrane skeleton in with it and adherent membrane follows. This idea can receive further consideration now that it is known the VLDs are lined by the spectrin skeleton.

CRITIQUE OF THESIS INTERPRETATIONS

Intracellular calcium experiments

Could other processes have been occurring which could also explain the VLD observations? As explained in chapter 2, no appreciable intracellular calcium concentration increases were detected during neuronal swelling, therefore ruling out that the addition of membrane at the cell surface is mediated by release of calcium from intracellular stores that could stimulate exocytosis. However could calcium mediated exocytosis have been occurring near the membrane invaginations that VLDs arise from (Mills and Morris, 1998), resulting in addition of membrane at the invaginations and therefore causing the growth of the invaginations into VLDs? Our data appear to rule this out. Neurons loaded with BAPTA, a calcium chelator, for 1 and 3 hours were able to form VLDs (fig 2.6a, b, and c). Likewise FURA-2 (a calcium concentration indicator) loaded neurons elicited VLDs in normal and low extracellular calcium and exhibited very small intracellular calcium concentration increases during swelling (fig 2.3 and 2.4), which could not stimulate calcium dependent exocytosis. Neurons loaded with BAPTA and FURA-2, in normal extracellular calcium, correspondingly exhibited small intracellular calcium concentration increases (fig 2.6d) but not enough to elicit calcium dependent exocytosis. We are confident that BAPTA did indeed chelate intracellular calcium, as the resting intracellular calcium concentration before osmotically perturbing the neurons was almost one-half that of neurons not incubated in BAPTA (compare fig 2.6d to fig 2.3). Overall we are confident that subtle calcium signalling was not necessary during neuronal swelling and shrinking. Since calcium mediated effects are not important in neuronal RVD (Morán *et al.*, 1997) and since our data rule out that osmotic perturbations make big calcium signals, we can therefore use this preparation to look further at the possible role of tension in surface area regulation.

F-actin experiments

Our F-actin experiments of how cells undergo VLD recovery lead to a very interesting observation of F-actin reorganized around the VLD peripheries upon shrinking. The most striking evidence for this was at the substrate where a ring of filopodia and lamellipodia were observed to sweep and project into the VLD opening (fig 3.8). We termed these actin-rich rings of filopodia and lamellipodia "actipodia" and hypothesize that actipodia, which constrict, begin the process of reinternalization of excess surface membrane (ie. VLD membrane). The actipodia dynamics of projecting and retracting (fig 3.8) appeared similar to the dynamics exhibited by new leading edge at cell margins. Previous experiments revealed that new outgrowth is stimulated upon membrane tension increases produced by pulling or swelling (Lamoureux *et al.*, 1989; Zheng *et al.*, 1991; Lin *et al.*, 1995). We hypothesize that VLDs must form at substrate sites under locally increased membrane tension. Therefore it may be valid to regard actipodia, F-actin rich structures associated with these same membrane sites, as new leading edge triggered by the tension changes. However, we observed filopodia in larger VLDs but the smaller VLDs, whose actipodia appeared more like a ring of lamellipodium and which had the most intense staining, appeared to be the best candidates for pinching off from the substrate. Larger VLDs with actipodia did not appear to pinch off during our observation times and the smaller ones were hard to resolve as time went on. More data involving both bath dyes and G-actin is required to determine if the smaller VLDs pinch off from the substrate in comparison to the larger VLDs. Since both actipodia and leading edge formation appear to be stimulated by membrane tension decreases and since both contain F-actin, study of actipodia formation and dynamics in larger VLDs could be a good model to study leading edge dynamics.

Spectrin skeleton experiments

Phospholipid molecules spontaneously assemble into lipid bilayers in aqueous solution (Alberts *et al.*, 1989). A flat lipid bilayer is, however, innately unstable and lowers its energy by forming closed surfaces (Lipowsky, 1991) such as vesicles. Lipid bilayer does no,t however, always form into vesicles, especially if there is a stabilizing framework (Bray and White, 1988).

Beneath the plasma membrane such a framework is provided by the cortical cytoskeleton network of actin and spectrin filaments. The cortical cytoskeleton gives mechanical strength to the plasma membrane, allowing cells to change shape and exhibit motility. Shape changes and motility are brought about by cytoskeletal alterations (ie. filament polymerization, depolymerization, contraction, elongation and position changes) (Ingber and Folkman, 1989).

In erythrocytes, spectrin and actin provide critical mechanical support; extraction of the erythrocyte cytoskeleton causes the membrane to fragment into small vesicles (Alberts *et al.*, 1989). Identification of spectrin and/or its non-erythroid counterpart, fodrin, lining vacuolar membranes in a variety of cells (Bonder *et al.*, 1989; Fujimoto and Ogawa, 1989; Fishkind *et al.*, 1990a and 1990b; De Bleecker *et al.*, 1993; Vita *et al.*, 1994) lead us to investigate if these proteins lined VLD membrane. We observed that the spectrin skeleton lined osmotically induced VLDs in rat skeletal myotubes. This suggests, as others have concluded (Porter *et al.*, 1992; De Bleecker *et al.*, 1993; Vita *et al.*, 1994; Pumplin, 1995), that spectrin's known role of stabilizing erythrocyte membrane also applies in non-erythrocytes. However, in a review of spectrin and fodrin's roles, Morrow (1989) suggested that non-erythrocyte spectrin and fodrin do not serve to stabilize membranes. Surface membrane areas lacking spectrin and/or fodrin was used as evidence that spectrin and fodrin were unnecessary for membrane support (Nelson and Veshnock, 1986). Further evidence was a lymphocyte study (Black *et al.*, 1988) in which α-fodrin was observed in a previously undescribed cytoplasmic meshwork or aggregate of filaments and membranous vesicles. However cytoplasmic localization of spectrin and/or fodrin as observed by us and many others (Goodman *et al.*, 1981; Messina and Lemanski, 1991; Kobayashi *et al.*, 1995; Porter *et al.*, 1997) does not constitute counter-evidence for a mechanical support role at the cell surface. The view that spectrin and/or fodrin supports and stabilizes erythrocyte membrane as well as non-erythrocyte membrane is widely held today (Porter *et al.*, 1992; De Bleecker *et al.*, 1993; Doctor *et al.*, 1993; Vita *et al.*, 1994; Pumplin, 1995).

Glogauer *et al.* (1998) extended this by showing that membrane stability during increases in membrane tension was enhanced by another spectrin superfamily member, the actin-binding protein 280 (ABP-280). ABP-280 was recruited into human gingival fibroblast cortical areas upon

increased tension, resulting in stimulation of actin assembly. A magnet was used to generate a constant upward force on collagen-coated magnetic beads bound to extracellular integrin receptors, which were directly attached to the actin cytoskeleton. In a human melanoma cell line that does not express ABP-280, actin accumulation could not be stimulated upon application of force, whereas in the equivalent cell line stably transfected with ABP-280, actin accumulation was stimulated upon force application. After force application, greater than 90% of the ABP-280 deficient cells died in comparison to ABP-280 positive cells after force application. Therefore it was concluded that ABP-280's role in mechanically stabilizing cell membranes may be to stimulate interactions between the actin cytoskeleton and the plasma membrane.

Another member of the spectrin superfamily, dystrophin, is likewise found beneath the plasma membrane in muscle cells. Muscle that lacks dystrophin (ie. the dystrophic muscle of the disease muscular dystrophy) is characterized by progressive loss of muscle tissue due to myofiber degradation (Porter *et al.*, 1992). Dystrophin has also been shown to contribute to the stability of mouse muscle fibers (Menke and Jockusch, 1991). Hyposmotic shocks just less than 50% were used to assess whether the amount of tension that muscle fibers deficient in dystrophin could withstand differed from that in muscle fibers expressing dystrophin. Based on the number of survivors, dystrophin-less muscle cells were more sensitive to hyposmotic shocks suggesting that dystrophin-less membrane was physically weaker. Elevated levels of α-spectrin are found lining avian dystrophic muscle (versus non-dystrophic) (Repasky *et al.*, 1986); this would be in line with the idea that in healthy muscle, dystrophin and α-spectrin together stabilize muscle surface membranes but in dystrophic muscle, spectrin overexpression may be an attempt to compensate for the lack of dystrophin.

Assuming that membrane skeleton serves in part to mechanically support plasma membrane in cells like muscles and neurons, what role might the spectrin skeleton play in surface area regulation? If, as we suspect from our findings with VLDs and the spectrin skeleton, the network stays in intimate contact with membrane as it is invaginated and retrieved, it might serve to define a pool of readily accessible reserve membrane that does not coalesce with other endomembrane pools. In this regard it is interesting that Cheng and Reese (1987) in an

ultrastructural study of recycling plasmalemma in chick tectal growth cones found that individual membrane disks were kept as ready-to-use but discretely separated entities via regularly spaced, filamentous, electron-dense cross-links that may well have been spectrin-like membrane skeleton. Shortly after Cheng and Reese's publication, Fujimoto and Ogawa (1989) showed that following hyperstimulation, the retrieved excess membrane was fodrin coated. We have hypothesized that VLD membrane, which we now know to be associated with membrane skeleton, could also represent a distinct pool of reserve membrane. Since transmission electron micrographs of *Aplysia* neurons revealed that these cells have large membrane cisternae or infoldings, which were postulated to represent reserve membrane for enlarging cells (Fejtl *et al.*, 1995), it may be possible to exploit this preparation further and determine if membrane skeleton is associated with a readily accessible but distinct pool of endomembrane.

BROADER IMPLICATIONS

Surface area regulation and regulatory volume decrease

Some swollen cells undergo cell-mediated shrinkage in hypotonic medium to ensure that a preferred volume is maintained. This reshrinking of cells in a hypotonic solution is termed regulatory volume decrease (RVD). Cells that undergo RVD return to their normal volume by loss of organic and inorganic solutes and by a concomitant loss of cell water (Spring and Hoffmann, 1992). Little is known about how cell surface area adjustments are made during RVD, yet for optimal cell function, cellular volume and surface area changes must somehow be coordinated. *Lymnaea* neurons (used in chapters 2 and 3) do not undergo a rapid RVD (Morris *et al.*, 1989) and so we were able to use exogenously driven volume changes (rather than cell-mediated ones) to look at the question of surface area regulation. There are some interesting correlations between RVD and swell/shrink driven VLD formation.

The first is that extracellular fluid-filled vesicles form in cells shrinking by RVD (Czekay *et al.*, 1994). The vesicles formed during RVD may be directly related to the cell-mediated VLDs observed to form during prolonged hyposmia in *Lymnaea* neurons (fig 3.5) and in shrinking plant protoplasts (Wartenburg *et al.*, 1992). Therefore shrinkage-induced vesicle and/or vacuole

formation, whether it be cell-mediated (RVD) or exogenously mediated (VLDs in shrinking neurons), may be a universal indicator of membrane retrieval and therefore of surface area regulation.

Upon swelling of cells that undergo RVD, cellular F-actin is first depolymerized but then repolymerized as shrinkage occurs over the next few minutes (Ziyadeh *et al.*, 1992; Cornet *et al.*, 1993 and 1994; Czekay *et al.*, 1994; Mills *et al.*, 1994; Morán *et al.*, 1996). This 5 minute time course is comparable to what we observed for substantial reorganization of F-actin in *Lymnaea* neurons. Five minutes after eliciting VLDs by shrinking, we observed that F-actin had reorganized around the VLD periphery as actipodia. At this time, F-actin also covered the entire dilated region of VLDs (fig 3.6A-G).

One hypothesis for actin's role in RVD is that it is a resistive element to cell swelling during pathophysiological conditions when cell volume control mechanisms have been compromised. This role has also been suggested for *Lymnaea* neurons, not with respect to RVD per se, but with respect to swelling limitation (Wan *et al.*, 1995). Shrinking-induced actipodia suggest that F-actin's role in surface area regulation may extend beyond limiting cell expansion. It may also provide a mechanism whereby excess membrane (ie. VLD), once invaginated, is pinched off and hence reinternalized. The mechanism of VLD recovery depends upon a dynamic F-actin network; although cells preincubated in cytochalasin form VLDs, they do not undergo VLD recovery (Reuzeau *et al.*, 1995). Intact and/or dynamic F-actin cytoskeleton is not needed in all cells that undergo RVD. Cytochalasin inhibits RVD in many cells including Jurkat cells (Downey *et al.*, 1995) and Ehrlich ascites tumor cells (Cornet *et al.*, 1993), but in human neutrophils, HL-60 cells (Downey *et al.*, 1995) and rat cerebellar astrocytes (Morán *et al.*, 1996) cytochalasin had no effect on RVD. The disposition of actin in these cells during RVD has not been examined at the level of detail that was possible for VLDs in large molluscan neurons.

Many cells exhibit an intracellular calcium concentration increase during swelling which mirrors the time course of volume regulation (O'Connor and Kimelberg, 1993; Raat *et al.*, 1995). Sources of increased calcium can be influx of extracellular calcium or calcium release from intracellular stores (Spring and Hoffmann, 1992). In cerebellar granule neurons, the RVD response was, however, found to be independent of the swelling induced intracellular calcium concentration

increase (Morán *et al.*, 1997). Known blockers of endogenous calcium release had no affect on neuronal RVD, therefore suggesting that intracellular calcium concentration increases have no role in neuronal RVD. Likewise, neither extracellular (Reuzeau *et al.*, 1995) nor intracellular calcium (Herring *et al.*, 1998) is required for VLD formation in molluscan neurons. Molluscan neurons formed VLDs in normal and low calcium media (fig 2.3 and 2.4) and in BAPTA loaded neurons (fig 2.6) without a corresponding intracellular calcium concentration increase.

The primary cell volume sensor is unknown to date. Our VLD experiments point to membrane tension changes as a likely candidate to instigate surface area regulation. Since cells must regulate both their volume and membrane area, the same sensor might operate in both capacities. Membrane changes that translate into membrane tension gradients over the cell surface could be the primary sensor and effector in surface area regulation and membrane tension could be the trigger for RVD.

Membrane tension

Membrane tension is emerging as an important parameter that appears to control neurite outgrowth (Bray, 1984; Bray *et al.*, 1991; Zheng *et al.*, 1991; Lin *et al.*, 1995; Dai and Sheetz, 1995a; Dai *et al.*, 1998), exocytosis, endocytosis (Dai and Sheetz, 1995b and Sheetz and Dai, 1996), embryogenesis (Fink and Cooper, 1996), morphogenesis and CNS wiring (Van Essen, 1997).

As discussed through out this thesis, it was hypothesized for many years (Bray, 1984; Bray *et al.*, 1991; Zheng *et al.*, 1991; Lin *et al.*, 1995), but only recently demonstrated that membrane tension, as measured by membrane tethers, differs regionally over a neuron depending on whether net retrieval or insertion of membrane is occurring and differs according to whether a cell is swollen or reshrunk (Dai and Sheetz, 1995a; Dai *et al.*, 1998).

The idea that tension may control exocytosis and endocytosis is currently being investigated in animal cells (Dai and Sheetz, 1995a and b; Sheetz and Dai, 1995) but was first examined in plant protoplasts (Wolfe and Steponkus, 1981; Wolfe *et al.*, 1985 and 1986). Dai and Sheetz (1995b) proposed that for membrane area homeostasis, the surface membrane which is endocytosed

approximately every 30-60 minutes, a coupling of exocytosis and endocytosis is needed. The signal which couples these two processes was postulated to be membrane tension (Dai and Sheetz, 1995b). In rat basophilic leukemia cells it was confirmed that membrane tension increases stimulate exocytosis and that decreases stimulate endocytosis (Dai *et al.*, 1997). Exocytosis would cause addition of membrane at the cell surface, thereby relieving the increased membrane tension, while endocytosis would cause retrieval of membrane from the cell surface, thereby helping to reset the membrane tension level. These tension experiments plus the finding that cytochalasin lowers the resting tension of dorsal root ganglia (Hochmuth *et al.*, 1996), lead Dai and Sheetz (1996) to conclude that tension is a tightly regulated cellular parameter and alterations in tension could signal major changes in cell function.

In keeping with this, in fibroblasts, membrane tension increases brought about by stretching prevented endocytosis (Hagmann *et al.*, 1992). Stretched fibroblasts that had previously incorporated rhodamine labelled vinculin (injected) and rhodamine labelled α_2-macroglobulin (incubated) into endosomes released their endosomal contents during 30-120 seconds of stretch. Elevated calcium and tension, in combination, were required to induce this endosomal release.

Recently the role of tension in embryogenesis was investigated in post-epiboly killifish embryos (Fink and Cooper, 1996). During epiboly, epithelial cells flatten and spread to completely cover the embryo as enveloping (EVL) cells. In embryos deformed between 2 coverglasses, EVL cells underwent an accelerated rate of membrane turnover with the fastest turnover occurring in regions of greatest deformation. It was therefore suggested that local mechanical tensions in EVL cells may modulate their apical membrane turnover during epiboly.

Van Essen (1997) proposed that mechanical tension was the major parameter that brings about CNS morphogenesis. More specifically he proposed that CNS tissues expand along the path of least resistance (ie. area of cell or tissue experiencing the lowest tension) and that neurites adjust their length by a negative feedback system that maintains a steady tension.

FUTURE WORK

Having characterized VLDs in molluscan neurons it would now be timely to investigate how

VLDs form and recover in a mammalian neuronal cell like PC12 cells, since we know PC12 cells form VLDs (Mills, unpublished observations). Four possible lines of inquiry that I think would be informative and interesting are: 1) is VLD recovery mediated by endocytosis? As a first step, fluorescence labelled endocytosis probes, such as transferrin, could be used. To confirm if VLD recovery is endocytosis-mediated, staining of neurons with an anti-clathrin antibody could also be done to determine if VLDs are reinternalized via clathrin coated vesicles. 2) Does brain spectrin and/or fodrin line VLDs and contribute to formation and recovery? Although evidence that the spectrin skeleton lines VLDs was obtained in muscle myotubes, VLDs have been more fully characterized in neurons. Brain fodrin lines retrieving vesicles in rat chromaffin cells (Fujimoto and Ogawa, 1989) and if spectrin and/or fodrin are found to line neuronal VLDs, as well as muscle VLDs (my work) and myopathic vacuoles (De Bleecker *et al.*, 1993; Vita *et al.*, 1994), this might indicate that membrane is generally retrieved, not naked, but supported by the membrane skeleton. 3) Do focal adhesion proteins colocalize with VLD peripheries? Here immunocytochemistry could be used to identify if proteins such as integrin and vinculin are present, which could be responsible for firmly attaching membrane regions adjacent to VLDs to the substrate. 4) What are the intracellular signals that trigger leading edge formation at VLDs? The forces that generate VLDs may also trigger new leading edge (ie. actipodia). Tyrosine kinases are widely implicated in cellular responses to mechanical signalling. It is known that cells initiate volume regulation through pathways involving protein tyrosine phosphorylation (Tilly *et al.*, 1993; Szászi *et al.*, 1997). Strain, via the tyrosine kinase pp60src, increases the phosphorylation of specific actin-binding proteins (Liu *et al.*, 1996). It would be interesting to exploit the dramatic shrinking-induced actipodia configuration to determine if the actin dynamics are regulated by pp60src. General and more specific inhibitors of pp60src are available, including herbimycin A and PP1 (Liu *et al.*, 1996). PC12 cells would be appropriate to use here since they form VLDs (Mills, unpublished observation) and also because a lot is known about how their filamentous actin network reorganizes upon swelling and RVD-mediated shrinking (Cornet *et al.*, 1994). Therefore if shrinking-induced actipodial formation is inhibited by compounds like herbimycin A and PP1, this would suggest that the mechanical signals trigger new leading edge at VLDs.

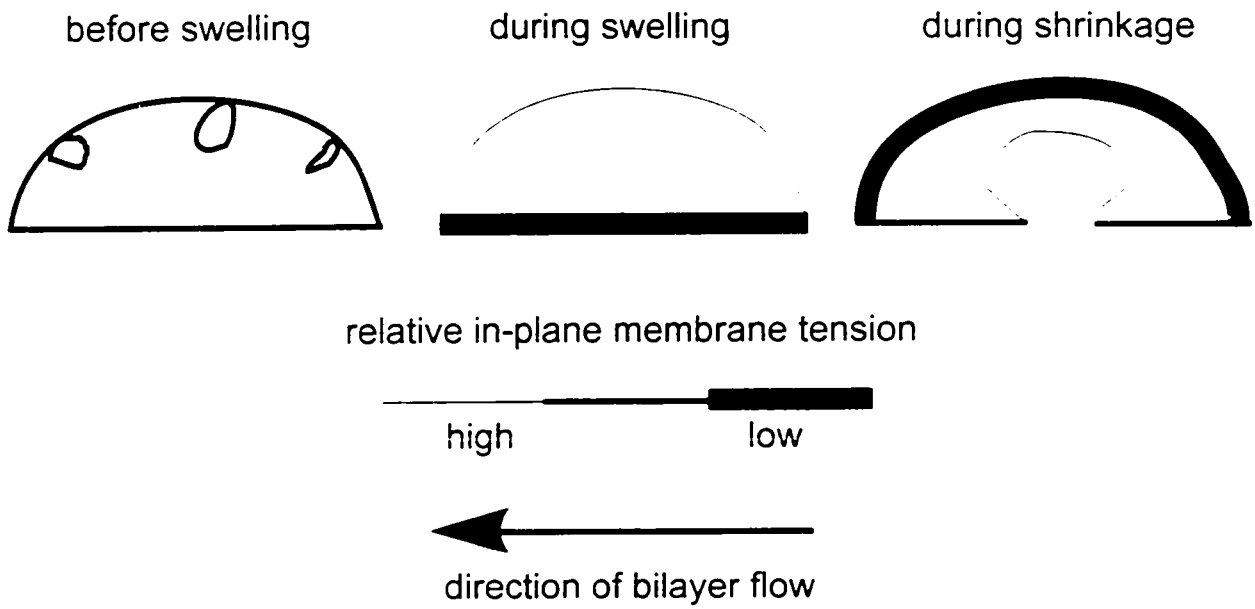

Figure 5.1 Model of how VLDs form in response to membrane tension changes. This model is based on the hypothesis that membrane under decreased tension flows to membrane areas under increased tension.

REFERENCES

Alberts, B., Bray, D., Lewis, J., Raff, M., Roberts, K., Watson, J.D. 1989. The Plasma Membrane. *In* Molecular Biology of the Ceil. 2nd edition. Garland Publishing Inc., New York, NY. pp. 275-340.

Allan, V., Vale, R. 1994. Movement of membrane tubules along microtubules in vitro: evidence for specialised sites of motor attachment. *Journal of Cell Science* 107: 1885-1897.

Amato, P.A., Taylor, D.L. 1986. Probing the mechanism of incorporation of fluorescently labeled actin into stress fibers. *The Journal of Cell Biology* 102: 1074-1084.

Andrew, R.D., Lobinowich, M.E., Oshehobo, E.P. 1997. Evidence against volume regulation by cortical brain cells during acute osmotic stress. *Experimental Neurology* 143: 300-312.

Auer, R.N., Coulter, K.C. 1994. The nature and time course of neuronal vacuolation induced by the N-methyl-D-aspartate antagonist MK-801. *Acta Neuropathologica* 87: 1-7.

Augustine, G.J., Adler, E. M., Charlton, M.P., Hans, M., Swandulla, D., Zipser, K. 1992. Presynaptic calcium signals during neurotransmitter release: detection with fluorescent indicators and other calcium chelators. *The Journal of Physiology* 86: 129-134.

Bennett, V. 1985. The membrane skeleton of human erythrocytes and its implications for more complex cells. *Annual Reviews of Biochemistry* 54: 273-304.

Black, J.D., Koury, S.T., Bankert, R.B., Repasky, E.A. 1988. Heterogeneity in lymphocyte spectrin distribution: ultrastructural identification of a new spectrin-rich cytoplasmic structure. *The Journal of Cell Biology* 106: 97-109.

Bonder, E.M., Fishkind, D.J., Cotran, N.M., Begg, D.A. 1989. The cortical actin-membrane cytoskeleton of unfertilized sea urchin eggs: analysis of the spatial organization and relationship of filamentous actin, nonfilamentous actin and egg spectrin. *Developmental Biology* 134: 327-341.

Bray, D. 1984. Axonal growth in response to experimentally applied mechanical tension. *Developmental Biology* 102: 379-389.

Bray, D., White, J.G. 1988. Cortical flow in animal cells. *Science* 239: 883-888.

Bray, D., Money, N.P., Harold, F.M., Bamburg, J.R. 1991. Responses of growth cones to changes in osmolality of the surrounding medium. *Journal of Cell Science* 98: 507-515.

Burridge, K., Kelly, T., Mangeat, P. 1982. Nonerythrocyte spectrins: actin-membrane attachment proteins occurring in many cell types. *The Journal of Cell Biology* 95: 478-486.

Cheek, T.R., Barry, V.A. 1993. Stimulus-secretion coupling in excitable cells: a central role for calcium. *The Journal of Experimental Biology* 184: 183-196.

Chen, C.S., Mrksich, M., Huang, S., Whitesides, G.M., Ingber, D.E. 1997. Geometric control of cell life and death. *Science* 276: 1425-1428.

Cheng, T.P.O., Reese, T.S. 1987. Recycling of plasmalemma in chick tectal growth cones. *The Journal of Neuroscience* 7: 1752-1759.
Cohan, C.S., Connor, J.A., Kater, S.B. 1987. Electrically and chemically mediated increases in intracellular calcium in neuronal growth cones. *The Journal of Neuroscience* 7: 3588-3599.

Coleman, T.R., Fishkind, D.J., Mooseker, M.S., Morrow, J.S. 1989. Contributions of the β-subunit to spectrin structure and function. *Cell Motility and the Cytoskeleton* 12: 248-263.

Cooper, M.S., Cornell-Bell, A.H., Chernjavsky, A., Dani, J.W., Smith, S.J. 1990. Tubulovesicular processes emerge from *trans*-golgi cisternae, extend along microtubules, and interlink adjacent *trans*-golgi elements into a reticulum. *Cell* 61: 135-145.

Cornet, M., Lambert, I.H., Hoffmann, E.K. 1993. Relation between cytoskeleton, hypo-osmotic treatment and volume regulation in Ehrlich ascites tumor cells. *The Journal of Membrane Biology* 131: 55-66.

Cornet, M., Isobe, Y., Lemanski, L.F. 1994. Effects of anisosmotic conditions on the cytoskeletal architecture of cultured PC12 cells. *Journal of Morphology* 222: 269-286.

Cunningham, C.C. 1995. Actin polymerization and intracellular solvent flow in cell surface blebbing. *The Journal of Cell Biology* 129: 1589-1599.

Czar, M.J., Welsh, M.J., Pratt, W.B. 1996. Immunofluorescence localization of the 90kDa heat-shock protein to cytoskeleton. *European Journal of Cell Biology* 70: 322-330.

Czekay, R-P., Kinne-Saffran, E., Kinne, R.K.H. 1994. Membrane traffic and sorbitol release during osmo- and volume regulation in isolated rat renal inner medullary collecting duct cells. *European Journal of Cell Biology* 63: 20-31.

Dabora, S.L., Sheetz, M.P. 1988. The microtubule-dependent formation of a tubulovesicular network with characteristics of the ER from cultured cell extracts. *Cell* 54: 27-35.

Dai, J., Sheetz, M.P. 1995a. Axon membrane flows from the growth cone to the cell body. *Cell* 83: 693-701.

Dai, J., Sheetz, M.P. 1995b. Regulation of endocytosis, exocytosis, and shape by membrane tension. *Cold Spring Harbor Symposia on Quantitative Biology* 60: 567-571.

Dai, J., Ting-Beall, H.P., Sheetz, M.P. 1997. The secretion-coupled endocytosis correlates with membrane tension changes in RBL 2H3 cells. *The Journal of General Physiology* 110: 1-10.

Dai, J., Sheetz, M.P., Morris, C.E. 1998. Membrane tension in swelling and shrinking molluscan neurons. Submitted for publication.

Dailey, M.E., Bridgman, P.C. 1993. Vacuole dynamics in growth cones: correlated EM and video observations. *The Journal of Neuroscience* 13: 3375-3393.

De Bleecker, J.L., Engel, A.G., Winkelmann, J.C. 1993. Localization of dystrophin and β-spectrin in vacuolar myopathies. *American Journal of Pathology* 143: 1200-1208.

de Ruijter, N., Emons, A. 1993. Immunodetection of spectrin antigens in plant cells. *Cell Biology International* 17: 169-182.

Dhermy, D. 1991. The spectrin super-family. *Biology of the Cell* 71: 249-254.

Doctor, R.B., Bennett, V., Mandel, L.J. 1993. Degradation of spectrin and ankyrin in the ischemic rat kidney. *American Journal of Physiology* 264: C1003-C1013.

Downey, G.P., Grinstein, S., Sue-A-Quan, A., Czaban, B., Chan, C.K. 1995. Volume regulation in leukocytes: requirement for an intact cytoskeleton. *Journal of Cellular Physiology* 163: 96-104.

Eckert, R., Randall, D., Augustine, G. 1988. Ions and Excitation. *In* Animal Physiology Mechanisms and Adaptations. 3rd edition. W. H. Freeman and Company. New York, NY. pp. 101-133.

Emery, D.G., Lucas, J.H. 1995. Ultrastructural damage and neuritic beading in cold stressed spinal neurons with comparisons to NMDA and A23187 toxicity. *Brain Research* 692: 161-173.

Evans, E.A., Waugh, R., Melnik, L. 1976. Elastic area compressibility modulus of red cell membrane. *Biophysical Journal* 16: 585-595.

Fabiato, A., Fabiato, F. 1979. Calculator programs for computing the composition of the solutions containing multiple metals and ligands used for experiments in skinned muscle cells. *Journal de Physiologie* 75: 463-505.

Fejtl, M., Szarowski, D.H., Decker, D., Buttle, K., Carpenter, D.O., Turner, J.N. 1995. Three-dimensional imaging and electrophysiology of live *Aplysia* neurons during volume perturbation: confocal light and high-voltage electron microscopy. *Journal of the Microscopic Society of America* 1: 75-85.

Fink, R.D., Cooper, M.S. 1996. Apical membrane turnover is accelerated near cell-cell contacts in an embryonic epithelium. *Developmental Biology* 174: 180-189.

Fishkind, D.J., Bonder, E.M., Begg, D.A. 1990a. Subcellular localization of sea urchin egg spectrin: evidence for assembly of the membrane-skeleton on unique classes of vesicles in eggs and embryos. *Developmental Biology* 142: 439-452.

Fishkind, D.J., Bonder, E.M., Begg, D.A. 1990b. Sea urchin spectrin in oogenesis and embryogenesis: a multifunctional integrator of membrane-cytoskeletal interactions. *Developmental Biology* 142: 453-464.

Forscher, P., Smith, S.J. 1988. Actions of cytochalasins on the organization of actin filaments and microtubules in a neuronal growth cone. *The Journal of Cell Biology* 107: 1505-1516.

Forscher, P., Lin, C.H., Thompson, C. 1992. Novel form of growth cone motility involving site-directed actin filament assembly. *Nature* 357: 515-518.

Fujimoto, T., Ogawa, K. 1989. Retrieving vesicles in secretion-induced rat chromaffin cells contain fodrin. *The Journal of Histochemistry and Cytochemistry* 37: 1589-1599.

Glacy, S.D. 1983. Subcellular distribution of rhodamine-actin microinjected into living fibroblastic cells. *The Journal of Cell Biology* 97: 1207-1213.

Glenney, J.R., Glenney, P. 1983a. Spectrin, fodrin and TW260/240: a family of related proteins lining the plasma membrane. *Cell Motility* 3: 671-682.

Glenney, J.R., Glenney, P. 1983b. Fodrin is the general spectrin-like protein found in most cells whereas spectrin and the TW protein have a restricted distribution. *Cell* 34: 503-512.

Glogauer, M., Arora, P., Chou, D., Janmey, P.A., Downey, G.P., McCulloch, C.A.G. 1998. The role of actin-binding protein 280 in integrin-dependent mechanoprotection. In Press.

Goodman, S.R., Zagon, I.S., Kulikowski, R.R. 1981. Identification of a spectrin-like protein in nonerythyroid cells. *Proceedings of the National Academy of Science. USA* 78: 7570-7574.

Goodman, S.R., Shiffer, K. 1983. The spectrin membrane skeleton of normal and abnormal human erythrocytes: a review. *American Journal of Physiology* 244: C121-C141.

Goodman, S.R., Krebs, K.E., Whitfield, C.F., Riederer, B.M., Zagon, I.S. 1988. Spectrin and related molecules. *CRC Critical Reviews in Biochemistry* 23: 171-234.

Gordon-Kamm, W.J., Steponkus, P.L. 1984. The behaviour of the plasma membrane during osmotic contraction of isolated protoplasts: implications in freezing injury. *Protoplasma* 123: 83-94.

Gratzer, W.B. 1981. The red cell membrane and its cytoskeleton. *Biochemical Journal* 198: 1-8.

Gruen, D.W.R., Wolfe, J. 1982. Lateral tensions and pressures in membranes and lipid monolayers. *Biochimica et Biophysica Acta* 688: 572-580.

Grynkiewicz, G., Poenie, M., Tsien, R.Y. 1985. A new generation of Ca^{2+} indicators with greatly improved fluorescence properties. *The Journal of Biological Chemistry* 260: 3440-3450.

Hagmann, J., Dagan, D., Burger, M.M. 1992. Release of endosomal content induced by plasma membrane tension: video image intensification time lapse analysis. *Experimental Cell Research* 198: 298-304.

Haydon, P.G., Cohan, C.S., McCobb, D.P., Miller, H.R., Kater, S.B. 1985. Neuron-specific growth cone properties as seen in identified neurons of *Helisoma*. *Journal of Neuroscience Research* 13: 135-147.

Hemphill, A., Seebeck, T., Lawson, D. 1991. The *Trypanosoma brucei* cytoskeleton: ultrastructure and localization of microtubule-associated and spectrin-like proteins using quick-freeze, deep-etch, immunogold electron microscopy. *Journal of Structural Biology* 107: 211-220.

Herring, T.L., Slotin, I.M., Baltz, J.M., Morris, C.E. 1998. Neuronal swelling and surface area regulation: elevated intracellular calcium is not a requirement. American Journal of Physiology 274: C272-C281.

Hiller, G., Weber, K. 1977. Spectrin is absent is various tissue culture cells. *Nature* 266: 181-183.

Hitt, A.L., Luna, E.J. 1994. Membrane interactions with the actin cytoskeleton. *Current Opinion in Cell Biology* 6: 120-130.

Hochmuth, R.M., Shao, J-Y., Dai, J., Sheetz, M.P. 1996. Deformation and flow of membrane into tethers extracted from neuronal growth cones. *Biophysical Journal* 70: 358-369.

Hopkins, C.R., Gibson, A., Shipman, M., Miller, K. 1990. Movement of internalized ligand-receptor complexes along a continuous endosomal reticulum. *Nature* 346: 335-339.

Ingber, D.E., Folkman, J. 1989. Tension and compression as basic determinants of cell form and function: utilization of a cellular tensegrity mechanism. *In* Cell Shape: Determinants, Regulation, and Regulatory role. Editors: Stein, W.D., Bronner, F. Academic Press Inc., San Diego, CA. pp. 3-31.

Itoh, T., Kanmura, Y., Kuriyama, H. 1985. A23187 increases calcium permeability of store sites more than of surface membranes in the rabbit mesenteric artery. *The Journal of Physiology* 359: 467- 484.

Jensen, K.G., Palta, J.P. 1980. Plasma membrane surface during osmotically induced volume changes: evidence against membrane folding. *Plant Physiology* 65 [Supp]: 814.

Kell, A., Glaser R.W. 1993. On the mechanical and dynamic properties of plant cell membranes: their role in growth, direct gene transfer and protoplast fusion. *Journal of Theoretical Biology* 160: 41-62.

Kennedy, H.J., Thomas, R.C. 1996. Effects of injecting calcium-buffer solutions on $[Ca^{2+}]_i$ in voltage-clamped snail neurons. *Biophysical Journal* 70: 2120-2130.

Kobayashi, T., Ohno, S., Park-Matsumoto, Y., Kameda, N., Baba, T. 1995. Developmental studies of dystrophin and other cytoskeletal proteins in cultured muscle cells. *Microscopy Research and Technique* 30: 437-457.

Koenig, E., Kinsman, S., Repasky, E., Sultz, L. 1985. Rapid mobility of motile varicosities and inclusions containing α-spectrin, actin and calmodulin in regenerating axons *in vitro*. *The Journal of Neuroscience* 5: 715-729.

Kosaka, T., Nagatsu, I., Wu, J-Y., Hama, K. 1986. Use of high concentrations of glutaraldehyde for immunocytochemistry of transmitter-synthesizing enzymes in the central nervous system. *Neuroscience* 18: 975-990.

Kostyuk, P.G., Mironov, S.L., Tepikin, A.V., Belan, P.V. 1989. Cytoplasmic free Ca in isolated snail neurons as revealed by fluorescent probe Fura-2: mechanisms of Ca recovery after Ca load and Ca release from intracellular stores. *The Journal of Membrane Biology* 110: 11-18.

Kreis, T.E., Winterhalter, K.H., Birchmeier, W. 1979. *In vivo* distribution and turnover of fluorescently labeled actin microinjected into human fibroblasts. *Proceedings of the National Academy of Science. USA* 76: 3814-3818.

Krolenko, S.A., Amos, W.B., Lucy, J.A. 1995. Reversible vacuolation of the transverse tubules of frog skeletal muscle: a confocal fluorescence microscopy study. *Journal of Muscle Research and Cell Motility* 16: 401-411.

Kwiatkowska, K., Sobota, A. 1990. Alpha-spectrin immunoanalog in *Acanthamoeba* cells. *Histochemistry* 94: 87-93.

Lamoureux, P., Buxbaum R.E., Heidemann, S.R. 1989. Direct evidence that growth cones pull. *Nature* 340: 159-162.

Lee, C., Chen, L.B. 1988. Dynamic behavior of endoplasmic reticulum in living cells. *Cell* 54: 37-46.

Letourneau, P.C. 1981. Immunocytochemical evidence for colocalization in neurite growth cones of actin and myosin and their relationship to cell-substratum adhesions. *Developmental Biology* 85: 113-122.

Levina, N.N., Lew, R.R., Heath, I.B. 1994. Cytoskeletal regulation of ion channel distribution in the tip-growing organism *Saprolegnia ferax*. *Journal of Cell Science* 107:127-134.

Levine, J., Willard, M. 1981. Fodrin: axonally transported polypeptides associated with the internal periphery of many cells. *The Journal of Cell Biology* 90: 631-643.

Lewis, S.A., Diamond, J.M.J. 1976. Na^+ transport by rabbit urinary bladder, a tight epithelium. *The Journal of Membrane Biology* 28: 1-40.

Lewis, S.A., de Moura, J.L.C. 1982. Incorporation of cytoplasmic vesicles into apical membrane of mammalian urinary bladder epithelium. *Nature* 297: 685-688.

Lin, C., Lamoureux, P., Buxbaum, R.E., Heidemann, S.R. 1995. Osmotic dilution stimulates axonal outgrowth by making axons more sensitive to tension. *Journal of Biomechanics* 28: 1429-1438.

Lipowsky, R. 1991. The conformation of membranes. Nature 349: 475-481.

Lippincott-Schwartz, J., Donaldson, J.G., Schweizer, A., Berger, E.G., Hauri, H-P., Yuan, L.C., Klausner, R.D. 1990. Microtubule-dependent retrograde transport of proteins into the ER in the presence of Brefeldin A suggests an ER recycling pathway. *Cell* 60: 821-836.

Lippincott-Schwartz, J., Yuan, L., Tipper, C., Amherdt, M., Orci, L., Klausner, R.D. 1991. Brefeldin A's effects on endosomes, lysosomes, and the TGN suggest a general mechanism for regulating organelle structure and membrane traffic. *Cell* 67: 601-616.

Liu, M., Qin, Y., Liu, J., Tanswell, A.K., Post, M. 1996. Mechanical strain induces pp60src activation and translocation to cytoskeleton in fetal rat lung cells. *The Journal of Biological Chemistry* 271: 7066-7071.

Liu, S-C., Palek, J. 1980. Spectrin tetramer-dimer equilibrium and the stability of erythrocyte membrane skeletons. *Nature* 285: 586-588.

Liu, S-C., Derick, L.H., Agre, P., Palek, J. 1990. Alteration of the erythrocyte membrane skeletal ultrastructure in hereditary spherocytosis, hereditary elliptocytosis, and pyropoikilocytosis. *Blood* 76: 198-205.

Low, P.S., Willardson, B.M., Mohandas, N., Rossi, M., Shohet, S. 1991. Contribution of the band 3-ankyrin interaction to erythrocyte membrane mechanical stability. *Blood* 77: 1581-1586.

Lux, S.E., Pease, B., Tomaselli, M.B., John, K.M., Bernstein, S.E. 1979. *In* Normal and Abnormal Red Cell Membranes. Editors: Lux, S.E., Marchesi, V.T., Fox, C.F. A.R. Liss, New York. pp. 463-469.

Marchesi, V.T. 1985. Stabilizing infrastructure of cell membranes. *Annual Review of Cell Biology* 1: 531-561.

Mattson, M.P., Kater, S.B. 1987. Calcium regulation of neurite elongation and growth cone motility. *The Journal of Neuroscience* 7: 4034-4043.

McGough, A.M., Josephs, R. 1990. On the structure of erythrocyte spectrin in partially expanded membrane skeletons. *Proceedings of the National Academy of Science, USA* 87: 5208-5212.

Menke, A., Jockusch, H. 1991. Decreased osmotic stability of dystrophin-less muscle cells from the mdx mouse. *Nature* 349: 69-71.

Messina, D.A., Lemanski, L.F. 1991. Studies of hamster cardiac myofibrillogenesis in vivo with antibodies to spectrin, desmin, and alpha-actinin. *The American Journal of Anatomy* 191: 85-94.

Mills, J.W., Schwiebert, E.M., Stanton, B.A. 1994. Evidence for the role of actin filaments in regulating cell swelling. *The Journal of Experimental Zoology* 268: 111-120.

Mills, L.R., Morris, C.E. 1998. Neuronal plasma membrane dynamics evoked by osmomechanical perturbations. Submitted for publication.

Morán, J., Sabanero, M., Meza, I., Pasantes-Morales, H. 1996. Changes of actin cytoskeleton during swelling and regulatory volume decrease in cultured astrocytes. *American Journal of Physiology* 271: C1901-C1907.

Morán, J., Morales-Mulia, S., Hernandez-Cruz, A., Pasantes-Morales, H. 1997. Regulatory volume decrease and associated osmolyte fluxes in cerebellar granule neurons are calcium independent. *Journal of Neuroscience Research* 47: 144-154.

Morimoto, T., Ginsberg, M.D., Dietrich, W.D., Zhao, W. 1997. Hyperthermia enhances spectrin breakdown in transient focal cerebral ischemia. *Brain Research* 746: 43-51.

Morisaki, J.H., Heuser, J.E., Sibley, L.D. 1995. Invasion of *Toxoplasma gondii* occurs by active penetration of the host cell. *Journal of Cell Science* 108: 2457-2464.

Morris, C.E., Williams, B., Sigurdson, W.J. 1989. Osmotically-induced volume changes in isolated cells of a pond snail. *Comparative Biochemistry and Physiology* 92A: 479-483.

Morris, C.E., Horn, R. 1991. Failure to elicit neuronal macroscopic mechanosensitive currents anticipated by single-channel studies. *Science* 251: 1246-1249.

Morris, C.E., Lesiuk, H., Mills, L.R. 1997. How do neurons monitor their mechanical status? *Biological Bulletin* 192: 118-120.

Morrow, J.S. 1989. The spectrin membrane skeleton: emerging concepts. *Current Opinion in Cell Biology* 1: 23-29.

Mulholland, J., Preuss, D., Moon, A., Wong, A., Drubin, D., Botstein, D. 1994. Ultrastructure of the yeast actin cytoskeleton and its association with the plasma membrane. *The Journal of Cell Biology* 125: 381-391.

Müller, T.H., Partridge, L.D., Swandulla, D. 1993. Calcium buffering in bursting *Helix* pacemaker neurons. *Pflugers Archiv - European Journal of Physiology* 425: 499-505.

Myers, P.Z., Bastiani, M.J. 1993. Growth cone dynamics during the migration of an identified commissural growth cone. *The Journal of Neuroscience* 13: 127-143.

Neher, E., Augustine, G.J. 1992. Calcium gradients and buffers in bovine chromaffin cells. *The Journal of Physiology* 450: 273-301.

Nelson, W.J., Lazarides, E. 1983. Switching of subunit composition of muscle spectrin during myogenesis *in vitro*. *Nature* 304: 364-368.

Nelson, W.J., Lazarides, E. 1985. Posttranslational control of membrane-skeleton (ankyrin and αβ-spectrin) assembly in early myogenesis. *The Journal of Cell Biology* 100: 1726-1735.

Nelson, W.J., Veshnock, P.J. 1986. Dynamics of membrane-skeleton (fodrin) organization during development of polarity in Madin-Darby canine kidney epithelial cells. *The Journal of Cell Biology* 103: 1751-1765.

Nichol, J.A., Hutter, O.F. 1996a. Tensile strength and dilatational elasticity of giant sarcolemmal vesicles shed from rabbit muscle. *The Journal of Physiology* 493: 187-198.

Nichol, J.A., Hutter, O.F. 1996b. Ca^{2+} loading reduces the tensile strength of sarcolemmal vesicles shed from rabbit muscle. *The Journal of Physiology* 493: 199-209.

Norberg, R., Lidman, K., Fagraeus, A. 1975. Effects of cytochalasin B on fibroblasts, lymphoid cells and platelets revealed by human anti-actin antibodies. *Cell* 6: 507-512.

Nusse, O., Lindau, M., Cromwell, O., Kay, A.B., Gomperts, B.D. 1990. Intracellular application of guanosine-5'-O-(3-thiotriphosphate) induces exocytotic granule fusion in guinea pig eosinophils. *Journal of Experimental Medicine* 171: 775-786.

O'Connor, E.R., Kimelberg, H.K. 1993. Role of calcium in astrocyte volume regulation and in the release of ions and amino acids. *The Journal of Neuroscience* 13: 2638-2650.

Okabe, S., Hirokawa, N. 1989. Incorporation and turnover of biotin-labelled actin microinjected into fibroblastic cells: an immunoelectron microscopic study. *The Journal of Cell Biology* 109: 1581-1595.

Okabe, S., Hirokawa, N. 1991. Actin dynamics in growth cones. *The Journal of Neuroscience* 11: 1918-1929.

Okada, Y., Hazama, A., Hashimoto, A., Maruyama, Y., Kubo, M. 1992. Exocytosis upon osmotic swelling in human epithelial cells. *Biochimica et Biophysica Acta* 1107: 201-205.

Palek, J. 1987. Hereditary elliptocytosis, spherocytosis and related disorders: consequences of a deficiency or a mutation of membrane skeletal proteins. *Blood Reviews* 1: 147-168.

Penner, R., Neher, E. 1988. The role of calcium in stimulus-secretion coupling in excitable and non-excitable cells. *The Journal of Experimental Biology* 139: 329-345.

Porter, G.A., Dmytrenko, G.M., Winkelmann, J.C., Bloch, R.J. 1992. Dystrophin colocalizes with β-spectrin in distinct subsarcolemmal domains in mammalian skeletal muscle. *The Journal of Cell Biology* 117: 997-1005.

Porter, G.A., Scher, M.G., Resneck, W.G., Porter, N.C., Fowler, V.M., Bloch, R.J. 1997. Two populations of β-spectrin in rat skeletal muscle. *Cell Motility and the Cytoskeleton* 37: 7-19.

Pumplin, D.W. 1995. The membrane skeleton of acetylcholine receptor domains in rat myotubes contains antiparallel homodimers of β-spectrin in filaments quantitatively resembling those of erythrocytes. *Journal of Cell Science* 108: 3145-3154.

Raat, N.J.H., Van Os, C.H., Bindels, R.J.M. 1995. Effects of osmotic perturbation on $[Ca^{2+}]_i$ and pH_i in rabbit proximal tubular cells in primary cuiture. *American Journal of Physiology* 269: F205-F211.

Repasky, E.A., Pollina, C.M., Menold, M.M., Hudecki, M.S. 1986. Increased concentration of spectrin in observed in avian dystrophic muscle. *Proceedings of the National Acadeny of Science, USA* 83: 802-806.

Reuzeau, C., Mills, L.R., Harris, J.A., Morris, C.E. 1995. Discrete and reversible vacuole-like dilations induced by osmomechanical perturbation of neurons. *The Journal of Membrane Biology* 145: 33-47.

Ross, P.E., Garber, S.S., Cahalan, M.D. 1994. Membrane chloride conductance and capacitance in Jurkat T lymphocytes during osmotic swelling. *Biophysical Journal* 66: 169-178.

Saido, T.C., Sorimachi, H., Suzuki, K. 1994. Calpain: new perspectives in molecular diversity and physiological-pathological involvement. *FASEB Journal* 8: 814-822.

Sánchez-Olea, R., Pasantes-Morales, H., Schousboe, A. 1993. Neurons respond to hyposmotic conditions by an increase in intracellular free calcium. *Neurochemical Research* 18: 147-52.

Schlaepfer, W.W. 1977. Structural alterations of peripheral nerve induced by the calcium ionophore A23187. *Brain Research* 136: 1-9.

Schliwa, M. 1982. Action of cytochalasin D on cytoskeletal networks. *The Journal of Cell Biology* 92: 79-91.

Séguin, D.G., Baltz, J.M. 1997. Cell volume regulation by the mouse zygote: mechanism of recovery from a volume increase. *American Journal of Physiology* 272: C1854-C1861.

Sheetz, M.P., Dai J. 1996. Modulation of membrane dynamics and cell motility by membrane tension. *Trends in Cell Biology* 6: 85-89.

Sikorski, A.F., Swat, W., Brzezinska, M., Wróblewski, Z., Bisikirska, B. 1993. A protein cross-reacting with anti-spectrin antibodies is present in higher plant cells. *Zeitschrift fur Naturforsch* 48c: 580-583.

Speicher, D.W., Marchesi, V.T. 1984. Erythrocyte spectrin is comprised of many homologous triple helical segments. *Nature* 311: 177-180.

Spring, K.R., Hoffmann, E.K. 1992. Cellular volume control. *In:* The Kidney: Physiology and pathophysiology. 2nd edition. Editor: Seldin, D.W., Giebisch, G. Raven Press, Ltd., New York. pp. 147-169.

Springall, D.R., Polak, J.M. 1995. Samples and preparation methods. *In* Conventional and confocal microscopy. Image analysis in histology. Editors: Wootton, R., Springall, D.R., Polack, J.M. Cambridge University Press, Cambridge, UK. pp. 123-133.

Steinhardt, R.A., Bi, G., Alderton, J.M. 1994. Cell membrane resealing by a vesicular mechanism similar to neurotransmitter release. *Science* 263: 390-393.

Sukhorukov, V.L., Arnold, W.M., Zimmermann, U. 1993. Hypotonically induced changes in the plasma membrane of cultured mammalian cells. *The Journal of Membrane Biology* 132: 27-40.

Swanson, J., Bushnell, A., Silverstein, S.C. 1987. Tubular lysosome morphology and distribution within macrophages depend on the intergrity of cytoplasmic microtubules. *Proceedings of the National Academy of Science, USA* 84: 1921-1925.

Szászi, K., Buday, L., Kapus, A. 1997. Shrinkage-induced protein tyrosine phosphorylation in Chinese hamster ovary cells. *Journal of Biological Chemistry* 272: 16670-16678.

Taylor, D.L., Wang, Y.L. 1978. Molecular cytochemistry: incorporation of fluorescently labeled actin into living cells. *Proceedings of the National Academy of Science, USA* 75: 857-861.

Terasaki, M., Song, J., Wong, J.R., Weiss, M.J., Chen, L.B. 1984. Localization of endoplasmic reticulum in living and glutaraldehyde-fixed cells with fluorescent dyes. *Cell* 38: 101-108.

Terasaki, M., Chen, L.B., Fujiwara, K. 1986. Microtubules and the endoplasmic reticulum are highly interdependent structures. *The Journal of Cell Biology* 103: 1557-1568.

Tilly, B.C., van de Berghe, N., Tertoolen, L.G.J., Edixhoven, M.J., de Jonge, H.R. 1993. Protein tyrosine phosphorylation is involved in osmoregulation of ionic conductances. *Journal of Biological Chemistry* 268: 19919-19922.

Ursitti, J.A., Wade, J.B. 1993. Ultrastructure and immunocytochemistry of the isolated human erythrocyte membrane skeleton. *Cell Motility and the Cytoskeleton* 25: 30-42.

Van Essen, D.C. 1997. A tension-based theory of morphogenesis and compact wiring in the central nervous system. *Nature* 385: 313-318.

Vita, G., Migliorato, A., Toscano, A., Bordoni, A., Bresolin, N., Fiumara, A., Messina, C. 1994. Immunocytochemistry of muscle cytoskeletal proteins in acid maltase deficiency. *Muscle and Nerve* 17: 655-661.

Wan, X., Harris, J.A., Morris, C.E. 1995. Responses of neurons to extreme osmomechanical stress. *The Journal of Membrane Biology* 145: 21-31.

Wartenburg, M., Hamann, J., Pratsch, I., Donath, E. 1992. Osmotically induced fluid-phase uptake of fluorescent markers by protoplasts of *Chenopodium album*. *Protoplasma* 166: 61-66.

Weber, K., Rathke, P.C., Osborn, M., Franke, W.W. 1976. Distribution of actin and tubulin in cells and in glycerinated cell models after treatment with cytochalasin B. *Experimental Cell Research* 102: 285-297.

Weber, K., Rathke, P.C., Osborn, M. 1978. Cytoplasmic microtubular images in glutaraldehyde-fixed tissue culture cells by electron microscopy and by immunofluorescence microscopy. *Proceedings of the National Academy of Science, USA* 75: 1820-1824.

Welnhofer, E.A., Zhao, L., Cohan, C.S. 1997. Actin dynamics and organization during growth cone morphogenesis in *Helisoma* neurons. *Cell Motility and the Cytoskeleton* 37: 54-71.

Wilkerson, E.H., DiBona, D.R., Schafer, J.A. 1986. Analysis of structural changes during hypotonic swelling in Ehrlich ascites tumor cells. *American Journal of Physiology*. 251: C104-C114.

Winkelmann, J.C., Chang, J-G., Tse, W.T., Scarpa, A.L., Marchesi, V.T., Forget, B.G. 1990a. Full length sequence of the cDNA for human erythroid β-spectrin. *The Journal of Cell Biology* 265: 11827-11832.

Winkelmann, J.C., Costa, F.F., Linzie, B.L., Forget, B.G. 1990b. β-spectrin in human skeletal muscle. Tissue-specific differential processing of 3' β spectrin pre-mRNA generates a β spectrin isoform with a unique carboxyl terminus. *The Journal of Biological Chemistry* 265: 20449-20454.

Winkelmann, J.C., Forget, B.G. 1993. Erythroid and nonerythroid spectrins. *Blood* 81: 3173-3185.

Wolfe, J., Steponkus, P.L. 1981. The stress-strain relation of the plasma membrane of isolated plant protoplasts. *Biochimica et Biophysica Acta* 643: 663-668.

Wolfe, J., Dowgert, M.F., Steponkus, P.L. 1985. Dynamics of membrane exchange of the plasma membrane and the lysis of isolated protoplasts during rapid expansions in areas. *The Journal of Membrane Biology* 86: 127-138.

Wolfe, J., Dowgert, M.F., Steponkus, P.L. 1986. Mechanical study of the deformation and rupture of the plasma membranes of protoplasts during osmotic expansions. *The Journal of Membrane Biology 93*: 63-74.

Wood, S.A., Park, J.E., Brown, W.J. 1991. Brefeldin A causes a microtubule-mediated fusion of the trans-golgi network and early endosomes. *Cell* 67: 591-600.

Wu, D-Y., Goldberg, D.J. 1993. Regulated tyrosine phosphorylation at the tips of growth cone filopodia. *The Journal of Cell Biology* 123: 653-664.

Zheng, J., Lamoureux, P., Santiago, V., Dennerll, T., Buxbaum, R.E., Heidemann, S.R. 1991. Tensile regulation of axonal elongation and initiation. *The Journal of Neuroscience* 11: 1117-1125.

Zhou, D., Ursitti, J.A., Bloch, R.J. 1998. Developmental expression of spectrins in rat skeletal muscle. *Molecular Biology of the Cell* 9: 47-61.

Ziyadeh, F.N., Mills, J.W., Kleinzeller, A. 1992. Hypotonicity and cell volume regulation in shark rectal gland: role of organic osmolytes and F-actin. *American Journal of Physiology* 262: F468-F479.

Zorec, R., Tester, M. 1993. Rapid pressure driven exocytosis-endocytosis cycle in a single plant cell: capacitance measurements in aleurone protoplasts. *FEBS* Letters 333: 283-286.

APPENDIX: L6E9 MYOTUBES MAKE VLDs

These experiments were performed by Jenni McNally, a summer student in Dr. Cathy Morris' lab in 1996 and 1997. She observed and characterized VLD formation (fig A.1 and A.2), reversal (fig A.1), recovery (fig A.2), repeatability (fig A.1) and VLD size distributions (fig A.3) in rat skeletal muscle myotubes (L6E9 cells). Together with her Western blot analysis of muscle spectrin skeleton expression in L6E9 cells (fig A.4), this lead to the experiments presented in chapter 4 of localizing the spectrin skeleton in L6E9 cells by immunocytochemistry.

METHODS AND MATERIALS

Cells and solutions

L6E9 muscle myotubes were grown as outlined in the methods and materials section in chapter 4, except that myoblasts were plated onto 22x22mm autoclaved glass coverslips.

Flow through chamber construction and viewing of cells

A double coverslip chamber with a 150µm gap, similar to the flow through chamber described in chapter 2, was constructed for viewing the cells during solution changes. Solution changes were effected using 250µL (5x 50µL drops). VLDs were elicited by swelling in 50% L6NS for 4 minutes and then returning to L6NS (recipe in methods and materials, chapter 4) to bring about shrinkage and VLD formation. Cells were viewed with an inverted Olympus IMT-2 microscope fitted with Hoffman modulation contrast optics (40x objective).

All experiments were video recorded using a Sony CCD video camera (AVC-D5) either with a JVC BR-S601 MU super VHS or with a time lapse JVC BR-905 OU recorder. Taped video frames were digitized by a Data Translations 3155 frame grabber using Image Tool software. Digitized images were processed in Corel Photo Paint and Corel Draw. VLD size measurements (fig A.3) were made from videotaped experiments displayed on a monitor. Measurements from the screen were then converted to absolute sizes with a stage micrometer.

Western Blot

The following protocols were according to Porter *et al.* (1992 and 1997).

Tissue preparation

0.5g of L6E9 myoblasts or myotubes (plus any non-differentiated myoblasts still in the culture) and 500µL of protease inhibitor cocktail (10mM benzamidine, 2 units/mL aprotinin, 10µg/mL leupeptin, 10µg/mL antipain, 200µg/mL soybean trypsin; all from Sigma, St. Louis, MO) was added to 20mL of GP buffer (10mM $NaPO_4$, 2mM EDTA, 10mM NaN_3, 140mM NaCl, 1% deoxycholate, 1% NP40; all from Sigma, St. Louis, MO). To this cell-solution cocktail, a 1mM final concentration of phenylmethylsulfonylfluoride (PMSF) (Sigma, St. Louis, MO) was added and the mixture was homogenized at 15 000 rpm for 4x30 second bursts. Tissue was then incubated on ice at 4°C for 1 hour then spun at 14 000 rpm for 1 hour at 4°C. The pellet was resuspended in 1mL of GP buffer and supernant was assayed for protein concentrations. To determine the protein concentrations, protein aliquots (1µL, 10µL and 100µL) were added to water and Biorad protein dye and vortexed (ie. 1µL of protein + 799µL water + 200µL protein dye; 10µL of protein + 790µL water + 200µL protein dye). Absorbance at 595nm was recorded and blank buffer aliquots were subtracted from this value to get real protein concentrations. Protein aliquots of 50µg were then frozen at -20°C until needed for the Western blot protocol.

Western blot protocol

For Western blots, blocking buffer (0.2% I-block, 0.1% Tween-20 in PBS), wash buffer (0.1% Tween-20 in PBS), goat anti-rabbit secondary antibody conjugated to alkaline phosphastase, assay buffer, CSPD ready-to-use substrate solution and Nitro-block were all supplied in the Western-Light chemiluminescent detection kit (Tropix Inc., Bedford, MA).

A 7.5% separating gel and 4% stacking gel were prepared on the day of the experiment. Protein samples (50µg/lane) and molecular weight markers were loaded and run for 1.5 hours at a constant voltage of 100V. The gel was then cut into two: one half was stained in coomassie blue and other half was transfered to nitrocellulose at 120mA for 2 hours and blocked for 3 days in

blocking buffer. Detection of the muscle spectrin skeleton was by the Western-Light chemiluminescent detection system (Tropix Inc., Bedford, MA). Nitrocellulose was incubated in the primary 4I12 antibody (diluted 1:10000 in blocking buffer) for 2 hours, washed 6 times, 5 minutes each, in wash buffer, incubated in goat anti-rabbit conjugated to alkaline phosphatase (diluted 1:5000 in blocking buffer) for 1 hour, washed 6 times, 5 minutes each, in wash buffer, washed 2 times, 5 minutes each, in assay buffer. Blots were drained, placed on saran wrap and incubated for 5 minutes in CSPD ready-to-use substrate solution (a chemiluminescent substrate for alkaline phosphatase) in Nitro-block (a chemiluminescent enhancer), drained off and exposed to film for 30 minutes.

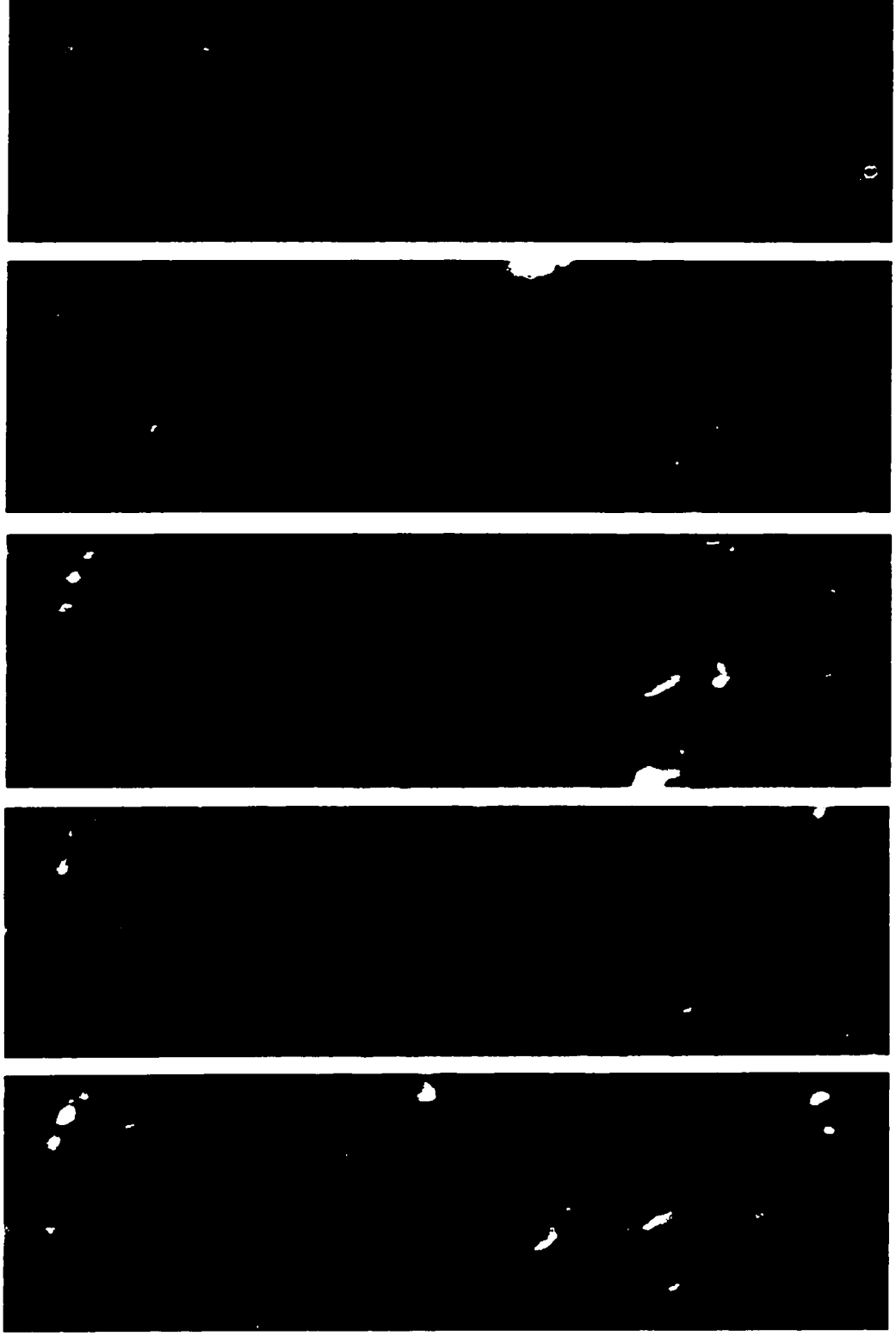

Figure A.1 VLD formation and reversal in L6E9 myotubes. View of myotubes before being osmotically shocked (A), swollen in 50% NS (B) and shrunk in NS causing VLD formation (C). Reswelling of myotubes results in VLD reversal (D) and reshrinkage caused VLDs to reform at the same discrete sites (arrowheads in E). Notice the VLD-like structure that persisted through out the osmotic perturbations (arrows) and the formation of membrane blebs in swollen cells (asterisks in B). B, D were taken 4 minutes after first being swollen and C, E were taken 2 minutes after being shrunk. Scale: 10μm.

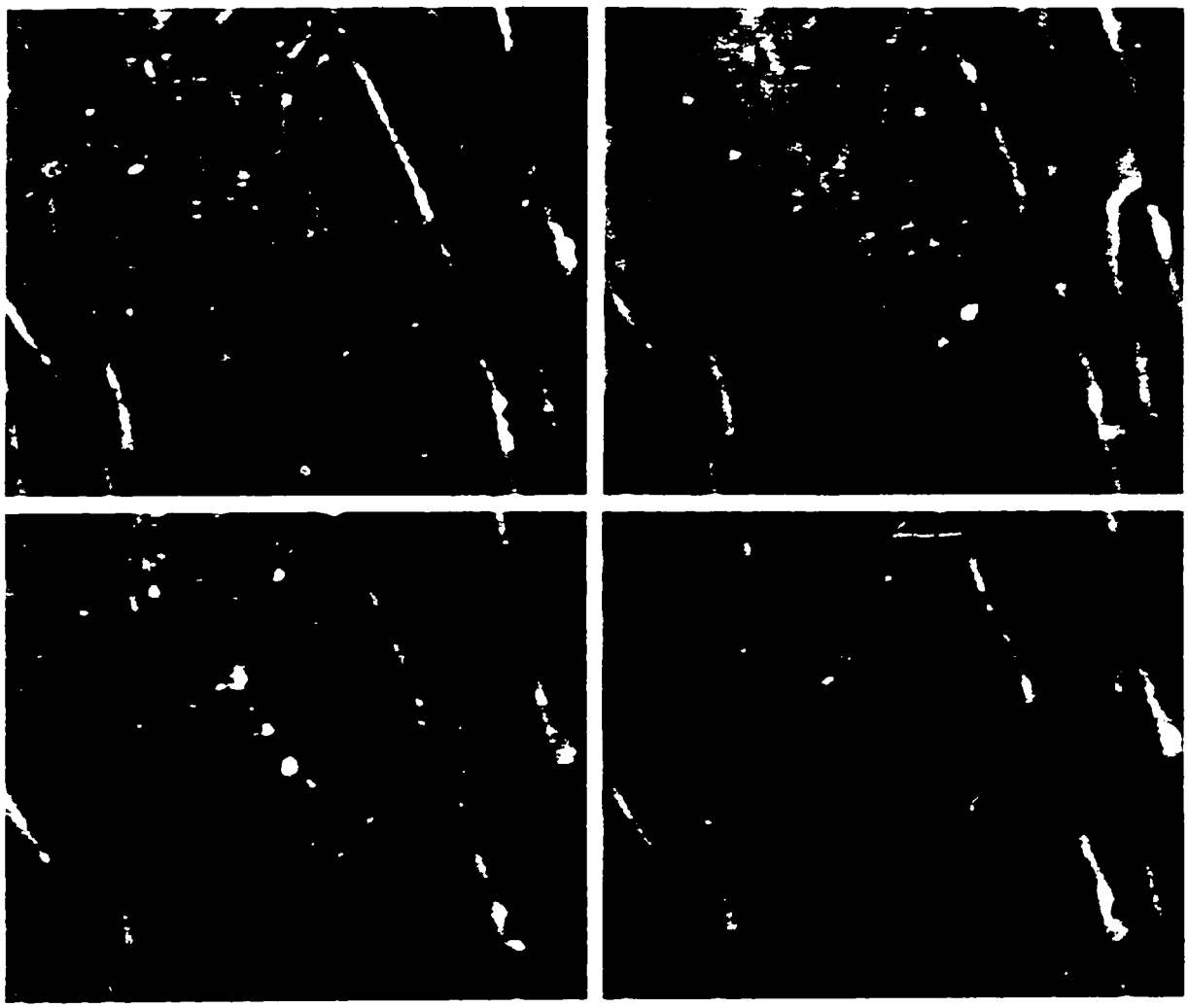

Figure A.2 VLD formation and recovery in L6E9 myotubes. View of myotubes before being osmotically shocked (A), swollen in 50% NS (B) and shrunk in NS causing VLD formation (C). VLD recovery occurs when myotubes are left in NS, as shown in D. B, C were taken 4 and 3 minutes after swelling and shrinking were initiated, respectively. D was taken 8 minutes after VLDs were first observed. Scale: 10μm.

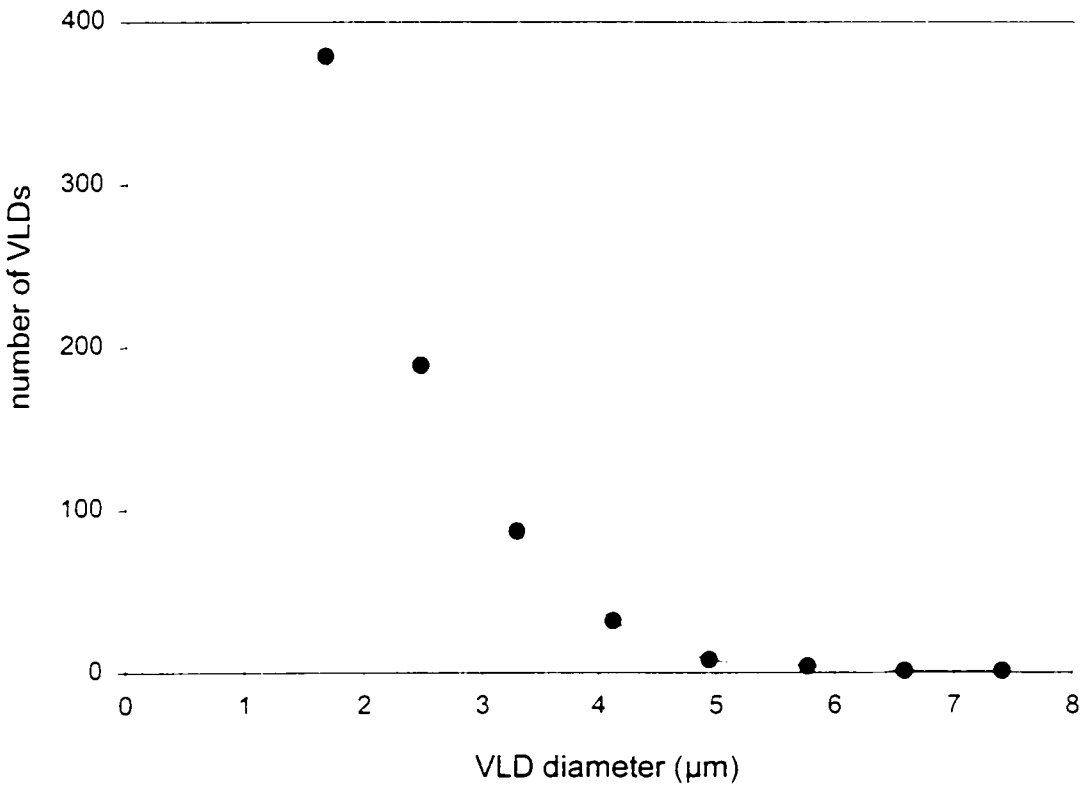

Figure A.3 Frequency distribution of the sizes of VLDs elicited in rat L6E9 skeletal myotubes. The line is a single exponential fit to the data. Smaller VLDs could not be resolved, but if it is assumed that the size fit a Poisson distribution, the mean diameter would be 1µm, the decay constant of the fitted line.

Figure A.4 Western blot of L6E9 muscle cells probed with muscle spectrin skeleton antibodies. Anti-muscle spectrin was expressed in myoblasts (MB) and myotubes (MT) at a molecular weight of 235kDa. However a very light myotube band of approximately 200kDa was evident in the original Western blot. Molecular weight markers (MWM) were *E. coli* MBP-β-galactosidase (175kDa), *E. coli* MBP-paramyosin (83kDa) and bovine liver glutamine dehydrogenase (62kDa). MBP = maltose binding protein.

Jan 21/98

Dear Miss Green,

I am writing to request permission to include manuscript #C388-7 titled: Neuronal swelling and surface area regulation: elevated intracellular calcium is not a requirement in my Master's thesis. I am attending the University of Ottawa and want to ensure that this manuscript can be added as a chapter to my thesis without any problems. A letter stating that submission of this paper to my thesis has been approved by the journals management & editors would be all that is required.

Thank-you very much. Please attention any responses to myself.

AJP 274. Pg 272 - 281

*

Post-it™ Fax Note 7671	Date	# of pages ▶
To T. Herring	From S. Green	
Co./Dept.	Co APS	
Phone #	Phone # 301 571 5742	
Fax #	Fax # 301 571 1814	

THE AMERICAN PHYSIOLOGICAL SOCIETY
9650 Rockville Pike — Bethesda, MD 20814

Permission is granted for use of the material requested, provided the publication is credited as the source.

1/21/98 Date — Brenda Hamm, Publ Mgr & Exec Editor

* Please use for reference information

TEST TARGET (QA-3)

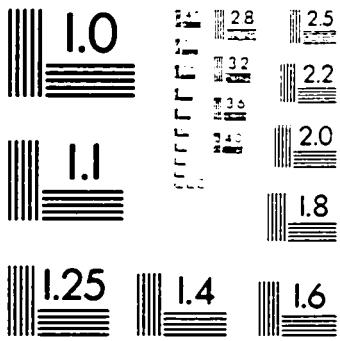

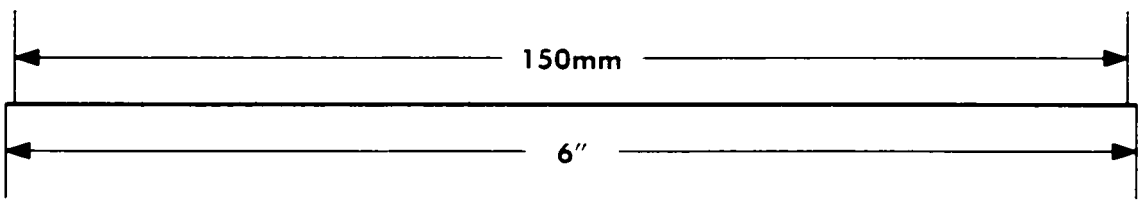

APPLIED IMAGE, Inc
1653 East Main Street
Rochester, NY 14609 USA
Phone: 716/482-0300
Fax: 716/288-5989